



UNIVERSITEIT VAN PRETORIA  
UNIVERSITY OF PRETORIA  
YUNIBESITHI YA PRETORIA

**CONDENSATION INSIDE  
HORIZONTAL AND INCLINED  
SMOOTH TUBES AT LOW MASS  
FLUXES**

by

**Daniel Raphael Ejike EWIM**

**Submitted in partial fulfilment of the requirements for the degree**

**Doctor of Philosophy (PhD)**

**in Engineering**

**Department of Mechanical and Aeronautical Engineering**

**Faculty of Engineering, Built Environment and Information Technology**

**University of Pretoria**

**January 2019**

**Supervisor: Prof JP Meyer**

# Abstract

---

Title: Condensation inside horizontal and inclined smooth tubes at low mass fluxes

Supervisor: Prof JP Meyer

Department: Mechanical and Aeronautical Engineering

Degree: Doctor of Philosophy (Mechanical Engineering)

Condensation has been extensively investigated from as early as 1914. However, there are several gaps in the literature, especially for in tube condensation at low mass fluxes and inclined tubes. Until now, no study has systematically investigated the influence of temperature difference, vapour quality, and inclination on the heat transfer coefficients and pressure drops during condensation inside horizontal and inclined smooth tubes at low mass fluxes. Thus, the purpose of this study was to increase the fundamental understanding of two – phase flow behaviour at low mass fluxes by experimentally investigating the heat transfer, flow pattern, and pressure drop characteristics during condensation inside horizontal and inclined smooth tubes at low mass fluxes.

An existing experimental set-up was modified to accommodate the “*low mass flux*” needs of this study and the initial results were successfully validated against literature. A smooth circular copper tube in tube test condenser with an inner tube 1.49 m long, an inner diameter of 8.38 mm and an outer diameter of 9.54 mm was designed and built. The annulus had an inner diameter of 14.5 mm and an outer diameter of 15.88 mm. Heat transfer and pressure drop experiments were conducted for mass fluxes of 50, 75, 100, 150, and 200 kg/m<sup>2</sup>s, at 15 different inclination angles from  $-90^\circ$  (vertically downwards) to  $+90^\circ$  (vertically upwards). The temperature differences (differences between the average refrigerant saturation temperature and tube wall temperature) were varied from 1 °C to 10 °C, while the average saturation (condensation) temperature was maintained at 40 °C. The mean vapour qualities were varied between 0.1 to 0.9. R134a was used as the test fluid while water was used in the annulus to cool the test section. A total of 2 178 videos, 2 920 mass flow rate measurements, 56 301 temperature measurements and 1 536 pressure drop measurements were taken. The flow patterns were recorded in grey levels with two high-speed video cameras installed at the inlet and outlet of the test section through sight glasses made from borosilicate. To improve the image quality and ensure uniformity in the distribution of the light, a uniform (LED) backlight was used. This LED backlight was a 99% uniform, 50 by 50 mm red light. An uncertainty analysis

showed that the maximum uncertainties of the pressure drops, heat transfer coefficients and vapour qualities presented in this study were 9%, 12%, and 5% respectively.

For horizontal flow, it was found that the flow patterns were predominantly stratified and stratified wavy. It was also found that the heat transfer coefficients were dependent on the temperature difference between the temperature of the wall on which condensation occurs and the temperature of the condensing refrigerant. Furthermore, it was found that the heat transfer coefficient decreased with an increase in the temperature difference. When comparing the heat transfer results at low mass fluxes to the literature, it was found that the absolute mean deviation varied by up to 42%. An amendment was suggested in a stratified heat transfer coefficient term from literature. It was found that with this amendment, the heat transfer coefficients of low mass fluxes could be estimated with errors of an average of  $\pm 5\%$ .

For inclined flow, six flow patterns namely — stratified, stratified wavy, annular, annular wavy, intermittent, and churns flows were observed. Bubbly flow was not observed on its own but was observed during intermittent flows. These flow patterns were adopted using the descriptions of flow regimes as prescribed by Thome. It was found that the inclination angles significantly influenced the flow patterns and the heat transfer coefficients. Downwards flows accounted for an increase in heat transfer coefficient with the maximum heat transfer coefficient found at inclinations of  $-15^\circ$  and  $-30^\circ$  at the corresponding minimum temperature difference tested for in each case. The maximum inclination effect was approximately 60% and was obtained at the lowest mass flux of  $50 \text{ kg/m}^2\text{s}$ . In general, it was concluded that the heat transfer coefficients were more sensitive to the temperature difference for downwards flows than for upwards flows. Furthermore, there was no significant effect of the temperature difference on the heat transfer coefficients for upwards flows. It was also found that the vertical downwards ( $-90^\circ$ ) and upwards ( $+90^\circ$ ) orientations were almost independent of the temperature difference. With respect to the inclination effect, it was found that in general, they decreased with increase in temperature difference, but increased with a decrease in mass flux and vapour quality.

With respect to pressure drops in smooth and inclined tubes, it was found that they increased with an increase in mass flux, temperature difference and vapour quality. Furthermore, the lowest and highest measured pressure drops were obtained during the downward and upward flows respectively. On the other hand, the opposite was found for the frictional pressure drops.

**Keywords:** Inclination angles, condensation, temperature difference, mass flux, smooth tube, vapour quality, heat transfer coefficient, flow patterns, pressure drop, inclination effect.

## Publications

---

The following journal and conference papers were produced as progress was made during the preparation of this thesis. They provided independent peer reviews from subject matter experts whose valuable feedbacks were implemented.

### Articles

1. J.P. Meyer and **D.R.E. Ewim**, Heat transfer coefficients during the condensation of low mass fluxes in smooth horizontal tubes, *International Journal of Multiphase Flow*, Volume 99, Pages 485–499, 2018.
2. **D.R.E. Ewim**, J.P. Meyer, and S. M. A. Noori Rahim Abadi, Condensation heat transfer coefficients in an inclined smooth tube at low mass fluxes, *International Journal of Heat and Mass Transfer*, Volume 123, Pages 455–467, 2018.
3. **D.R.E. Ewim** and J.P. Meyer, Pressure drop during condensation at low mass fluxes in smooth horizontal and inclined tubes, *International Journal of Heat and Mass Transfer*, Volume 133, Pages 686–701, 2019.

### Conferences

1. A. O. Adelaja, **D.R.E. Ewim**, J. Dirker and J. P. Meyer, Experimental investigation on pressure drop and friction factor in tubes at different inclination angles during the condensation of R134a. *Proceedings of the 15th International Heat Transfer Conference, IHTC-15*. 10 – 15 August 2014, Kyoto, Japan.
2. **D.R.E. Ewim** and J.P. Meyer, Condensation heat transfer coefficients of enhanced tubes. *Proceedings of the 3rd Southern African Solar Energy Conference, SASEC-2015*. 11 – 13 May 2015, Kruger National Park, South Africa.
3. **D.R.E. Ewim**, R. Kombo and J.P. Meyer. Flow pattern and experimental investigation of heat transfer coefficients during the condensation of R134a at low mass fluxes in a smooth horizontal tube. *Proceedings of the 11th Heat Transfer, Thermodynamics and Fluid Mechanics Conference, HEFAT- 2016*. 11 – 14 July 2016, Costa del Sol, Spain.
4. **D.R.E. Ewim** and J.P. Meyer. Experimental investigation of condensation heat transfer coefficients in an inclined smooth tube at low mass fluxes. *Proceedings of the 16th International Heat Transfer Conference, IHTC-16*, 10 – 15 August 2018, Beijing, China.

An additional article, which was prepared during the preparation and completion of this thesis:

1. **D.R.E. Ewim**, M. Mehrabi and J.P. Meyer, Modelling of heat transfer coefficients during condensation at low mass fluxes inside smooth horizontal and inclined tubes. Submitted to *Heat Transfer Engineering* on 11 April 2019.

## Dedication

---

This thesis is dedicated to God Almighty, *Deus Scientiarum*.

## Acknowledgements

---

I will like to thank the following for their contributions to the success and completion of my PhD programme.

- My study leader and supervisor – Professor JP Meyer, who funded my PhD. He also supported and motivated me throughout this learning process. His enthusiasm and passion for the thermal sciences is indeed contagious, and his desire to see his students succeed kept me going throughout this long journey. His critical review of my papers significantly enhanced my writing skills. I owe him deep and sincere appreciation because without his guidance and mentorship, the body of this work would not have been possible.
- The Federal Government of Nigeria through the Nigeria Atomic Energy Commission for granting my study leave to pursue my “*PhD dream*”.
- The members of the Clean Energy Research Group have been an incredible support structure, both as friends, colleagues and as technical advisors. While I have benefited greatly from the advice of almost every member of the group, I would like to specially mention Mr Danie Gouws, Mr Charles Moon and Mr Koos Mthombeni for their massive technical support with the building, commissioning and testing of the experimental set-up.
- Sincere appreciation also goes to the departmental administrative officers – Ms Tersia Evans, Ms Ilka Meyer and Ms Elzabe Pieterse for their assistance, guidance and support.
- I am grateful to my loving fiancée, Zama, and my beautiful daughter, Chizitelu for their unconditional love and support. They stood by me during this process. I could never have done this without them.
- Special mention to my parents – Mr Innocent Ewim and Mrs Josephine Ewim for raising me up and for their prayers, motivation and support. I could never have done this without them and I am eternally indebted to them.

- To my siblings — Chioma Ann Udeh, Nkeiru Ewim, Chikezie Ewim and Chinedu Ewim. They supported and prayed for me throughout this long journey. I am nothing without them!!
- To my in-laws — Mr and Mrs JI Mhlongo, Asanele Mhlongo, Njabulo Mhlongo and Nolwazi Shezi. I am grateful for their love and support.
- To my friends and mentors — Dr AO Adelaja, Dr OA Jejeniwa, Barr (Dr) AC Onuora-Oguno, Mrs Blessing Onuora-Oguno, Engr UU Oteh, Emmanuel Owoicho Ijiga, Dr OT Olakoyejo, Dr OO Adewumi, Dr AC Eloka-Eboka, Victoria Eloka-Eboka, Nsisong Eyo-Udo, Engr Nwakamma Ninduwezuor-Ehiobu, Odinaka and Zama Nwokediegwu, Dr Victor Alumona, Nkemefuni Ninduwezuor-Ehiobu, Abiodun Ayodeji, Wonderful Modo Ndlovu, Errol Pilusa, Stanislaus Nnadih, Barr Godwin and Chioma Odo, Muhtahir Oloyede, Ntswalo Mabuza, Nike Adelakun, Tolulope Babawarun, Chulumanco Giyose, Dr AG Dosunmu, Michael Odeyemi, Barr (Dr) Anwuli Ofuani-Sokolo, Abubakar Idris Bashir, Godfrey and Lora Akpakwu, Stephen Oyewobi, Dr and Mrs Ayo Imoru, Chibuike DaraOjimba, Mosella Rasutha, Rev Fr Sunday Ikpe, Sogo and Laide Abolarin, Uche Izuka, Francis Effah, Nyeleti Fortunate Mashaba, Mr & Mrs Udochukwu Nwankwo, Mr & Mrs Francis Ijiga, Boniswa Muthaphuli, Rev Fr Hubert Obaedo, Rev Fr Chidi Iyiegbu, Rev Fr Samuel Alabi, Rev Fr Manuel Graca, Rev Fr Fidelis Alabi, Raymond Kene, Rainah Kombo, Gerard Muteba Kandindi, Abiodun Aasa, Prince Obinna Nwawuike, Dr Eucharia Igbafe, Dr Suvanjan Bhattacharyya, Dr IF Okafor, Dr Saheed Adio, The DaraOjimbass', The Ibehs', Ngbede Junior Awodi, and my other colleagues at the Nigeria Atomic Energy Commission. I thank them most sincerely for their encouraging words, love and support.
- Above all, I give honour, praise and sincere thanks to my Lord and Saviour Jesus Christ — it is He who provided me with enduring strength, perseverance and grace. I love you, Lord!!



# Table of Contents

---

Abstract.....	i
Publications.....	iii
Dedication.....	v
Acknowledgements.....	vi
List of Figures.....	xiii
List of Tables.....	xvi
Nomenclature.....	xvii
Chapter 1: Introduction.....	1
1.1. Background to the study.....	1
1.2. Problem statement.....	3
1.3. Aim.....	4
1.4. Objectives.....	5
1.5. Original outcomes.....	5
1.6. The scope of the study.....	7
1.7. Overview of the thesis.....	7
Chapter 2: Literature Review.....	8
2.1. Introduction.....	8
2.2. Fundamentals of condensation.....	8
2.3. Modes of condensation.....	8
2.4. Two-phase flow terminology.....	8
2.4.1. Vapour quality.....	9
2.4.2. Void fraction.....	9
2.4.3. Mass flux.....	9
2.5. Dimensionless parameters.....	9
2.5.1. Dimensionless vapour velocity.....	10
2.5.2. Reynolds number.....	10
2.5.3. Prandtl number.....	10
2.5.4. Lockhart- Martinelli parameter.....	10
2.5.5. Jakob number.....	11
2.5.6. Nusselt number.....	11
2.5.7. Liquid Froude number.....	11
2.6. Flow regimes.....	11

2.6.1.	Annular flow regimes.....	12
2.6.2.	Intermittent flow regimes.....	12
2.6.3.	Stratified flow regimes.....	12
2.6.4.	Stratified wavy flow.....	13
2.6.5.	Bubbly flow.....	13
2.6.6.	Churn flow regimes.....	13
2.7.	Flow regime maps.....	14
2.8.	First generation correlations of heat transfer during in tube condensation.....	15
2.8.1.	Correlation of Chato.....	17
2.8.2.	Correlation of Jaster and Kosky.....	17
2.8.3.	Correlation of Shah.....	17
2.8.4.	Correlation of Akers <i>et al.</i> .....	18
2.8.5.	Correlation of Moser <i>et al.</i> .....	18
2.9.	Review of state of the art of condensation heat transfer coefficient correlations.....	18
2.9.1.	Correlation of Dobson and Chato.....	18
2.9.2.	Correlation of Thome <i>et al.</i> .....	19
2.9.3.	Correlation of Cavallini <i>et al.</i> .....	20
2.9.4.	Correlation of Shah.....	20
2.10.	Condensation in smooth horizontal tubes.....	20
2.10.1.	Initial works.....	20
2.10.2.	Low mass fluxes (horizontal tubes).....	21
2.10.2.1.	Work of Aprea <i>et al.</i> .....	22
2.10.2.2.	Work of Suliman <i>et al.</i> .....	22
2.10.2.3.	Work of Lee and Son.....	22
2.10.2.4.	Work of Azzolin <i>et al.</i> .....	22
2.11.	Condensation in smooth inclined tubes.....	23
2.11.1.	Work of Tepe and Muller.....	23
2.11.2.	Work of Chato.....	24
2.11.3.	Work of Nitheanandan and Soliman.....	24
2.11.4.	Work of Meyer and co-workers.....	24
2.11.5.	Work of Mohseni and co-workers.....	25
2.11.6.	Work of Xing <i>et al.</i> .....	26
2.11.7.	Low mass fluxes (inclined tubes).....	26
2.11.8.	Work of Davies <i>et al.</i> .....	26
2.11.9.	Work of Lyulin <i>et al.</i> .....	27
2.11.10.	Work of Arslan and Eskin.....	27

2.12.	Physics of pressure drop.....	28
2.13.	Pressure drop in horizontal tubes .....	29
2.14.	Pressure drop in inclined tubes.....	31
2.15.	Summary and conclusion .....	34
Chapter 3: Experimental Set-Up.....		35
3.1.	Introduction .....	35
3.2.	Experimental apparatus and procedure .....	35
3.3.	Data reduction .....	43
3.4.	Uncertainty analysis and repeatability .....	48
3.5.	Test matrix for smooth tubes.....	49
3.6.	Test matrix for inclined tubes.....	49
3.7.	Summary and conclusion .....	51
Chapter 4: Validation.....		53
4.1.	Introduction .....	53
4.2.	Validation of heat transfer coefficients in horizontal tubes .....	53
4.3.	Validation of flow pattern in horizontal tubes.....	54
4.4.	Validation of heat transfer coefficients in inclined tubes.....	55
4.5.	Validation of pressure drop results.....	56
4.6.	Summary and conclusion .....	57
Chapter 5: Heat Transfer Coefficients in Smooth Tubes .....		58
5.1.	Introduction .....	58
5.2.	Flow patterns .....	58
5.3.	Heat transfer coefficients .....	63
5.4.	Comparison with literature.....	67
5.5.	Revised theoretical model .....	68
5.6.	Summary and conclusion .....	71
Chapter 6: Heat Transfer Coefficients in Inclined Tubes .....		73
6.1.	Introduction .....	73
6.2.	Flow patterns .....	73
6.3.	Heat transfer coefficients .....	76
6.4.	Summary and conclusion .....	84
Chapter 7: Pressure Drops in Smooth and Inclined Tubes .....		86
7.1.	Introduction.....	86

7.2.	Flow pattern visualisation results .....	86
7.3.	Measured pressure drops .....	86
7.3.1.	Effect of inclination angles .....	86
7.3.2.	Effect of temperature differences .....	88
7.3.3.	Effect of mass flux and vapour quality .....	90
7.4.	Frictional pressure drops .....	91
7.4.1.	Effect of inclination angles .....	91
7.4.2.	Effect of temperature differences .....	94
7.4.3.	Effect of vapour qualities .....	94
7.4.4.	Effect of mass fluxes .....	94
7.5.	Summary and conclusion .....	96
Chapter 8: Summary, Conclusions and Recommendations .....		98
8.1.	Summary .....	98
8.2.	Conclusions .....	99
8.3.	Recommendations .....	101
References .....		102
Appendix A: Experimental Uncertainty Analysis .....		122
A.1.	Introduction .....	122
A.2.	General uncertainty analysis procedures .....	122
A.3.	Temperature measurement uncertainties .....	123
A.4.	Wall temperature uncertainty .....	124
A.5.	Temperature difference uncertainty .....	125
A.6.	Refrigerant mass flow rate uncertainty .....	125
A.7.	Mass flux uncertainty .....	125
A.8.	Water mass flow rates uncertainty .....	126
A.9.	Pressure measurement uncertainty .....	126
A.10.	REFPROP uncertainty analysis .....	126
A.11.	Uncertainty in the measurement of condenser length .....	127
A.12.	Uncertainty in the measurement of tube diameter .....	127
A.13.	Uncertainty in the thermal conductivity of the copper tubes .....	127
A.14.	Uncertainty in the measurement of surface area .....	128
A.15.	Uncertainty in the wall thermal resistance .....	128
A.16.	Refrigerant side heat balance uncertainty .....	129
A.17.	Waterside heat balance uncertainty .....	129

A.18.	Inlet and outlet vapour quality uncertainty .....	130
A.18.1.	Inlet vapour quality uncertainty .....	130
A.18.2.	Outlet vapour quality uncertainty .....	131
A.18.3.	Average test vapour quality uncertainty .....	132
A.19.	Inner wall temperature uncertainty .....	132
A.20.	Heat transfer coefficient uncertainty analysis .....	132
A.21.	Pressure drop uncertainty analysis .....	133
A.21.1.	Measured pressure drop uncertainty .....	133

## List of Figures

---

Fig. 2.1: Flow regimes for high-velocity flow (adapted from Palen <i>et al.</i> [182]).....	12
Fig. 2.2: Flow regimes for low-velocity flow (adapted from Palen <i>et al.</i> [182]).....	13
Fig. 2.3: Improved flow pattern map (adapted from Suliman <i>et al.</i> [81]).....	16
Fig. 3.1: Schematic of the experimental set-up and test section (horizontal tube). ....	36
Fig. 3.2: Schematic of the experimental set-up and test section (inclined tube).....	38
Fig. 3.3: Schematic of the measurement points in the test section. ....	40
Fig. 4.1: Validation results of experimental heat transfer coefficients as functions of quality at a mass flux of 300 kg/m <sup>2</sup> s compared to experimental data at a saturation temperature of 40 °C. ...	54
Fig. 4.2: General description of flow patterns found at mass fluxes of 50, 75, and 100 kg/m <sup>2</sup> s (horizontal flow). ....	55
Fig. 4.3: Validation results of experimental heat transfer coefficients as a function of inclination angle at a mass flux of 300 kg/m <sup>2</sup> s and mean vapour quality of 0.5.....	56
Fig. 5.1: Flow regimes at different temperature differences and vapour qualities at a mass flux of 100 kg/m <sup>2</sup> s. ....	60
Fig. 5.2: Flow regimes at different temperature differences and vapour qualities at a mass flux of 75 kg/m <sup>2</sup> s. ....	61
Fig. 5.3: Flow regimes at different temperature differences and vapour qualities at a mass flux of 50 kg/m <sup>2</sup> s ....	62
Fig. 5.4: Verification experimental data points generated in this study plotted on the El Hajal <i>et al.</i> [97] map. ....	63
Fig. 5.5: Heat transfer coefficients as a function of different wall and refrigerant saturation temperature differences, $\Delta T$ , at different mean qualities during condensation at a mass flux of 200 kg/m <sup>2</sup> s. ....	64
Fig. 5.6: Heat transfer coefficients as a function of different wall and refrigerant saturation temperature differences, $\Delta T$ , at different mean qualities during condensation at a mass flux of 150 kg/m <sup>2</sup> s. ....	65
Fig. 5.7: Heat transfer coefficients as a function of different wall and refrigerant saturation temperature differences, $\Delta T$ , at different mean qualities during condensation at a mass flux of 100 kg/m <sup>2</sup> s. ....	65
Fig. 5.8: Heat transfer coefficients as functions of different wall and refrigerant temperature differences, $\Delta T$ , at different mean qualities during condensation at a mass flux of 75 kg/m <sup>2</sup> s. ....	66
Fig. 5.9: Heat transfer coefficients as functions of different wall and refrigerant temperature differences, $\Delta T$ , at different mean qualities during condensation at a mass flux of 50 kg/m <sup>2</sup> s. ....	66
Fig. 5.10: Comparison of experimental data with several theoretical models from literature. ....	67

Fig. 5.11: Measured heat transfer coefficients compared to the Cavallini <i>et al.</i> [48] equation as functions of mass flux using the original values of $T_1$ and $T_2$ , i.e., 0.25 and 0.087, respectively as proposed by Cavallini <i>et al.</i> [48].....	70
Fig. 5.12: Measured heat transfer coefficients compared to the modified Cavallini <i>et al.</i> [48] using the revised values of $T_1$ and $T_2$ , i.e., 0.245 and 0.25, respectively, (which take into consideration the temperature differences at low mass fluxes) as suggested.....	71
Fig. 6.1: Description of flow patterns found in the study. ....	74
Fig. 6.2: Flow regimes at different temperature differences for a vapour quality of 0.5 at a mass flux of $G = 100 \text{ kg/m}^2\text{s}$ .....	74
Fig. 6.3: Flow regimes at different temperature differences for a vapour quality of 0.25 at a mass flux of $G = 50 \text{ kg/m}^2\text{s}$ .....	75
Fig. 6.4: Condensation heat transfer coefficients, $\alpha$ , as a function of inclination angle, $\beta$ , at different wall and refrigerant temperature differences, $\Delta T$ , at a mean quality of 0.25 during condensation: (a) Mass flux of $100 \text{ kg/m}^2\text{s}$ , (b) mass flux of $75 \text{ kg/m}^2\text{s}$ , and (c) mass flux of $50 \text{ kg/m}^2\text{s}$ . ....	77
Fig. 6.5: Condensation heat transfer coefficients, $\alpha$ , as a function of inclination angle, $\beta$ , at different wall and refrigerant temperature differences, $\Delta T$ , at a mean quality of 0.50 during condensation: (a) Mass flux of $100 \text{ kg/m}^2\text{s}$ , (b) mass flux of $75 \text{ kg/m}^2\text{s}$ , and (c) mass flux of $50 \text{ kg/m}^2\text{s}$ . ....	80
Fig. 6.6: Condensation heat transfer coefficients, $\alpha$ , as a function of inclination angle, $\beta$ , at different wall and refrigerant temperature differences, $\Delta T$ , at a mean quality of 0.75 during condensation: (a) Mass flux of $100 \text{ kg/m}^2\text{s}$ , (b) mass flux of $75 \text{ kg/m}^2\text{s}$ , and (c) mass flux of $50 \text{ kg/m}^2\text{s}$ . ....	81
Fig. 6.7: Condensing heat transfer coefficients as a function of temperature differences, $\Delta T$ , and different inclination angles, $\beta$ , at a mean quality of 0.50: (a) Mass flux of $100 \text{ kg/m}^2\text{s}$ and (b) mass flux of $50 \text{ kg/m}^2\text{s}$ .....	83
Fig. 6.8: Inclination effect as a function of temperature differences, $\Delta T$ , at different mass fluxes during condensation: (a) Vapour quality of 0.25 and (b) Vapour quality of 0.50. ....	84
Fig. 7.1: Measured pressure drop, $\Delta P_{meas}$ as a function of inclination angle, $\beta$ , at different wall and refrigerant temperature differences, $\Delta T$ , at a mass flux of $100 \text{ kg/m}^2\text{s}$ during condensation: (a) at a mean quality of 0.25, (b) at a mean quality of 0.50 and (c) at a mean quality of 0.62. ....	87
Fig. 7.2: Measured pressure drop, $\Delta P_{meas}$ as a function of inclination angle, $\beta$ , at different wall and refrigerant temperature differences, $\Delta T$ , at a mass flux of $75 \text{ kg/m}^2\text{s}$ during condensation: (a) at a mean quality of 0.25, (b) at a mean quality of 0.50 and (c) at a mean quality of 0.62. ....	89
Fig. 7.3: Measured pressure drop, $\Delta P_{meas}$ as a function of inclination angle, $\beta$ , at different wall and refrigerant temperature differences, $\Delta T$ , at a mass flux of $50 \text{ kg/m}^2\text{s}$ during condensation: (a) at a mean quality of 0.25, (b) at a mean quality of 0.50 and (c) at a mean quality of 0.62. ....	90

Fig. 7.4: Frictional pressure drop,  $\Delta P_{fri}$  as a function of inclination angle,  $\beta$ , at different wall and refrigerant temperature differences,  $\Delta T$ , at a mass flux of 100 kg/m<sup>2</sup>s during condensation: (a) at a mean quality of 0.25, (b) at a mean quality of 0.50 and (c) at a mean quality of 0.62. .... 92

Fig. 7.5: Frictional pressure drop,  $\Delta P_{fri}$  as a function of inclination angle,  $\beta$ , at different wall and refrigerant temperature differences,  $\Delta T$ , at a mass flux of 75 kg/m<sup>2</sup>s during condensation: (a) at a mean quality of 0.25, (b) at a mean quality of 0.50 and (c) at a mean quality of 0.62. .... 93

Fig. 7.6: Frictional pressure drop,  $\Delta P_{fri}$  as a function of inclination angle,  $\beta$ , at different wall and refrigerant temperature differences,  $\Delta T$ , at a mass flux of 50 kg/m<sup>2</sup>s during condensation: (a) at a mean quality of 0.25, (b) at a mean quality of 0.50 and (c) at a mean quality of 0.62. .... 95



## List of Tables

---

Table 2.1: Pure vapour condensation inside smooth tubes: First generation heat transfer models...	19
Table 3.1: Operating conditions and average energy balances for the experimental matrix.....	41
Table 3.2: Equipment used by LabVIEW in the experimental test rig.....	42
Table 3.3: Experimental parameters, ranges, and uncertainties.....	48
Table 3.4: Summary of experimental test points for smooth tubes.....	50
Table 3.5: Summary of experimental test points for inclined tubes.....	51
Table 4.1: Summary of validation heat transfer coefficient experiments conducted at different qualities.....	53
Table 4.2: Summary of validation test points.....	56

# Nomenclature

---

$A$	area (m <sup>2</sup> )
$C$	constant
$C_p$	constant pressure specific heat (J/kgK)
$d$	diameter (mm)
$EB$	energy balance (%)
$f$	function
$F_I$	Fixed error
$Fr$	Froude number
$g$	gravitational acceleration (m/s <sup>2</sup> )
$G$	mass flux (kg/m <sup>2</sup> s)
$h$	specific enthalpy
$h_{fg}$	specific latent heat of vaporization
$I$	inclination effect
$Ja$	Jakob number
$J_V$	dimensionless gas velocity
$J_V^T$	transition dimensionless gas velocity
$k$	thermal conductivity (W/mK)
$L$	length of the test section (m)
$L_{\Delta P}$	distance between pressure taps (m)
$\Phi_v$	two-phase multiplier for Lockhart-Martinelli parameter
$Nu$	Nusselt number
$\dot{m}$	mass flow rate (kg/s)
$n$	Akers index, number of thermocouples
$P$	pressure (Pa)
$P_I$	Precision error
$\Delta P$	pressure drop (Pa)
$Pr$	Prandtl number
$\dot{q}$	heat flux (W/m <sup>2</sup> )
$\dot{Q}$	heat transfer rate (W)
$R$	thermal resistance (K/W)
$Re$	Reynolds number
$T$	temperature (°C)
$\bar{T}$	average wall temperature (°C)

$\Delta T$	temperature difference (°C)
$V$	velocity (m/s)
$We$	Weber number
$x$	vapour quality
$X_1,$	experimental variable
$X_{tt}$	Lockhart–Martinelli parameter
$Z$	experimental quantity
$z$	axial direction

### Greek symbols

$\alpha$	heat transfer coefficient (W/m <sup>2</sup> K)
$\beta$	inclination angle (>0: upward, <0 downward) (deg)
$\delta$	uncertainty
$\varepsilon$	void fraction
$\mu$	dynamic viscosity (kg/ms)
$\rho$	density (kg/m <sup>3</sup> )
$\sigma$	surface tension (N/m)
$\sigma$	standard deviation

### Subscripts

$A$	$\Delta T$ independent annular flow regime
$avg$	average
$cond$	conduction
$conv$	convection
$crit$	critical
$Cu$	copper
$cs$	cross section
$D$	$\Delta T$ dependent flow regime/total heat transfer coefficient
$e$	equivalent
$fri$	frictional
$h$	hydraulic
$i$	inner
$in$	inlet
$ind$	indicated
$j$	measurement location
$l$	liquid

<i>line</i>	lines between pressure taps and transducer
<i>lo</i>	liquid phase with total flow
<i>m</i>	mean
<i>max</i>	maximum
<i>meas</i>	measurement
<i>min</i>	minimum
<i>mom</i>	momentum
<i>o</i>	outer
<i>out</i>	outlet
<i>post</i>	post-condenser
<i>pre</i>	pre-condenser
<i>r</i>	refrigerant
<i>red</i>	reduced
<i>rh</i>	Rouhani and Axelsson
<i>s</i>	surface
<i>sat</i>	saturation
<i>stat</i>	static
<i>strat</i>	fully stratified regime, stratified
<i>test</i>	test-condenser
<i>tot</i>	total
<i>tp</i>	two-phase
<i>tr</i>	transducer
<i>v</i>	vapour
<i>w</i>	wall, water

# Chapter 1: Introduction

---

## 1.1. Background to the study

With soaring energy costs and the grave concerns about the environmental impact of some working fluids, efforts are now being stepped up more than ever before to ensure the proper design and optimisation of condensers used in refrigeration and air-conditioning systems, desalination plants, solar systems and power generation plants [1-57].

Heat transfer and pressure drops are perhaps the two most important parameters needed to design and characterise condensers correctly. In general, the aim is to maximize the heat transfer coefficients and minimize the pressure drops through the use of accurate and unified predictive methods. The goal to maximize heat transfer coefficients and minimize pressure drop has led to numerous studies (but not at low mass fluxes below  $200 \text{ kg/m}^2\text{s}$  in smooth horizontal and inclined tubes). Reviews of these works in both macro- and micro-channels are available in [2, 4, 6, 7, 12, 18, 28, 33, 58-93]. The state of the art is that some correlations [76, 90, 94-96] were developed based on flow regimes, and for that reason, new flow regime maps [81, 97] were developed. This is possibly occasioned by the general agreement in the open technical literature that the mechanisms of pressure drop and heat transfer are closely linked to the prevailing flow regime. However, in general, most of the works referred to above were conducted at mass fluxes varying from approximately  $200 - 1\,000 \text{ kg/m}^2\text{s}$ .

Some of these and other studies [7, 11, 33, 72, 77, 79, 83] found that the temperature difference between the wall on which condensation occurs and the saturation temperature (hereafter referred to in this thesis as the “*temperature difference*”) had a negligible influence on the heat transfer coefficients. The results were, in general, dependent on mass flux and vapour quality. The results generated at low mass fluxes were generally secondary data and were not the foci of previous works. Furthermore, Thome [62] pointed out that, as opposed to external condensation, the heat transfer coefficients during in-tube condensation were independent on the temperature difference, except at low mass fluxes. However, there are very limited extensive studies during condensation at low mass fluxes.

Another subject of limited studies is inclination. It is an option when designing condenser tubes that cannot be oriented horizontally or vertically owing to space constraints, operating conditions, performance optimization, or environmental conditions [4, 7, 8, 18, 32, 33, 71, 72, 91, 92, 98-103]. Examples where condensation occurs in inclined tubes, include steam condensers used for air-cooling, specific rooftop industrial air-cooled refrigeration systems, and in the condensers of motor vehicles

and trucks driving up and down hills. However, little work [4, 32] has been published in the open literature which justifies the angles being used or which gives performance data at different inclination angles. This implies that design and engineering know-how on inclination is rather limited.

An example in which the environmental and space conditions are important factors is in dry regions of the world that lack large water resources for power-plant cooling. In such cases, large forced-convection, air-cooled power plant condensers are used. The condensers are normally constructed in an 'A' or 'V' frame configuration with the condensing steam in a downwards flow direction of approximately  $-60^\circ$ . At least three countries (South Africa, Australia, and the U.S.) are currently using this technology increasingly. Some of the largest dry-cooling plants at present are found in South Africa, with an installed capacity of more than 10 GW. The typical water consumption of a dry-cooling plant is approximately 0.1 l of water per kilowatt-hour of electricity produced. In comparison, a traditional wet-cooled plant requires nearly 2 l per kWh. The cross-sectional geometry of the condensing channels of a dry-cooled power plant is finned on the outside. The channels are in many cases flat and rectangular and relatively large with dimensions of approximately 214 mm by 13 mm. The tubes are about 10 m long with steam mass fluxes lower than  $10 \text{ kg/m}^2\text{s}$  [31, 104, 105]. The reasons for these choices of inclination angle and low mass fluxes have not been addressed in the literature.

Previous studies [4, 8, 9, 18, 32, 33, 46, 71, 72, 91, 92, 98-103, 106-123] on inclined tubes were at moderate to high mass fluxes. In those studies, it was found that varying the inclination angles altered the flow patterns with consequent effects on the heat transfer coefficients, pressure drops, and void fractions. It was also found that the effects of inclination became more pronounced as the mass flux decreased. For downwards inclinations, it was found that the effect of the gravity was dominant and caused a thinning of the liquid layer which led to a reduction in the thermal resistance within the tube surface, leading to higher heat transfer coefficients [7, 18, 32, 33, 71, 72, 124]. For upwards inclinations, no concrete trend was established. However, there are two main challenges. The first is that there is no study that has systematically coupled the effect of inclination and temperature difference on the heat transfer coefficients and flow patterns at low mass fluxes ( $\leq 100 \text{ kg/m}^2\text{s}$ ). The other challenge is that there are contradictory reports [32, 72, 99, 100, 102] on the recommended inclination angle for optimum heat transfer performance. This is further evidenced by the fact that there is no unifying correlation that can properly predict the heat transfer coefficients in inclined smooth tubes. This may be attributed to the fact that the available models are either limited by tube size, working fluid, saturation temperature, mass flux, or tube orientation. There is thus a gap in the literature that addresses condensation at different inclination angles as well as condensation at low mass fluxes. A review of the most relevant works on inclination will be presented in the next chapter.

The last subject of limited studies is pressure drops. Pressure drop is particularly crucial in forced convective systems because it is synonymous with pumping or compressor power consumption. In natural (free) convective systems, pressure drop determines the circulation rate; in nuclear power plants, high-pressure steam and water flow as a two-phase mixture within the piping networks and pressure vessels of different sizes and orientations. It is therefore imperative in this case, to predict the pressure drop and void fraction in the heat transport loop of nuclear reactors for safety and design analyses [10, 13, 24, 125]. In general, the pressure drop is intimately linked to the quantity of energy needed to move flow through a two-phase system and is a fundamental parameter in two-phase flow design and modelling.

There have been various experimental studies on pressure drops during condensation inside smooth horizontal tubes [5-7, 10, 12, 13, 17, 18, 20, 24, 27, 28, 35, 37, 40, 46, 126-139]. Most of these studies were conducted at mass fluxes greater than 200 kg/m<sup>2</sup>s and typically reaching up to 1 000 kg/m<sup>2</sup>s. It was found that an increase in vapour quality and mass flux led to an increase in the pressure drop. It was also found that higher pressure drops were recorded at lower saturation temperatures and that low-pressure fluids gave higher pressure drop. However, the effect of temperature difference was never studied. There have also been quantitative studies [3, 19, 26, 134, 140-144] aimed at comparing pressure drop models with the results of empirical studies. Furthermore, various two-phase pressure drop predictive models [14, 16, 21, 22, 25, 41, 57, 141, 145-164] have been developed. The challenge is that these models are at variance with one another. Also, of all the models developed, those of Moreno et al. [21] (developed for evaporation), Chen et al. [165], Garimella [41], Cavallini et al. [154], Quiben et al. [21] and Xiao and Hrnjak [166] were the most prominent derived as a function of the prevailing flow pattern. Other models have either been empirical or analytical and are limited to particular working fluids, tube size, heat fluxes, and mass flow rates. This implies that they are not expected to be very accurate. On the other hand, general frictional pressure drop correlations have been formulated based on either separated or homogeneous flow. However, the separated models are mostly used for two-phase flows. A comprehensive review of the general literature on pressure drop inside smooth tubes is presented in the next chapter.

## **1.2. Problem statement**

It can therefore be concluded from previous studies that insufficient work has been conducted during in tube condensation in horizontal and inclined smooth tubes at low mass fluxes, specifically to determine the heat transfer coefficients, pressure drops and capture the flow regimes as functions of inclination angles, temperature differences and vapour quality.

With respect to horizontal flow, there has been no study that captured the flow patterns and systematically quantified the effect of temperature difference on the heat transfer coefficients during in tube condensation at low mass fluxes. With respect to inclination, there are two primary challenges. The first is that there is no study that has systematically coupled the effect of inclination and temperature difference on the heat transfer coefficients and flow patterns at low mass fluxes ( $\leq 200$  kg/m<sup>2</sup>s). The other challenge is that there are contradictory reports [32, 72, 99, 100, 102] on the recommended inclination angle for optimum heat transfer performance. This is further evidenced by the fact that there is no unifying correlation that can adequately predict the heat transfer coefficients in inclined smooth tubes. This may be attributed to the fact that the available models are either limited by tube size, working fluid, saturation temperature, mass flux, or tube orientation. With respect to pressure drops, it can be concluded from the literature that there is a gap in the open literature during condensation in smooth and inclined tubes at specifically low mass fluxes where the pressure drops may be temperature difference dependent. To the best of our knowledge, there has been no study on the effect of temperature differences (defined in this study as the temperature difference between the saturation temperature and the wall temperature) on pressure drop at low mass fluxes. In fact, there is no single published work on pressure drops in the low mass flux region in smooth and tubes covering the whole range of inclination angles and temperature differences. When evaluating various correlations, it was found they did not agree with another. While the Friedel [16] correlation seems to be the most cited, it was developed for high reduced pressures and high mass fluxes. On the other hand, the correlations of Muller-Steinhagen and Heck [22], Sun and Mishima [147], Chen *et al.* [13], and Grønnerud [146] usually gave the best predictions when compared with various experimental results (at high mass fluxes). It implies that further research needs to be carried out to develop more pressure drop correlations.

To summarise, insufficient comprehensive work has been conducted at mass fluxes lower than 200 kg/m<sup>2</sup>s in horizontal and inclined smooth tubes to specifically characterise low mass fluxes by determining the heat transfer coefficients, pressure drops and capture the flow regimes as a function of inclination angle, vapour quality and temperature difference between the tube wall temperature and condensing temperature.

### **1.3. Aim**

The purpose of this study was to experimentally investigate the heat transfer coefficients and pressure drops and the flow pattern characteristics during the condensation of R134a in horizontal and inclined smooth tubes at low mass fluxes ( $50 \leq G \leq 200$  kg/m<sup>2</sup>s).



## 1.4. Objectives

The main objectives of the study were:

- To modify an experimental set-up that can be used to investigate heat transfer, flow patterns and pressure drops during condensation at low mass fluxes.
- To develop a fundamental understanding of condensation in inclined smooth tubes at low mass fluxes.
- To experimentally determine the heat transfer coefficients in a smooth horizontal tube at low mass fluxes and different vapour qualities
- To investigate the effect of the temperature difference on heat transfer coefficients in smooth and inclined tubes.
- To identify the flow patterns at different mass fluxes, inclination angles, and temperature differences.
- To investigate the effect of the temperature difference on the inclination effect.
- To investigate the effect of flow pattern on the heat transfer and pressure drops at low mass fluxes.
- To examine the effect of the temperature difference on pressure drops in smooth and inclined tubes.
- To investigate the effect of inclination on heat transfer coefficients at low mass fluxes.
- To investigate the effect of inclination on pressure drops at low mass fluxes.
- To investigate the effect of mass flux and mean vapour quality on the pressure drops at different inclination angles.
- To investigate the optimum angle(s) for maximum heat transfer coefficients.
- To compare the experimental data to literature.
- To develop new heat transfer correlations for low mass fluxes.

## 1.5. Original outcomes

The work in this study was published as part of this thesis mainly in three articles. The original contributions of the three articles, with relevant chapters, are as follows:

### **Chapter 5, Meyer and Ewim [52, 167]**

Heat transfer coefficients during the condensation of low mass fluxes in smooth horizontal tubes;

Highlights

- Measured condensing heat transfer coefficients at low mass fluxes in a smooth horizontal tube at different temperature differences.
- The experiments were also conducted at different wall and saturation temperature differences are varying between 1–10 °C.
- The flow patterns were recorded with a high-speed video camera at the inlet and outlet of the test section through sight glasses.
- Results showed that the flow patterns during condensation were predominantly stratified and stratified wavy.
- It was also found that the heat transfer coefficients were dependent on the temperature difference between the temperature of the wall on which condensation occurs and the temperature of the condensing refrigerant.
- Furthermore, it was found that the heat transfer coefficient decreased with an increase in this temperature difference.
- When comparing the results of this study at low mass fluxes to the literature, it was found that the absolute mean deviation varied up to 38%.
- An amendment was suggested in a stratified heat transfer coefficient term from literature. It has been found that, with this amendment, the heat transfer coefficients of low mass fluxes could be estimated with errors of  $\pm 5\%$ .

### **Chapter 6, Ewim, Meyer and Noori Rahim Abadi [54]**

Condensation heat transfer coefficients in an inclined smooth tube at low mass fluxes

#### Highlights

- Measured heat transfer coefficients during condensation at low mass fluxes.
- Inclination angle effects on heat transfer coefficients.
- Temperature difference effects on heat transfer coefficients in inclined tubes.
- Optimum angle and temperature difference effects at low mass fluxes.
- Heat transfer coefficients were more sensitive to temperature difference for downward flow.

### **Chapter 7, Ewim and Meyer [168]**

Pressure drop during the condensation at low mass fluxes in smooth horizontal and inclined tubes.

#### Highlights

- Experimental pressure drops at low mass fluxes during condensation.
- Pressure drops at different inclination angles and temperature differences.

- Pressure drops increased as temperature and inclination angles increased.
- Frictional pressure drops are maximum during downward flows.
- Frictional pressure drops increased with mass flux and vapour quality.

## **1.6. The scope of the study**

As the aim of this study was to investigate flow patterns, heat transfer and pressure drop during in tube condensation at low mass fluxes ( $50 \text{ kg/m}^2\text{s} - 200 \text{ kg/m}^2\text{s}$ ), a test section with an inner diameter of 8.38 mm and a length of 1.49 m was used. The fluid used to conduct the experiments in this study was limited to R134a. The test sections were designed and built while the set-up was modified to cater for the low mass flux requirements. Local experiments were conducted with R134a at an average condensation temperature of  $40 \text{ }^\circ\text{C}$ , various mean vapour qualities ( $0.1 \leq x_m \leq 0.9$ ), inclination angles ( $-90^\circ \leq \beta \leq +90^\circ$ ) and mass fluxes with a particular focus on low mass flux range (below  $200 \text{ kg/m}^2\text{s}$ ). The flow regime at the inlet and outlet of the test condenser was visualised by two high-speed cameras.

## **1.7. Overview of the thesis**

In the next chapter, a state of the art review is presented with emphasis on work done at low mass fluxes. In Chapter 3, the experimental layout used is described and discussed. In the same chapter, an exhaustive discussion on the instrumentation, data acquisition and data reduction (deduction) is presented. Chapter 4 is dedicated to the validation of the experimental set-up. Chapter 5 [52, 167] covers the experimental heat transfer results and discussion as well as results of the flow visualization results in smooth tubes. A revised heat transfer model is also suggested in this chapter. Chapter 6 [54] covers the experimental heat transfer results and discussion as well as results of the flow visualization results in inclined tubes. Chapter 7 [168] includes the pressure drop results and analysis. The final chapter will focus on the summary, conclusion and recommendations for further studies. There will also be Appendix A which will cover the full details of the experimental uncertainties.

## Chapter 2: Literature Review

---

### 2.1. Introduction

The objective of this chapter is to give a state of the art review on condensation in smooth and inclined tubes with particular emphasis on low mass fluxes. The fundamentals of condensation will be briefly discussed. A quick overview of basic two-phase flow dimensionless parameters will be presented. This will be followed by a review of heat transfer correlations. Next up will be a description of flow regimes and flow regime maps. This chapter will finally be capped up by the most relevant experimental investigations during condensation inside horizontal and inclined smooth tubes with a view to identifying the gaps in the literature.

### 2.2. Fundamentals of condensation

Condensation is the change of the physical state of matter from the vapour phase into the liquid phase and is the reverse of evaporation. Heat transfer to a surface occurs by condensation when the surface temperature is less than the saturation temperature of an adjoining vapour. It normally occurs when a vapour is in contact with a subcooled liquid [90, 164, 165].

### 2.3. Modes of condensation

The two distinct forms of condensation are film condensation and dropwise condensation. In the former, the condensate wets the surface, forming a liquid film which falls under the effect of gravity. The thickness of this film increases in the direction of flow as more vapour condenses on the film while in the latter, the condensed vapour forms droplets on the surface instead of continuous films and the surface are covered with a countless number of droplets of varying diameter. In the industry, dropwise condensation is preferred to film condensation because most of the tube surface remains uncovered by liquid, so there is little heat transfer resistance and very high heat transfer rates whereas in film condensation, the liquid film serves as a resistance to heat transfer. In both cases, nucleation is typically the rate-limiting step, rather than heat transfer. Most industrial applications are based on film mechanisms because it is tricky and expensive to build non-wetting surfaces.

### 2.4. Two-phase flow terminology

It is important to discuss the most basic terminologies that appear in a majority of the heat transfer and pressure drop correlations.

### 2.4.1. Vapour quality

Vapour quality ( $x$ ) is the mass fraction in a saturated mixture that contains vapour. It is an intensive property of a two-phase flow system. It is particularly crucial because flow patterns are vapour quality and mass flux dependent.

Mathematically, it can be written as

$$x = \frac{\dot{m}_v}{\dot{m}_l + \dot{m}_v} \quad (2.1)$$

### 2.4.2. Void fraction

Void fraction ( $\varepsilon$ ) is a critical parameter in the design of condensers and heat exchangers in general. It is an important factor in determining pressure drop, flow patterns, two-phase specific volume and viscosity. It helps in the determination of the refrigerant charge. It can be defined as the ratio of the geometric area occupied by the vapour to the total area of flow.

Mathematically,

$$\varepsilon = \frac{A_v}{A_l + A_v} \quad (2.2)$$

Many void fraction models have been developed for condensation in smooth and inclined tubes and to summarize, the void fraction correlations available can be grouped into four categories namely: homogeneous, slip-ratio, drift-flux and empirical correlations wherein the drift-flux models have been found to give the best predictions relative to experimental data. Of particular importance is the Rouhani and Axelsson [169, 170] drift flux model which was used for friction pressure drop prediction in this study.

### 2.4.3. Mass flux

The mass flux or velocity ( $G$ ) is defined as the ratio of the mass flow rate and the cross-sectional area of the flow channel expressed as:

$$G = \frac{\dot{m}}{A_{cs}} \quad (2.3)$$

Considering the continuity equation, the mass flux (velocity) is the expression of the mean flow velocity multiplied by the mean density of the fluid.

## 2.5. Dimensionless parameters

It is important to discuss the dimensionless parameters as they relate to flow regime maps and flow regime transitions. Some correlations [94, 95] use these dimensionless parameters because they are useful in determining flow regime transitions. Furthermore, several researchers [171-177] have studied

condensation in macro-sized tubes and have attempted to give the transition criteria from one flow regime to another using dimensionless parameters. The section below discusses the most important dimensionless parameters relevant to this study.

### 2.5.1. Dimensionless vapour velocity

It is defined as:

$$J_v = \frac{xG}{[gd_i\rho_v(\rho_l - \rho_v)]^{0.5}} \quad (2.4)$$

Transition criteria in condensation flows are often determined by the dimensionless vapour velocity and the Lockhart Martinelli parameter for the turbulent- turbulent flow ( $X_{tt}$ ). In 1980, Breber *et al.* [172] used the dimensionless vapour mass flux ( $J_v$ ) in the prediction of horizontal tube-side condensation of pure components using flow regime criteria. It has often been used by other researchers in determining flow regimes during the condensation of vapour inside a smooth horizontal tube or in the prediction of flow pattern and flow patterns transitions [174, 175, 178].

### 2.5.2. Reynolds number

Named after Osborne Reynold, it is arguably the most critical dimensionless number in fluid mechanics and the thermal sciences. It is defined as the ratio of inertia to viscous forces. It is mostly used to determine whether the flow is laminar or turbulent. Mathematically, it is written as:

$$Re = \frac{\rho V d}{\mu} \quad (2.5)$$

### 2.5.3. Prandtl number

The Prandtl number ( $Pr$ ) represents a measure of the rate of momentum diffusion against the rate of thermal diffusion. The Prandtl number contains no such length scale in its definition and is dependent only on the fluid and the state of the fluid. As a result, the Prandtl number is often found in property tables alongside other properties like viscosity and thermal conductivity. It is used to characterize heat transfer in fluids and is independent of the behaviour of flow. Mathematically, it is written as:

$$Pr = \frac{\mu C_p}{k} \quad (2.6)$$

### 2.5.4. Lockhart- Martinelli parameter

Developed by Lockhart-Martinelli [179], it is defined as the ratio between the theoretical pressure gradients which would occur if either fluid were flowing alone in the pipe with the original flow rate of each phase. In other words, it is the ratio of the two-phase flow frictional pressure gradient to some reference single-phase flow frictional pressure gradient, usually based on one of the components

flowing by itself. The two most common mathematical relationships of this parameter are given in Eqs. 2.7 and 2.8.

$$X_{tt} = \left(\frac{1-x}{x}\right)^{0.9} \left(\frac{\rho_v}{\rho_l}\right)^{0.5} \left(\frac{\mu_l}{\mu_v}\right)^{0.1} \quad (2.7)$$

$$X_{tt} = \frac{\dot{m}_l}{\dot{m}_v} \sqrt{\frac{\rho_v}{\rho_l}} \quad (2.8)$$

### 2.5.5. Jakob number

Named after Max Jacob in recognition of his early work on phase change. It is the ratio of sensible heat to latent heat released during a phase change process and given as:

$$Ja = \frac{C_p(T_{sat} - T_w)}{h_{fg}} \quad (2.9)$$

### 2.5.6. Nusselt number

When a fluid is in motion, heat transfer through the fluid layer is by convection. On the other hand, heat transfer is transferred by conduction when the fluid layer is stationary. The Nusselt number defines the ratio of the convection heat transfer to conduction heat transfer, and therefore represents the enhancement of heat transfer through a fluid due to the fluid motion. Hence for 100% conduction heat transfer, the Nusselt number is unity. The Nusselt number is named after the great German Physicist cum Engineer Wilhelm Nusselt, who made significant contributions to study of convective heat transfer [180, 181]. The Nusselt number for a circular cross-section is defined as follows:

$$Nu = \frac{\dot{q}_{conv}}{\dot{q}_{cond}} = \frac{hd}{k} \quad (2.10)$$

### 2.5.7. Liquid Froude number

The Froude number represents the ratio of the inertial force to the gravitational force. The general expression is:

$$Fr = \frac{V^2}{gd} \quad (2.11)$$

## 2.6. Flow regimes

A particular type of geometric distribution of the components of flow is referred to as a flow pattern or flow regime. For this study, five different flow regimes namely annular, intermittent, stratified, stratified wavy, bubbly, and churn flow regimes will be discussed. Fig 2.1 depicts the flow regimes for high mass flow rates while Fig 2.2 depicts the flow regimes for low mass flow rates. The detection method for flow regimes are well described by Rouhani and Sohal [177] and can be either by

visualization, X-ray and statistical analysis of fluctuations in measured pressures or void fraction which yield probability density and power spectral density functions.

### 2.6.1. Annular flow regimes

In annular flow, the dominant force is the vapour shear force and this flow regime typically occurs at high mass fluxes and high qualities. Here, the core (centre) of the tube is filled with vapour and the perimeter with the thin liquid film due to the great difference between shear and gravity forces wherein the shear force is much greater than the gravity force causing the expulsion of the liquid to the perimeter of the tube. This flow regime is stable and is the predominant flow regime for most practical applications.

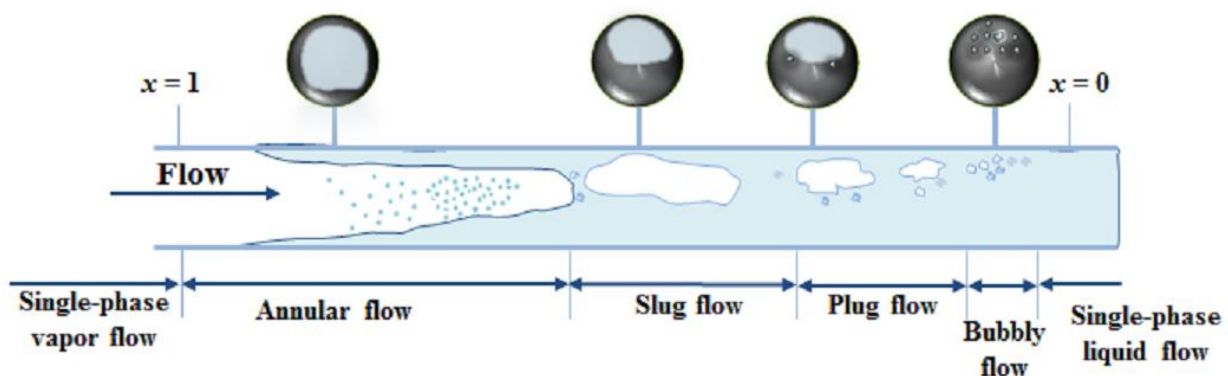


Fig. 2.1: Flow regimes for high-velocity flow (adapted from Palen *et al.* [182]).

### 2.6.2. Intermittent flow regimes

In this regime, both liquid plugs and vapour slugs can be noticed. This can also be referred to as the probabilistic flow regime. For slug flows, it occurs at high flow rates and low qualities and the diameters of elongated bubbles become similar in size to the channel height. The liquid slugs separating such elongated bubbles can also be described as large amplitude waves. Slug flow consists of a long bubble that moves between the liquid slugs and some dispersed bubbles following behind this bubble. They are formed as a result of the growth in the amplitude of the interfacial waves that blocks the cross-section of the tube at certain sections along the tube. The slugs are typically formed by the liquid condensate flowing down the tube. Plug flow regime has liquid plugs that are separated by elongated gas bubbles. The diameters of the elongated bubbles are smaller than the tube such that the liquid phase is continuous along the bottom of the tube below the elongated bubbles. Plug flow is also sometimes referred to as elongated bubble flow.

### 2.6.3. Stratified flow regimes

Also known as gravity controlled flow regime, stratified flows typically occur at low mass fluxes and quality. Here, top of the tube is wetted by the condensate film and the bottom of the tube is wetted by



thick liquid condensate, the distribution and separation of the two phases by an undisturbed horizontal interface are due to density difference and gravity. This flow regime can either be stratified smooth or stratified wavy flow.

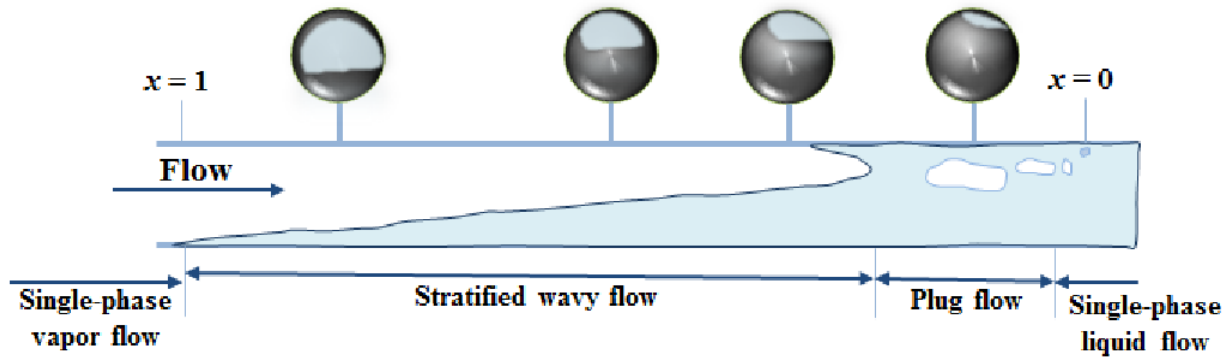


Fig. 2.2: Flow regimes for low-velocity flow (adapted from Palen *et al.* [182]).

#### 2.6.4. Stratified wavy flow

Increasing gas velocity in stratified flow results in the formation of surface waves on the gas-liquid interface giving the stratified wavy flow regime. The amplitude of the waves is notable and depends on the relative velocity of the two phases; however, their crests do not reach the top of the tube. The waves climb up the sides of the tube, leaving thin films of liquid on the wall after the passage of the wave.

#### 2.6.5. Bubbly flow

This flow regime is dominated by buoyancy forces which makes bubbles flow at the top of the tube. The gas bubbles are dispersed in the liquid with a high concentration of bubbles in the upper half of the tube due to their buoyancy. When shear forces are dominant, the bubbles tend to disperse uniformly in the tube. In horizontal flows, the regime typically only occurs at high mass flow rates.

#### 2.6.6. Churn flow regimes

Increasing the velocity of the flow, the structure of the flow becomes unstable with the fluid travelling up and down in an oscillatory fashion but with the net upward flow. The instability is the result of the relative parity of the gravity and shear forces acting in opposing direction on the thin liquid film surrounding Taylor bubbles. This flow pattern is in fact an intermediate regime between the slug flow and annular flow regimes.

## 2.7. Flow regime maps

Most studies in the open literature show a nexus between the prevailing flow pattern which is a result of shear, capillary and gravitational force balancing and the distribution of the phases of the working fluid which consequently affects heat transfer coefficients and pressure drops. There have been some reviews [183, 184] in the past. However, the last most comprehensive review of flow pattern was by Doretti *et al.* [59]. Accurate predictions of these factors are strongly dependent on suitable predictions of the various flow regimes experienced during two flow processes [4, 6, 17, 21, 59, 72, 76, 81, 94, 97, 99, 100, 108, 177, 184-193].

Flow patterns are also dependent on the properties of the working fluids, mass flux, and vapour quality and inclination effects. Many flow pattern maps are available in the literature. It is important to note that the transition from one flow regime to another is analogous to the progression of flow from laminar to turbulent in a single phase flow process. This implies that accurate prediction of flow regime and flow pattern maps will be invaluable to the designer of the heat exchange equipment in building effective ones. The transition from one flow regime to another are usually characterised by some dimensionless numbers which were discussed briefly in Section 2.5. Hence it follows that a thorough understanding of the prevailing flow regime ultimately helps in the characterisation of the condensation two-phase flow problems and the formulation of various models and correlations [62, 76, 81, 85, 99-101, 184, 194].

Flow regimes can be designated in flow pattern maps. Most of these maps were developed for horizontal flow in adiabatic conditions and a limited number of fluids, covering a limited experimental range, based on subjective flow pattern identification criteria. Although there is a nexus between condensation flow regimes and those for adiabatic two-phase flows, the condensate forms all around the perimeter (even for stratified flows) with diabatic cases but this is not applicable with adiabatic flows. However, many researchers working on diabatic flow have used them as a guide. The first map used for condensation was the Baker [195] map which was developed for the petroleum industry. However, the most widely used flow pattern map for horizontal flows is that of Taitel and Dukler [196]. Their map was based on a semi-theoretical method and is computationally challenging to use. Their map also assumes that the liquid-vapour interface during stratified flow is flat. However, Grolman and Fortuin [107] revealed that the model of Taitel and Dukler [196] which assumed a flat liquid-vapour interface was not applicable for upward flows as it led to errors.

Barnea [115] developed a unified model for predicting flow pattern transitions in pipes covering the whole inclination angles. However, the Mandhane *et al.* [197] map seems to be the most accepted map from the first generation of maps. For vertical tubes with upward flow, the flow pattern maps of Hewitt

and Roberts [198] and Fair [199] are the most widely used. However, they were mainly developed for air-water flows.

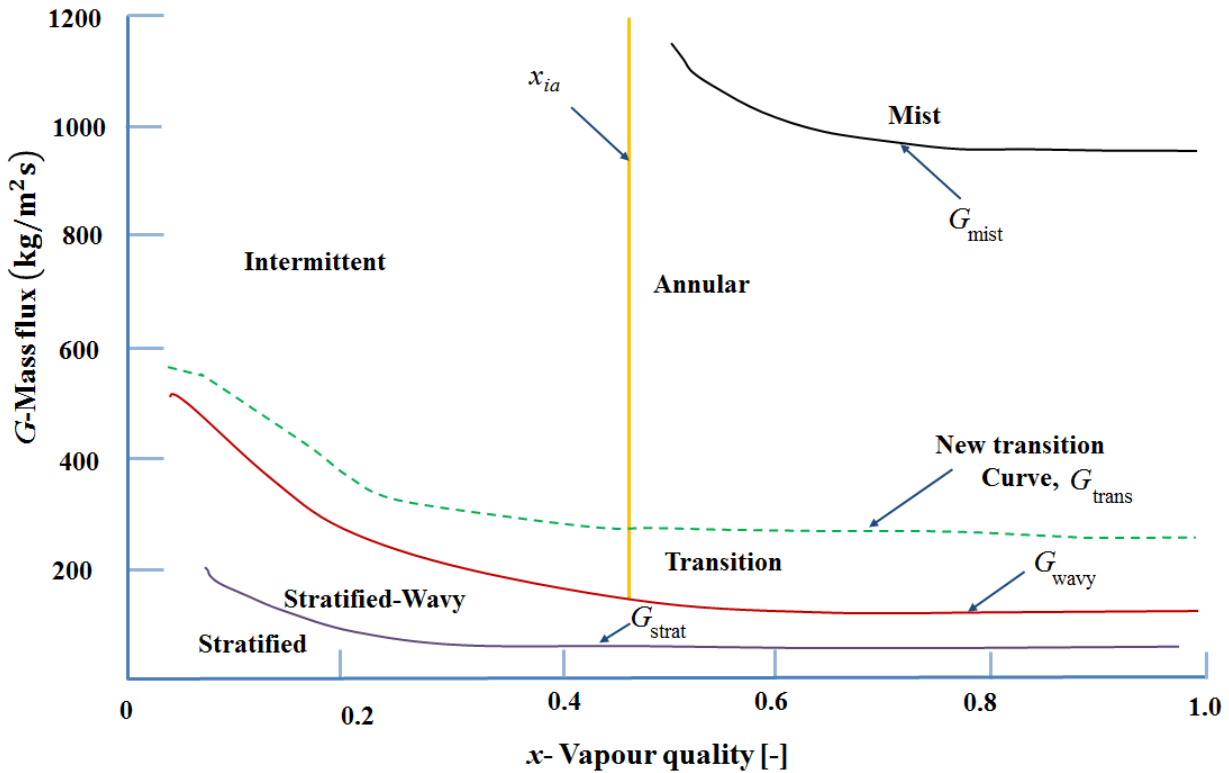
The premier map for condensation was introduced by Breber *et al.* [172] and later Tandon *et al.* [174] proposed their flow pattern map. The Breber *et al.* map when plotted on the Taitel and Dukler map [196], shows that the transition between annular and wavy regime is not abrupt and that a transition region rather than a single line was necessary to separate the flow patterns. However, the ‘breakthrough’ came when Kattan *et al.* [200] proposed the first comprehensive flow boiling model for evaporation in horizontal tubes wherein they relied on the local flow pattern and a novel diabatic flow pattern map. El-Hajal *et al.* [97] and Thome and El-Hajal [201] adapted the Kattan *et al.* [200, 202] map and simplified the two-phase flow structure perspective from flow boiling to condensation simplified the implementation of the map by using the Rouhani and Axelsson [169] cross-sectional void fraction equation into the method to eliminate its iterative solution scheme. This can be said to be a modification of the Steiner map [203]. Also, the changes proposed by Zürcher *et al.* [204] were implemented to ensure better prediction of the transition curves from annular to stratified/wavy flow, and from stratified/wavy to wavy flow. Spurred by these advances, Cavallini *et al.* [205], Shao and Granryd [192, 193] and El-Hajal *et al.* [97] have proposed some condensation models based on flow pattern and flow pattern transitions. They assumed a flow structure that uses a truncated liquid film and a liquid film of constant thickness, necessitated by the complexity of predicting film distribution. Of essence here are the complexities of the interactions between a turbulent liquid film and a turbulent vapour core, the added effect of gravity on flows in horizontal or angled tubes, the effects of heat and mass transfer occurring continually, and the behaviour of different wave structures at the vapour-liquid interface. Most recently, Suliman *et al.* [81] improved on the El-Hajal *et al.* [97] map by using experimental data during the condensation of R134a in smooth horizontal tubes at low mass fluxes. They used an iterative method to get a new transition line for annular to stratified wavy flow as described in Fig 2.3.

Despite the progress made in the development of new flow pattern maps, more work is needed in the prediction of correct flow pattern transition boundaries for condensation inside inclined smooth tubes and for low mass fluxes.

## **2.8. First generation correlations of heat transfer during in tube condensation**

There have been many studies in the technical literature aimed at modelling the condensation physics of heat transfer and pressure drop behaviour of refrigerants and other working fluids. These efforts have either been experimental, analytical or an integration of both experimental and analytical. Each

of these approaches has its advantages and disadvantage and are classified as either shear based, boundary layer based, two-phase flow multiplier based or flow pattern based.



**Fig. 2.3: Improved flow pattern map (adapted from Suliman *et al.* [81]).**

For instance, empirical correlations are limited in terms of sufficient variables to describe condensate flow correctly. On the other hand, analytical and semi-analytical approaches usually give less accurate results than purely empirical correlations. In general, the first generation correlations like that of [88, 171, 173, 176, 179, 206-212] have been shown not to agree with each other and some cases, differed by up to a factor of two. This discrepancy posed a serious challenge to the design engineer. This challenge is still with us until this present day. On the other hand, since there is a general agreement that the mechanisms of heat transfer, momentum and pressure drop are connected to the predominant local two-phase flow regime, most modern correlations [90, 94, 95, 165, 176, 200, 202, 212] dwelled on this. The relatively new flow pattern approach has led to the development of dimensionless parameters to predict and/or determine flow regime transitions. This has led to some level of accuracy in predicting heat transfer [4, 72, 76, 81, 84, 94, 97, 165, 176, 183, 185-187, 191-194, 200, 202]. The succeeding section below describes some of the correlation while Table 2.1 briefly lists and briefly explains selected first generation heat transfer correlations for smooth tubes.

### **2.8.1. Correlation of Chato**

Chato [213] developed analytical solutions for stratified laminar condensation in horizontal and inclined tubes. In his study, he assumed that the condensate depth decreased along the tube length hence he neglected the heat transfer in the liquid pool at the bottom of the tube. Furthermore, he assumed that the void fraction did not change significantly with respect to quality which led to large errors at high mass flux and low vapour quality because convective heat transfer prevails at those conditions. He also developed a Nusselt-type equation for condensation of refrigerants at low vapour velocities inside horizontal tubes based on the Chen [214] analysis of falling film condensation outside a horizontal cylinder.

### **2.8.2. Correlation of Jaster and Kosky**

Jaster and Kosky [215] also proposed a gravity-driven condensation correlation similar to that of Chato [213]. Before Jasper and Kosky were Rosson and Meyers [216]. They developed a correlation which was a remarkable improvement from the Chato correlation and which they recommended for use in the intermittent flow regime. They opined that Nusselt type film condensation occurred at the top of the tube with superimposed effects of vapour shear forces and for the bottom of the tube, they derived a forced convective heat transfer equation by applying the heat and momentum analogy. To conclude, they defined a parameter which represented a portion of the tube perimeter over which the film condensation was dominant.

### **2.8.3. Correlation of Shah**

Shah [88] was one of the pioneers of the two-phase multiplier method for determining condensation heat transfer coefficients. In his classic paper, he presented what he termed a general correlation for heat transfer during film condensation inside tubes. He verified his correlation by comparing it with experimental data from water, R11, R22, R12, R113, methanol, benzene, toluene and trichloroethylene condensing in horizontal, vertical and inclined pipes of diameters 7 mm to 40 mm and found the mean deviation for the data points analysed to be 15%. To achieve his correlation, he made use of the Dittus-Boelter model [217] for single-phase heat transfer and he also noted that there was a similarity between the mechanism of heat transfer during film condensation and that of boiling without bubble nucleation (evaporation). This correlation is one of the most cited in the literature and the simplicity of its formulation is heart-warming. However, Dobson and Chato [176] proved that Shah's correlation was only valid in the annular regime during the condensation process.

#### **2.8.4. Correlation of Akers *et al.***

Akers *et al.* [208] developed a two-phase multiplier-based correlation that became known as the “equivalent Reynolds number” model. This model defines the all-liquid mass flow rate that provides the same heat transfer coefficient as an annular flow during condensation.

#### **2.8.5. Correlation of Moser *et al.***

Moser *et al.* [212] applied the heat-momentum analogy to derive a shear based heat transfer correlation for in tube condensation in smooth tubes. Their aim was to rectify the problems associated with the Akers *et al.* [208] correlation which was based on the equivalent Reynolds number. They asserted that the assumptions for the derivation of Akers correlation was faulty and led to the underprediction of other experimental data of other researchers. In deriving their correlation, they made three assumptions: The static pressure drop of the liquid was the same as that of the vapour, the volume occupied by the liquid phase plus the vapour phase volume at any instant was equal to the total volume of the tube, there was no liquid entrainment in the vapour core.

### **2.9. Review of state of the art of condensation heat transfer coefficient correlations**

This section presents a brief review of the most essential correlations relevant to this study. There have been various reviews on correlations by authors [38, 69, 100, 101]. These previous reviews have pointed out the strengths and shortcomings of the correlations. For the same conditions, these correlations give different varying values for heat transfer coefficients. In general, heat transfer correlations during in tube condensation can be classified as either shear based, boundary layer based (analytical), two-phase multiplier based and flow pattern based. For this study, the most relevant ones will be briefly discussed in chronological order. A compendium of selected correlations mentioned in Sec 2.7 and 2.8 are given in Table 2.1.

#### **2.9.1. Correlation of Dobson and Chato**

Dobson and Chato [47] carried out an empirical study of heat transfer and flow regimes during the condensation of R11, R12, R134a and near-azeotropic blends. They observed the flow regimes at the inlet and outlet of the test condenser and listed the flow regimes observed as stratified, wavy, wavy annular, annular mist and slug flows. They posited that heat transfer behaviours were controlled by the prevailing flow regime and on that basis grouped the flow regimes into gravity dominated and shear dominated flows and concluded that the gravity dominated regime was dependent on refrigerant temperature difference but independent of mass flux. Finally, they applied the two-phase multiplier approach in analysing annular flow which is dominated by vapour shear force.

### 2.9.2. Correlation of Thome *et al.*

Thome *et al.* [94] developed a flow pattern based heat transfer model by distinguishing between stratified and non-stratified flow regimes. They applied convection condensation to the perimeter wetted by the axial flow of liquid film which refers to the entire tube perimeter for annular, intermittent and mist flows but only the lower part of the tube perimeter for stratified wavy and smooth stratified flows. They assumed turbulent flow for non-stratified regimes and applied the Nusselt falling film type equation for the stratified flows thus ignoring the effect of vapour shear forces.

**Table 2.1: Pure vapour condensation inside smooth tubes: First generation heat transfer models**

Researcher(s)	Model
Akers <i>et al.</i> [208]	$\frac{\alpha d_i}{k_l} = C Re_e^n Pr_l^{0.333}$ $\dot{m}_e = \dot{m} \left[ (1-x) + x \left( \frac{\rho_l}{\rho_v} \right)^{0.5} \right]$ $C = 0.0265 \text{ and } n = 0.8 \text{ for } Re_e > 50,000$ $C = 5.03 \text{ and } n = 0.333 \text{ for } Re_e < 50,000$
Akers and Rosson [216]	$\frac{\alpha_{tp} d_h}{k_l} = 0.026 Pr_l^{0.333} \left\{ G \left[ (1-x) + x \left( \frac{\rho_l}{\rho_v} \right)^{0.5} \right] \frac{d_h}{\mu_l} \right\}^{0.8}$
Tang [211]	$\frac{\alpha d_i}{k_l} = 0.023 Re_l^{0.8} Pr_l^{0.4} \left[ 1 + 4.863 \left( \frac{-x \ln P_{red}}{1-x} \right)^{0.836} \right]$ $P_{red} = \frac{P_{sat}}{P_{crit}}$
Chato [213]	$\alpha = 0.296 \left[ \frac{\rho_l (\rho_l - \rho_v) h_{fg} g d^3}{k_l \mu_l (T_s - T_w)} \right]^{0.25} \left( \frac{k_l}{d} \right)$
Cavallini and Zecchin [207]	$Nu = 0.05 Re_e^{0.8} Pr_l^{0.33}$ $Re_e = Re_l + Re_v \frac{\mu_v}{\mu_l} \left( \frac{\rho_v}{\rho_l} \right)^{0.5}$
Jaster and Kosky [215]	$Nu_{strat} = 0.725 \left[ \frac{\rho_l (\rho_l - \rho_v) h_{fg} g d^3 \varepsilon^3}{k_l \mu_l (T_s - T_w)} \right]^{0.25}$ <p>where <math>\varepsilon</math> is calculated from the Zivi [218] void fraction model</p>
Shah [88]	$Nu = 0.023 Re_e^{0.8} Pr_l^{0.4} \left[ 1 + \frac{3.8}{P_{red}^{0.38}} \left( \frac{x_l}{1-x_l} \right)^{0.76} \right]$ <p>Valid for <math>Re_l \geq 350</math></p>
Haraguchi <i>et al.</i> [210]	$\frac{\alpha_{tp} d_h}{k_l} = 0.0152 (1 + 0.6 Pr_l^{0.8}) \frac{\Phi_v}{X_{tt}^{0.77}} Re_l^{0.77}$ $\Phi_v = 1 + 0.5 \left[ \frac{G}{\sqrt{g \rho_v (\rho_l - \rho_v) d_h}} \right]^{0.75} X_{tt}^{0.35}$

### **2.9.3. Correlation of Cavallini *et al.***

Cavallini *et al.* [95] developed new heat transfer coefficient and pressure drop models for predicting the condensation of halogenated refrigerants. Their motivation stemmed from the fact that other available models at that time failed to correctly predict to within acceptable limits the experimental results obtained from their earlier studies and the results from other independent laboratories. This problem was more noticeable for high-pressure refrigerants like R410A, R125 and R32. Their model was developed to cover the most relevant flow regime like annular, stratified, wavy and slug. To conclude, they tested their model with the experimental data of almost all the available refrigerants.

The starting point of their model comparing their earlier data with the Kosky and Staub [206] equation and used the Friedel [16] to compute interfacial shear stress. Their model was flow pattern based and divided into annular-stratified flow transition and stratified flow, stratified-slug transition and slug flow and bubbly-intermittent flow. For the first, they gave the limits and noted that if the dimensionless gas velocity  $J_v \geq 2.5$  and Lockhart Martinelli parameter  $X_{tt} < 1.6$ , then the flow could be considered to be fully annular, in that case they proposed a suitable correlation. For the stratified flow they noted that  $J_v$  was typically low and always less than 2.5 and the  $X_{tt} < 1.6$ . Their thinking was that since in stratified flows we have a thin liquid film which is gravity driven at the top of the tube and a thick liquid film at the bottom of the tube, it will be wise to represent the heat transfer as the sum of what happens during both phenomena. For the thin film at the top of the tube, they derived a Nusselt type temperature dependent equation which was a correction of the Jaster and Kosky [74] equation and for the bottom of the tube dominated by liquid, they derived another equation which is a correction of the Dittus-Boelter equation.

### **2.9.4. Correlation of Shah**

Shah [90, 96] presented a new flow pattern based general correlation for heat transfer during in-tube condensation in horizontal tubes. He divided the flow regimes into three. Regime I was for intermittent, annular and mist flows; regime II was for stratified – wavy flows and regime III was for stratified flows. These divisions were based on the values of the dimensionless vapour velocity  $J_v$ . This new correlation was a modification of his previous correlations [52, 100] and covered mass fluxes as low as 13 kg/m<sup>2</sup>s. The new correlation was able to predict 1568 data points with an average absolute deviation of 17%.

## **2.10. Condensation in smooth horizontal tubes**

### **2.10.1. Initial works**

Pioneering research work on condensation heat transfer was carried out by Nusselt [219]. For a vertical plate, he reduced the complexity of the real condensation phenomenon to an elementary model by



assuming that the only resistance for heat removal during condensation occurred in the condensate film. He assumed that the viscous shear of the vapour on the film was insignificant and solved the continuity, momentum and energy equations using some assumptions to simplify the complex process. The assumptions were that there was a uniform vapour temperature and vapour is saturated. He also assumed constant fluid properties; gravity is the only external force acting on the film (static force balance because momentum is ignored); the adjoining vapour is static and exerts zero drag on the film, and the latent heat is much greater than the sensible cooling of the film. The curvature of the interface is negligible hence the saturation temperature of the interface is that of a planar interface determinable from the vapour pressure curve of the fluid. For a horizontal tube, he used a numerical integration approach to derive the laminar film condensation on the outside of horizontal tubes obtaining the relation: In arriving at this, he assumed a laminar condensate flow round the tube and that the coefficient of heat transfer was highest at the centre of the tube decreasing around the surface as the intrinsic thermal resistance in the film grew with its thickness and finally resulting to nil at the bottom of the tube. A major shortcoming of Nusselt was that he neglected the surface tension forces that help up the condensate at the bottom of the tube until been overcome by the force of gravity resulting in the formation of condensate droplets instead of a continuous sheet. The Nusselt [219] equation can be applied to condensation inside horizontal tubes to calculate the falling film heat transfer coefficient when considering stratified flows.

In his PhD thesis, Crosser [208] examined the effect of vapour velocity, temperature difference and fluid properties on the condensation of propane. He concluded that there was no effect of liquid loading and temperature difference on the heat transfer coefficient over the range of his investigation then came up with a correlation for his heat transfer coefficients. Carpenter and Colburn [220], Soliman *et al.* [173] and Chen *et al.* [93] also developed shear based correlations for heat transfer coefficients while Kosky and Staub [206] and Traviss *et al.* [171, 221] developed boundary layer based correlations for heat transfer coefficients applying the momentum and heat transfer analogy to an annular flow model using the Von Karman [222] universal velocity in describing the liquid film wherein the total thermal resistance of the liquid film thickness was considered different from that of Carpenter and Colburn [220], Soliman *et al.* [173] and Chen *et al.* [93] who only considered theirs in the laminar sub-layer.

### **2.10.2. Low mass fluxes (horizontal tubes)**

A review of studies during in tube condensation at low mass fluxes in horizontal tubes is presented in this section.

#### **2.10.2.1. Work of Aprea *et al.***

Aprea *et al.* [86] measured the local heat transfer coefficients during the condensation of R22 and R407C in a 20 mm diameter, smooth horizontal tube at saturation temperatures varying between 37°C and 40°C. They conducted experiments at mass fluxes of 45 – 120 kg/m<sup>2</sup>s. They found that their experimental points at low mass fluxes fell into the stratified wavy flow regime. They compared the results of their experiments with some correlations [109, 215, 216, 223] and found that the correlation of Dobson and Chato [176] predicted their results to within an accuracy of 13%. However, they did not study the effect of temperature difference on the heat transfer coefficients.

#### **2.10.2.2. Work of Suliman *et al.***

Suliman *et al.* [81] performed heat transfer experiments at mass fluxes ranging between 75 – 300 kg/m<sup>2</sup>s during the in-tube condensation of R134a in a smooth horizontal tube with an inner diameter of 8.38 mm at a nominal saturation temperature of 40 °C. They found that at low mass fluxes, the heat transfer coefficients were dependent on temperature differences. They also presented an improved flow pattern map, which was a slight modification of the map proposed by El-Hajal *et al.* [97]. However, they only acquired two data points for the lowest mass flux of 75 kg/m<sup>2</sup>s.

#### **2.10.2.3. Work of Lee and Son**

Lee and Son [28] presented the results of their experiments during the condensation of R134a, R290a, R600a, and R22 in different smooth horizontal tubes at a saturation temperature of 40 °C. Their lowest mass flux was 35.5 kg/m<sup>2</sup>s, while their maximum was 210.4 kg/m<sup>2</sup>s. Their work was more of a comparative study between the heat transfer characteristics of the different refrigerants in the search for replacement refrigerants. They did not study the effect of the temperature difference on the heat transfer coefficients. However, just as other researchers, they found that the heat transfer coefficients increased with increasing quality and mass flux. Comparing the results of their experiments with correlations, they found that the Haraguchi *et al.* [210] correlation was the most reliable for predicting the range of their experimental data.

#### **2.10.2.4. Work of Azzolin *et al.***

Azzolin *et al.* [224] investigated the effect of gravity during the convective condensation occurs inside a circular channel with a diameter of 3.4 mm. An experimental apparatus was designed to perform microgravity experiments at mass fluxes between 70 kg/m<sup>2</sup>s and 170 kg/m<sup>2</sup>s with Hydrofluoroether (HFE-7000) as the working fluid. The results of the heat transfer coefficient and the flow pattern visualizations showed that, when gravity acted perpendicular to the channel flow, it had a beneficial effect on the heat transfer coefficient by acting on the liquid distribution along the tube perimeter. In microgravity conditions, this mechanism led to a penalization factor which increased as the mass flux increased.

## **2.11. Condensation in smooth inclined tubes**

Previous studies [4, 8, 9, 18, 32, 33, 46, 71, 72, 91, 92, 98-103, 106-117, 119-123, 225] on inclined tubes were at moderate to high mass fluxes. In those studies, it was found that varying the inclination angles altered the flow patterns with consequent effects on the heat transfer coefficients, pressure drops, and void fractions. It was also found that the effects of inclination became more pronounced as the mass flux decreased. For downwards inclinations, it was found that the effect of the gravity was dominant and caused a thinning of the liquid layer which led to a reduction in the thermal resistance within the tube surface, leading to higher heat transfer coefficients [7, 18, 32, 33, 71, 72, 124]. For upwards inclinations, no concrete trend was established. However, there are two main challenges. The first is that there is no study that has systematically coupled the effect of inclination and temperature difference on the heat transfer coefficients and flow patterns at low mass fluxes ( $\leq 100 \text{ kg/m}^2\text{s}$ ). The other challenge is that there are contradictory reports [32, 72, 99, 100, 102] on the recommended inclination angle for optimum heat transfer performance. This is further evidenced by the fact that there is no unifying correlation that can properly predict the heat transfer coefficients in inclined smooth tubes. This may be attributed to the fact that the available models are either limited by tube size, working fluid, saturation temperature, mass flux, or tube orientation. A review of the most relevant works on inclination is presented below.

### **2.11.1. Work of Tepe and Muller**

Tepe and Mueller [29] were arguably the first to publish their findings on the effect of inclination during condensation inside smooth tubes. They performed experiments during the condensation of benzene inside a smooth tube 18 mm in diameter at a single inclination angle of  $15^\circ$ . They observed that there existed an effect of inclination on their measured heat transfer coefficients. They also found that their measured heat transfer coefficients were approximately 50% higher than the predicted values when compared to the Nusselt [219] classical theory. Following closely were Hassan and Jakob [117], who performed numerical and empirical studies on the effect of inclination on the heat transfer coefficients during condensation outside horizontal tubes. They noticed an effect of inclination on the measured heat transfer coefficients. Furthermore, they applied the Nusselt [219] classical theory and compared the results of their experiments to that of their numerical analysis. They found that the heat transfer coefficients of their numerical study were between 28% and 100% lower than the results of their experiments. They attributed this to the rippling effect of the condensate film, which was not accounted for in their theoretical model. Later, Chato [116] also observed an inclination effect during condensation of R113, wherein he observed that slightly downwards inclinations led to an increase in heat transfer rates.

### **2.11.2. Work of Chato**

Chato [109] studied and developed analytical solutions for stratified laminar condensation in horizontal and inclined tubes. It was assumed that the condensate depth decreased along the tube length. Hence, he neglected the heat transfer in the liquid pool at the bottom of the tube and assumed that the void fraction did not change significantly with respect to vapour quality. These assumptions led to large errors at high mass fluxes and low vapour qualities because convective heat transfer prevailed in those conditions. He further developed a Nusselt-type equation for the condensation of refrigerants at low vapour velocities inside horizontal and inclined tubes based on Chen's [36] analysis of falling film condensation outside a horizontal cylinder.

### **2.11.3. Work of Nitheanandan and Soliman**

Nitheanandan and Soliman [113, 226] obtained flow regime data during the condensation of steam inside a 13.4 mm diameter tube at upwards and downwards inclinations within  $\pm 10^\circ$ . In all their experiments, they achieved complete condensation inside the condenser. They found that the zones occupied by the wavy and slug regimes experienced significant shifts, whereas the effect on the annular flow boundary appeared to be insignificant at the present small inclination angles. They also compared their data with adiabatic gas-liquid flow regime maps developed analytically and experimentally for horizontal and inclined tubes.

### **2.11.4. Work of Meyer and co-workers**

Lips and Meyer [7, 18, 71, 72] studied the heat transfer and pressure drops during the condensation of R134a inside a smooth inclined tube. They carried out experiments at different inclination angles for upwards and downwards flows. With the aid of a high-speed camera installed at the exit of their test section, they captured and studied the flow patterns by varying the mass fluxes, vapour qualities, and inclination angles. They found that at high mass fluxes and vapour qualities; the flow was independent of the angle of inclination and always remained annular. However, at high mass fluxes and low vapour qualities, the flow regime was mostly intermittent and dependent on the inclination angle. They defined the impact of gravity on the heat transfer coefficients as the 'Inclination effect' ( $I_a$ ) and presented an expression for it. They also found that the highest heat transfer coefficients were achieved at an inclination angle of between  $-15^\circ$  and  $-30^\circ$  (downwards flow). The gap in their work was that they did not investigate the combined effect of the temperature difference and inclination on the heat transfer coefficients.

Meyer *et al.* [33] conducted condensation heat transfer experiments in an 8.38 mm diameter inclined smooth tube at saturation temperatures in the range 30 – 50 °C. Their study was an extension of the work of Lips and Meyer [7, 71, 72], who carried out similar experiments but at a single saturation

temperature of 40 °C. They found out that in general, an increase in saturation temperature led to a decrease in the heat transfer coefficients. They also found out that the inclination effect on the heat transfer coefficients became more prominent as mass fluxes decreased. Similar to the result of Lips and Meyer [72] they found that the angle which gave the maximum heat transfer coefficients was between  $-15^\circ$  and  $-30^\circ$  (downwards flow). However, they did not investigate the influence of temperature difference on the heat transfer coefficients as they kept their heat transfer rate constant.

Recently, Olivier *et al.* [32] investigated the effect of inclination on void fraction and heat transfer coefficient during the condensation of R134a inside a smooth inclined tube at mass fluxes between 100 and 400 kg/m<sup>2</sup>s. They captured flow regimes and measured void fractions with a capacitive void fraction sensor mounted at both the inlet and outlet of their test section. They kept the heat transfer rate of their experiments at 200 W. They found that the inclination effect on heat transfer coefficients and measured void fractions became insignificant with increasing mass flux and vapour quality. The greatest effect of inclination on heat transfer coefficients was observed for combinations of low mass flux and low vapour quality. Their results at downwards inclinations were more sensitive to changes than for upwards inclinations. They also found that the void fraction and flow pattern map predictions were inadequate for inclined flow conditions. However, they did not investigate the influence of temperature difference on the heat transfer performance, keeping their heat transfer rate constant.

#### **2.11.5. Work of Mohseni and co-workers**

Mohseni and Akhavan-Behabadi, Mohseni *et al.* [99, 101] conducted experiments for seven different tube inclinations between  $-90^\circ$  and  $+90^\circ$  and six refrigerant mass fluxes between 53 and 212 kg/m<sup>2</sup>s to measure the heat transfer coefficients and observe the flow patterns of R134a condensing inside a smooth inclined tube. They found that the tube inclination noticeably influenced the heat transfer coefficients. In terms of the flow regimes, they found an effect of inclination on the vapour and condensed liquid flow distribution leading to eight distinct flow regimes with respect to the different tube inclinations. They also found that the best heat transfer performance was achieved at an inclination angle of  $+30^\circ$  (for all refrigerant mass fluxes). Their findings were in sharp contrast with the findings of Lips and Meyer [7, 18, 71, 72].

A holistic look at both studies showed that the difference between the experimental conditions was the length of the test sections, average saturation temperature, and the mass flux range, but would those variables be significant enough to sharply alter the inclination effect? They also found the effect of inclination angle on the heat transfer coefficient to be more prominent at low vapour qualities and mass fluxes. Furthermore, they developed an empirical correlation that predicted the results of the heat

transfer coefficient of their experiments. However, they did not investigate the combined effect of the temperature difference and inclination on the heat transfer coefficients.

#### **2.11.6. Work of Xing *et al.***

Xing *et al.* [102] performed experiments during the condensation of R245fa inside an inclined tube 14.81 mm in diameter and 1.2 m in length at an average saturation temperature of 55 °C. The mass fluxes considered to be in the range 191–705 kg/m<sup>2</sup>s with the vapour quality ranging between 0.19 and 0.95. Furthermore, they carried out a non – dimensional study wherein they found influences of inertia and gravity on the condensation heat transfer coefficients. Their analysis showed that surface tension forces were insignificant during the two-phase process. With respect to the heat transfer coefficients, they found an influence of inclination angle on the heat transfer coefficients and proposed that optimal inclination angles of 15° and 30° existed, at which the heat transfer coefficients reached a maximum. With respect to the flow patterns, they observed stratified-smooth flow, stratified-wavy flow, intermittent flow, churn flow, falling film, and annular flow. They developed a correlation which was also able to explain the influence of mass flux, vapour quality, and inclination angle on the condensation heat transfer coefficient. This correlation also predicts that the measured heat transfer coefficient.

#### **2.11.7. Low mass fluxes (inclined tubes)**

Despite its wide range of utilization and huge potential for future applications, little information is available on the thermal performance of inclined condensers at low mass fluxes. A review of the open literature [2, 4, 6-9, 11, 17, 18, 20, 32, 33, 46, 55, 58, 59, 71, 72, 74-76, 86, 91-94, 96-98, 101-103, 106, 107, 110, 111, 113, 114, 126-129, 171, 184, 214, 227-240] revealed that most studies on condensation inside smooth tubes focused on horizontal and vertical configurations at mass fluxes typically greater than 200 kg/m<sup>2</sup>s and normally reaching up to 1 000 kg/m<sup>2</sup>s. Other studies [11, 52, 75, 81, 104, 105, 119] showed that at low mass fluxes, the heat transfer coefficient was dependent on the temperature difference. Of these studies, none has quantitatively and systematically investigated the effects of both tube inclination and temperature difference on the heat transfer coefficients and flow patterns in smooth tubes at low mass fluxes. This underscores the need for more data collection by employing empirical studies to help in this regard. A review of the most relevant literature on low mass fluxes is presented below.

#### **2.11.8. Work of Davies *et al.***

Davies *et al.* [31, 104, 105] conducted experimental and flow visualization studies during the condensation of steam in noncircular inclined steel tubes brazed with aluminium fins at steam mass fluxes lower than 10 kg/m<sup>2</sup>s and a uniform air fin-face velocity of 2.2 m/s. Their test condenser was

approximately 11 m long and made of steel with brazed aluminium fins with a rectangular cross-section of dimensions 214 mm  $\times$  18 mm. Their test condenser was also cut in half lengthwise and covered with a polycarbonate viewing window to allow for simultaneous visualization and the heat transfer measurements. Their maximum inlet air temperature range was from 35 °C and the average condensing temperature of the steam were maintained at 100 °C. With respect to inclination angle, they varied it from horizontal (0°) to downwards (-75°) flow. Furthermore, they found that the depth of the condensate river at the bottom of the tube decreased with an increase in inclination angle. The average steam-side heat transfer coefficient was shown to increase with an increase in inclination angle. Overall, their results suggested that an improvement in steam-side heat transfer performance was achieved by varying the tube inclination angle. With respect to flow visualization, they found only the stratified flow regime for all test conditions at all locations along the condenser. They also observed both film-wise and drop-wise condensation on the tube wall. The steam-side heat transfer coefficient was found to be dependent on the wall-steam temperature difference, and not vapour quality or Reynolds number. As a result, the condensation heat transfer coefficient did not decrease along the condenser length, as is common for smaller condenser tubes with higher mass fluxes. Finally, they stated that the overall heat transfer coefficient of the condenser was found to increase linearly with increasing downwards inclination angle of the test condenser, at an approximate rate of 0.08% per degree of inclination beneath the horizontal reference. They attributed this increase to improved drainage and increased void fraction near the condenser outlet.

#### **2.11.9. Work of Lyulin *et al.***

Lyulin *et al.* [103] studied the laminar convective condensation of pure ethanol vapour inside an inclined smooth circular tube with an inner diameter 4.8 mm and a length of 200 mm. The experiments were conducted at an average saturation temperature of 58 °C. The vapour mass flux was varied from 0.24 to 2.04 kg/m<sup>2</sup>s. They investigated the dependence of the heat transfer coefficient on both the temperature difference between the saturated vapour and the wall and the condenser inclination. They found that the heat transfer coefficient reduced with an increase in the temperature difference. They also found that the heat transfer coefficient was a maximum at an inclination angle of 15°–35°. They attributed this to the complex gravity drainage mechanism of the condensate. They also proposed that their results would be valuable in the development of compact cooling systems for ground and space applications.

#### **2.11.10. Work of Arslan and Eskin**

Arslan and Eskin [75] measured the heat transfer coefficients during the condensation of R134a inside a smooth vertical tube. They covered only downwards flows for a mass flux range 20 to 175 kg/m<sup>2</sup>s. Their condensation temperatures varied from 20 – 30 °C. Their findings revealed that the heat transfer

coefficients decreased with an increase in saturation pressure and that at low mass fluxes, the heat transfer coefficients were dependent on the temperature difference between the inner tube wall temperature and saturation temperature. They also found that the measured heat transfer coefficients increased as the mass flux increased. They postulated that amongst the other correlations, that of Akers *et al.* [208] best predicted their results, with an average deviation of 23%. However, they did not represent their results as a function of vapour quality and only considered a vertical tube orientation, neglecting other possible inclinations.

## 2.12. Physics of pressure drop

The total pressure drop in a condensation process is intimately linked to the kinetic and potential energies of the working fluid, and the frictional interaction between the fluid and the tube wall in which the condensation occurs. These, in turn, are functions of the internal tube diameter, the length of the condenser, the mean fluid velocity and the mean value of the fluid density. While the kinetic energy is intimately linked to the momentum pressure drop, the gravitational energy is inextricably connected to the static pressure drop. Furthermore, the interaction between the fluid and the tube wall is linked to the frictional pressure drop.

It can also be shown that for horizontal flows, the static pressure drop reduces to zero thus is customarily neglected. Also, the frictional pressure drop is an essential component of the total pressure drop because it is typically more significant than the momentum and static pressure drop. Frictional pressure drop is a product of irreversible work due to shear forces on the tube wall and at the liquid-vapour interface. It is also the most challenging to determine, and more complicated to predict in comparison with single-phase flow. It has also been shown to be a function of the dominant flow pattern, tube diameter, interfacial contact area between the liquid and vapour phases, inclination angle, heat flux, pipe surface roughness, fluid properties, mean vapour quality, and mass velocity. The momentum pressure drop ( $\Delta P_{mom}$ ) accounts for the difference in pressure due to a change in momentum resulting from the acceleration or deceleration of the fluid in the test section. For condensing flow, the kinetic energy of the outgoing flow is usually less than that of the incoming flow which implies that the momentum pressure drop is always negative. Hence the momentum pressure head results in an increase in the pressure at the outlet i.e. a pressure recovery. The static pressure drop,  $\Delta P_{stat}$  results from an elevation difference between the inlet and the outlet due to the tube inclination angle. The mathematics of pressure drop will be treated in the data reduction section (Chapter 3) of this thesis.



### 2.13. Pressure drop in horizontal tubes

Ferguson and Spedding [133] conducted experimental and comparative studies on pressure drop during two-phase co-current air-water flow in a horizontal Perspex pipe with an internal diameter of 9.35 mm and a length of 12.8 m. The results of their experiments were used to test the prediction of pressure drop in a variety of models. They found that particularly with the stratified flow regimes, the model suggested by Olujic [241] was the most accurate. They also recommended different models for other flow regimes found in their study and explained why predictions in other specified flow regimes were unsuccessful.

Cavallini *et al.* [11] investigated heat transfer coefficient and pressure drop during the condensation of refrigerants R134a, R125, R32, R410A, and R236a within a vapour quality range between 0.15 to 0.85. Their saturation temperature range was between 30 and 50 °C. They found that pressure drop increased with mass flux and vapour quality and that the pressure drop was highest at the lowest saturation temperature (30 °C). They also found that lower pressure fluids resulted in higher pressure drop. The Rohuani [169, 170] void fraction model was used in estimating the momentum pressure drop. They chose this model because of the small change in vapour quality across the test section which implied that the momentum pressure drop was expected to be negligible. Finally, they concluded that pressure drop behaviour was crucial in ascertaining the overall thermal performance of different fluids.

Son and Oh [23] investigated pressure drop during the condensation of R22, R134a, and R410A at mass fluxes between 450 – 1 050 kg/m<sup>2</sup>s inside a circular microtube, 3.38 mm in outer diameter, at a saturation temperature of 40 °C. It was found that the condensation pressure drops for R22, and R410A were lower than that of R134a for the same mass fluxes. They also found that the pressure gradient decreased as the vapour quality decreased. Furthermore, their experimental results were compared with 14 two-phase flow pressure drop models, and it was found that the Chen *et al.* [13] correlation gave the lowest overall deviation for the three refrigerants. They attributed this to the fact that their tube diameter size and mass fluxes were in the same range as that used by Chen *et al.* [13] even though there was a difference in the range of saturation temperatures. After that, they leveraged on the results of their experiments and the Lockhart-Martinelli [145] two-phase multiplier method to develop a new correlation which predicted the results of their tests satisfactorily.

Bohdal *et al.* [10] presented the results of their experiments during the condensation of R134a, R407C, and R404A in mini-channels with their maximum tube being 3.3 mm in diameter. They found a significant dependence on pressure drop on the refrigerant type, process parameters, and structure of the two-phase flow. It was also found that an increase in the mass flux led to an increment of the flow resistances in local conditions. They proposed a correlation for determining the frictional pressure drop

in the annular, annular wavy, and stratified two-phase flow regimes covering a temperature range between 20 and 50 °C, vapour qualities between 0 and 1, and mass fluxes between 0 and 1 300 kg/m<sup>2</sup>s.

Goss *et al.* [39] investigated pressure losses during the convective condensation of R134a in horizontal and parallel circular microchannels. Their test conditions were saturation temperatures between 28 to 40 °C, qualities from 0.5 to 1, heat fluxes from 17 to 53 kW/m<sup>2</sup>, and mass fluxes from 230 to 445 kg/m<sup>2</sup>s. They quantified the contributions of fluid acceleration, contraction, expansion, flow direction changes and friction to the total pressure drop; they found that the frictional pressure drop component corresponded to 95% of the total pressure loss. They also investigated the influence of condensation temperature, heat flux, and mass velocity on the pressure drop and found that the pressure drops decreased with a decrease in mass flux but increased with a reduction in saturation temperature. They also found that the pressure drops were not affected as much by the heat flux. Finally, they compared the results of their experiments with various correlations and semi-empirical models and found that the model proposed by Cavallini *et al.* [242, 243] gave the best prediction performance.

Xu *et al.* [25] evaluated 29 frictional pressure drop models for two-phase flow in tubes by collecting 3 480 data points from previous experiments. The hydraulic diameters of the tubes considered ranged from 0.0695 mm to 14 mm, and mass fluxes ranged from 6 to 6 000 kg/m<sup>2</sup>s. They compared these experimental data with these models and investigated the significance of the mass flux, vapour quality, tube diameter and working fluid on the frictional pressure drop. They concluded that the correlations of Muller-Steinhagen and Heck [22], and Sun and Mishima [147] predicted the entire range of the experimental data under different conditions with the best accuracy and recommended them for use in the design of two-phase flow systems.

Dalkilic *et al.* [3] presented a comparative analysis of the results of their experiments against eleven different pressure drop models during the annular flow condensation of R600a in a horizontal tube and R134a in a vertical tube at condensation temperatures between 30 °C and 50 °C. Their test mass fluxes were between 75 and 400 kg/m<sup>2</sup>s. The diameter of their vertical tube was 8 mm, while the diameter of the horizontal tube was 4 mm. They used the Chisolm void fraction model [14] to calculate their momentum pressure drops. They asserted that compared to other correlations, that of Chen *et al.* [13] gave the best prediction in comparison with the results of their experiments. However, they found a considerable variation in the capability of the different models to correctly predict the results of their experiments.

Wang *et al.* [24] performed a theoretical study of friction pressure drops during laminar flow condensation in microchannels and reported a fair agreement at high vapour qualities and lower results when compared to some correlations at lower vapour qualities.

Wang *et al.* [37] conducted experiments to measure the frictional pressure drop during the condensation of steam in a horizontal vacuum tube. They varied the steam saturation temperature from 50 to 70 °C using mass fluxes from 2 to 10 kg/m<sup>2</sup>s across the whole vapour quality range. They maintained the temperature difference between the cooling water at 3, 5, and 8 °C. It was found that all their test points corresponded to the stratified flow regime. They also found that frictional pressure drop increased with mass flux and vapour quality but decreased with saturation temperature. Furthermore, they found that the frictional pressure drop did not depend much on the temperature difference. They compared the results of their experimental data with 25 existing frictional pressure drop models. It was found that the Quibén's and Thome model [21], Chisholm's model [14], Zhang's model [151], Sun's model [45, 147], Lee's model [150] had the best prediction accuracy.

Yan and Lin [35] investigated heat transfer and pressure drop during the condensation of R134a inside a horizontal circular tube with an internal diameter of 2 mm. Their test conditions were mass fluxes of 100-300 kg/m<sup>2</sup>s, and saturation temperatures between 25 and 50 °C. They investigated the effects of the mass and heat flux, vapour quality and saturation temperature on the measured pressure drops and heat transfer. They found that the pressure drop increased with mass flux. They also found that the pressure drops were lower at higher saturated temperatures. Based on their experimental data, they developed empirical correlations for friction factors.

Zhuang *et al.* [239] studied the thermal performance of R170 (ethane) undergoing condensation at saturation pressures that ranged from 1 MPa to 2.5 MPa, in a horizontal tube with an internal diameter of 4 mm. Their test mass fluxes were from 100 kg/m<sup>2</sup>s to 250 kg/m<sup>2</sup>s, and heat fluxes were from 55 kW/m<sup>2</sup> to 96 kW/m<sup>2</sup> over the complete range of vapour qualities. They examined the effects of vapour quality, mass flux and saturation pressure on condensation heat transfer and pressure drop. It was found that frictional pressure drop increased with mass flux. As saturation temperature was increased, the effect of mass flux weakened. They also found that frictional pressure drop decreased as the saturation pressure increased. However, at the lowest mass flux of 100 kg/m<sup>2</sup>s, both the saturation pressure and vapour quality had little influence on the frictional pressure gradients. In conclusion, it was found that the Yan and Lin correlation [35] predicted the experimental pressure drop with a mean absolute deviation of less than 18%.

#### **2.14. Pressure drop in inclined tubes**

Wongwises and Pipathattakul [244] studied pressure drops, flow patterns, and void fractions during horizontal and upward inclined air-water two-phase flow in a concentric annular test section with a length of 880 mm and an outer diameter of 12.5 mm. They found that their experimental test conditions corresponded to plug, slug, annular, annular/slug, bubbly/plug, bubbly/slug–plug, churn, dispersed

bubbly, and slug/bubbly flows. At low gas and liquid velocities, it was found that the pressure drops increased when the inclination angle changed from horizontal to 30° and 60°. At the same time, the void fractions increased with increasing gas velocity. They also found that the opposite was true for increasing liquid velocity.

Maddi and Rao [245] performed experiments during flow boiling of water in inclined tubes encountered in the design of solar collectors, The angle of inclination was varied from 0° to 90°. It was found that inclination had a significant influence on the transport process, particularly in the bubbly and the intermittent flow regimes. However, they found that inclination had only a marginal effect on the annular flow regime. The Baroczy [246] and the Lockhart – Martinelli [145] correlations were then used to evaluate the frictional pressure drop in the flow process.

Bhagwat and Ghajar [38] studied pressure drops, void fractions, flow patterns, and heat transfer coefficients for non-boiling air-water two-phase flow in the entire range of downward inclinations. Their test section was a tube with an inner diameter of 12.5 mm. Their measurements were taken over a vast range of liquid and gas phase mass fluxes to cater to the prevalent flow regimes experienced during downward inclined gas-liquid flow. It was found that there was an effect of the tilting on two-phase flow patterns, especially at low mass flow rates. A significant impact of pipe inclination was also seen in the transition between stratified and non-stratified (slug, intermittent) flow patterns. They concluded that the two-phase flow parameters such as void fraction, pressure drop and heat transfer coefficient were mainly influenced by the negative slippage at the gas-liquid interface controlled by the buoyancy-driven nature of the two-phase flow. Furthermore, they also found the two-phase flow parameters were not sensitive to the variation in downward pipe inclination in the inertia driven region of the flow patterns.

Autee *et al.* [247] performed an experimental study of pressure drops during the two-phase flow of air-water mixtures in transparent acrylic tubes with diameters of 4.0, 6.0, and 8.0 mm with a length of 400 mm orientated horizontally, vertically and at downward inclinations of 30° and 60°. The pressure drops were measured and compared with the six existing correlations frequently used in calculating the pressure drops in macro and mini-microchannels. It was found that the current models were inadequate in predicting the two-phase pressure drop for the three diameter sizes. Based on the results of their experiments, they proposed a new correlation for predicting pressure drops by modifying the Chisholm parameter [14] and integrating different parameters. It was found that the proposed correlation predicted two-phase pressure drops satisfactorily.

Lips and Meyer [7, 18] investigated pressure drops during the condensation of R134a in a smooth horizontal and inclined tubes at a saturation temperature of 40°C and a constant heat transfer rate of

200 W. For vertical upward flows; they found that the results of their experiments agreed with various pressure drop correlations. It was found that no model predicted their measurements correctly for downward flows. They defined an apparent gravitational pressure drop and a void fraction to study the inclination effect on the two-phase flow. For upward flows, they found that the void fraction and the frictional pressure drop did not depend on the inclination angle, but this was not the same for downward flows. In conclusion, they compared the results of their experiments with the model of Taitel and Dukler [196] for the stratified downward flow regime, and an excellent agreement was found.

Adelaja *et al.* [9] conducted experiments to determine the pressure drops during the condensation of R134a in an inclined smooth inclined tube with an inner diameter of 8.38 mm across a wide range of vapour qualities. The mass fluxes tested were between 100 kg/m<sup>2</sup>s and 400 kg/m<sup>2</sup>s at saturation temperatures from 30 – 50 °C. They computed their momentum pressure drop with the void fraction model of Bhagwat and Ghajar [248]. They found that the highest void fractions and pressure drops were for vertical downward flows. Furthermore, it was found that the pressure drops and void fractions increased with decreasing saturation temperatures. The opposite was true when the inclination angle was decreased. In conclusion, it was found that the maximum frictional pressure drops were for downward flow, while the lowest values were found for upward and horizontal flows.

Kang *et al.* [31] studied the effect of inclination angles on pressure drops during the condensation of steam in a flattened tube with a length of 10.7 m and a very low mass flux of 6.8 kg/m<sup>2</sup>s, as is typically found in air-cooled steam condensers in the power generation industry. The steam was superheated at the inlet, and the inclination angles varied from horizontal (0°) to 70°. A uniform velocity profile of 2.03 m/s was imposed on the air side to remove heat from the steam. Initial two-phase pressure drop measurements and flow visualizations showed a reduction of pressure drops due to enhancement in the gravity-assisted drainage of condensate inside the tube, although the growth was only seen at an early stage of inclination.

Most recently Noori Rahim Abadi *et al.* [53] performed a comprehensive numerical study that investigated the pressure drops during the condensation of R134a inside a smooth tube at different inclination angles. The tube had an internal diameter of 8.38 mm and a length of 1.488 m while the saturation temperature was maintained at 40 °C. Simulations were carried out throughout the possible angles of inclination from -90° to +90°. The heat flux was kept constant at approximately 5 kW/m<sup>2</sup> while the mass fluxes were varied from 100 – 600 kg/m<sup>2</sup> s. The volume of fluid multiphase flow formulation coupled with the ANSYS FLUENT™ CFD program was utilized to solve the fundamental governing equations. The simulated results showed good agreement with the results of the experiments of Adelaja *et al.* [8, 9], and in general, they found that the inclination effects on the void fractions and

pressure drops were negligible at high mass fluxes and vapour qualities. Furthermore, they found that the measured pressure drops increased as the void fractions, and mass fluxes increased. These increments were found to be more noticeable at high vapour qualities.

## **2.15. Summary and conclusion**

This chapter revised a few condensation concepts, the different flow regimes as well as relevant heat transfer correlations. A brief overview of previous work done on condensation in smooth and inclined tubes with particular reference to low mass fluxes was also given. It has been found that even though extensive research has been done on in tube condensation, studies were limited to condensation at high mass fluxes in smooth horizontal and vertical tubes. It was also found that there are gaps in the literature on low mass fluxes, the effect of temperature difference and inclination.

In previous studies, the results generated at low mass fluxes were generally secondary data and not part of the foci of those works. There has been no study to specifically determine the heat transfer coefficients and capture the flow regimes as functions of inclination, temperature differences and vapour quality.

Furthermore, despite its wide range of utilization and huge potential for future applications, little information is available on the thermal performance of inclined condensers at low mass fluxes. In fact, none has quantitatively and systematically investigated the effects of both tube inclination and temperature difference on the heat transfer coefficients and flow patterns in smooth tubes at low mass fluxes. This underscores the need for more data collection by employing empirical studies to help in this regard.

The other challenge is that there are contradictory reports on the recommended inclination angle for optimum heat transfer performance. This is further evidenced by the fact that there is no unifying correlation that can adequately predict the heat transfer coefficients in inclined smooth tubes. This may be attributed to the fact that the available models are either limited by tube size, working fluid, saturation temperature, mass flux, or tube orientation. It implies that further research needs to be carried out to develop more pressure drop correlations. Furthermore, the existing flow regime maps were also developed for either smooth or vertical tubes with none specifically for inclined tubes.

Overall, there needs to be a fundamental understanding between the relationship between temperature difference and inclination on heat transfer and pressure drops to enable designers optimize heat exchangers.

## Chapter 3: Experimental Set-Up

---

### 3.1. Introduction

The purpose of this chapter is to describe the experimental set-up which was used to conduct heat transfer, flow pattern and pressure drop experiments in the smooth horizontal and inclined tubes. An overview of the components of the experimental set-up, the test section, and the instrumentation used, is given. The experimental procedure and data reduction methods are also discussed. An overview of the uncertainty analysis is also given and the text matrix is discussed.

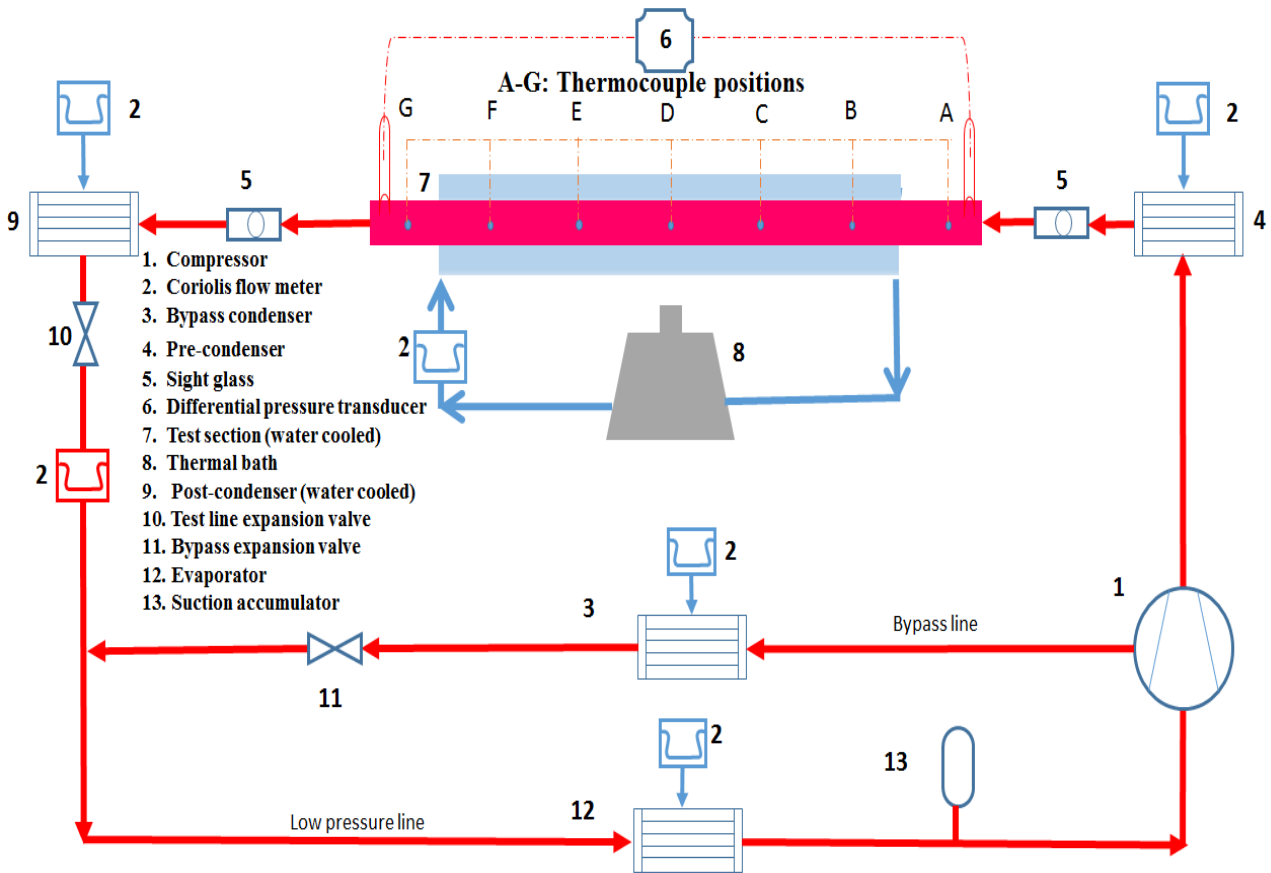
### 3.2. Experimental apparatus and procedure

The test bench used for this investigation is well established and has previously been used for condensation studies [4, 7-9, 18, 32, 33, 71, 76, 81, 92]. However, slight modifications were made to accommodate the low mass flux requirements of this study. The experimental test rig (Figure 3.1) and (Figure 3.2) for smooth and inclined tubes consisted of a vapour compression refrigerant cycle (red lines in the figure) and several water cycles (blue lines in the figure). The inclination angle ( $\beta$ ) of the test section could be varied in this study from  $-90^\circ$  (downwards flow) to  $90^\circ$  (upwards flow), with  $0^\circ$  (horizontal flow) as the reference. The inclination angles were measured with a digital inclinometer, which was calibrated to an accuracy of  $0.01^\circ$ .

The vapour compression cycle consisted of the test section line and the bypass line, which are both high-pressure lines, and a low-pressure line through which the R134a was pumped using a hermetic scroll compressor with a nominal capacity of 10 kW. Each of the lines had electronic expansion valves which controlled the mass flow rate of the refrigerant. The expansion valve in the test section line that was used in all previous work was replaced with an electronic expansion valve with a smaller valve port.

The test line had three condensers: the pre-condenser, the test condenser containing the test section, and the post-condenser. The pre-condenser was used to control the inlet vapour quality into the test section where the actual measurements and experiments were conducted. The post-condenser was used to ensure that complete condensation and subcooling occurred to ensure that only liquid flowed through the refrigerant mass flow meter. The bypass line had a bypass condenser that controlled the pressure, temperature, and mass flow rate of the refrigerant flowing into and through the test line. The majority of the refrigerant flowed through the bypass line with a smaller fraction through the test section line. The refrigerant from the two high-pressure lines was throttled in the electronic expansion

valves (EEV) into the low-pressure line, consisting of a water heated evaporator, suction accumulator, and a scroll compressor.



**Fig. 3.1: Schematic of the experimental set-up and test section (horizontal tube).**

The water that was used for the pre-condenser, post-condenser, and evaporator was stored and supplied from two storage tanks with capacities of 500 litres each. These tanks were kept at pre-selected temperatures and were thermostatically controlled to approximately 15°C and 40°C, respectively. These tanks were maintained at these constant temperatures because they were connected to a dual-function heat pump. The colder storage tank was connected to the pre- and post-condenser, and the warmer storage tank to the evaporator. A 1.5 kW thermal bath, with a 20-litre storage tank, was connected to the annulus of the test section. This thermal bath had a built-in pump and was operated with water inlet temperatures varying from 10 °C to 20 °C, depending on the required condensation experiments required in the test section.

The test section was a smooth copper tube that was assembled to correspond to a tube-in-tube heat exchanger configuration. The inner tube formed the test section in which the refrigerant flowed. The flow of water in the annulus was in a counter direction to that of the refrigerant. The water in the



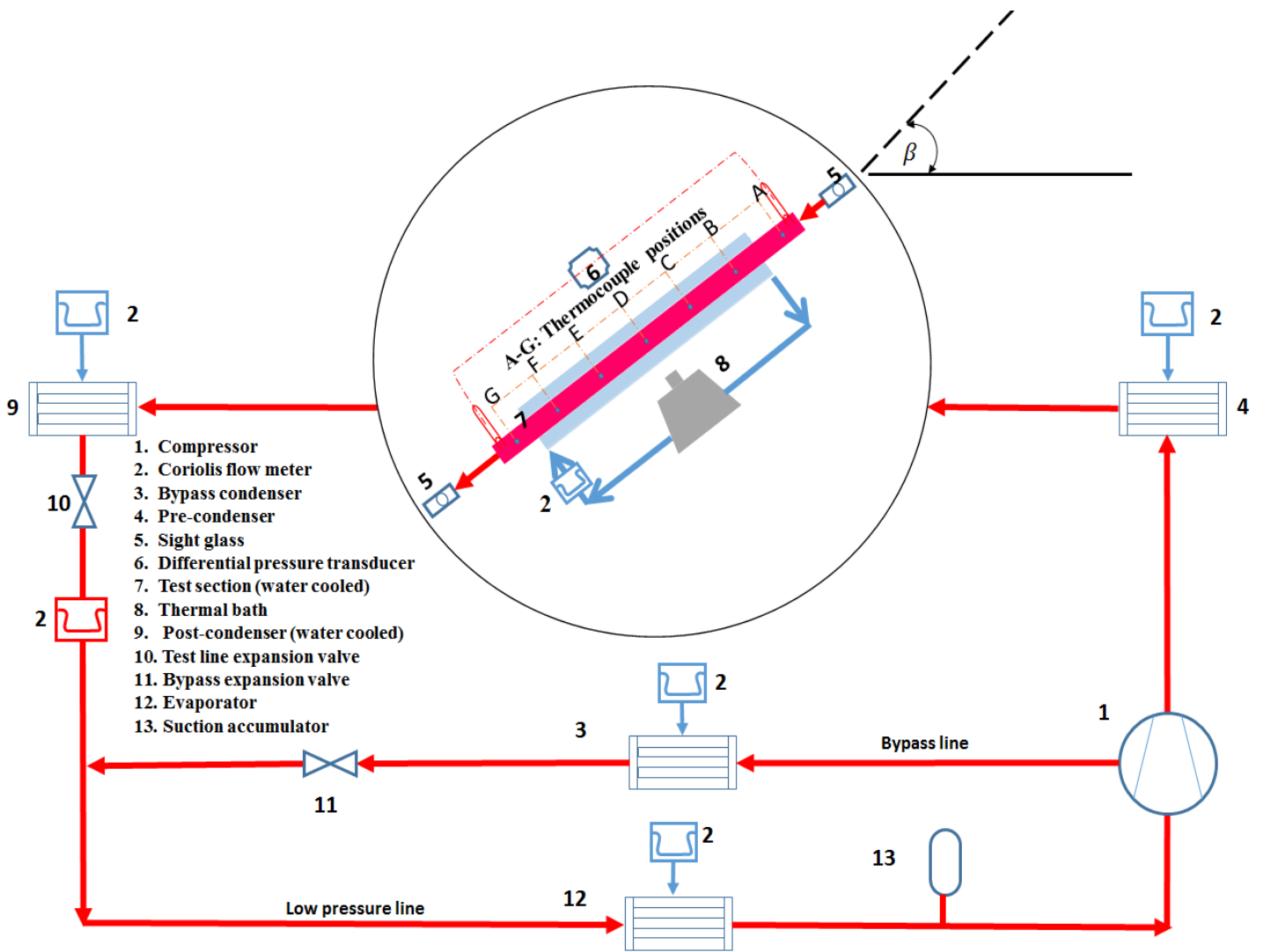
annulus was always operated at a temperature lower than that of the refrigerant gas, and therefore, condensation occurred on the inside of the test section tube.

The rate of condensation in the test section tube was manipulated with the refrigerant and/or water mass flow rates streams. The refrigerant stream was controlled by changing its mass flow rate, saturation temperature, and inlet quality. The refrigerant mass flow rate was controlled by opening the test section expansion valve. This also influenced the saturation temperature and pressure of the test section which was controlled with the opening or closing of the expansion valve of the bypass line and the water mass flow rate through the bypass condenser. It was found that the saturation values were more sensitive to water mass flow rate changes than changing the opening of the electronic expansion valve. Therefore, the water mass flow rate changes were mostly used to manipulate the saturation values close to the required values, while the expansion valve was used for precision control.

The vapour quality of the refrigerant before and after the test section was carefully controlled, as the overall test quality was defined as the average quality between the inlet and outlet qualities of the test section. This required quality was controlled by the water inlet temperatures and mass flow rates flowing through the annulus of the test section and flowing through the pre-condenser of the test section.

In the water stream through the test section, the mass flow rate and water inlet temperature were controlled. The mass flow rate of the water was controlled by two means. The first was adjusting the pump setting of the thermal bath while the other was the use of servo-actuated valves to control the flow through the test section while the remaining flow was bypassed to the bypass heat exchanger and immediately entered the return line back to the reservoirs. The water inlet temperature was set by changing the set point of the thermal bath. The refrigerant and water mass flow rates through the three condensers were measured with a Coriolis mass flow meter that could measure both the refrigerant and water mass flow rates with errors of less than 0.05%.

The test section inner tube was 1.49 m in length, with a measured inner diameter of 8.38 mm and an outer diameter of 9.54 mm. The annulus outer tube had an inner diameter of 14.5 mm and an outer diameter of 15.9 mm. The test section, pre-condenser, post-condenser, bypass-condenser, evaporator, and all refrigerant and water lines were insulated with 60 mm of a closed cell elastometric nitrile rubber that had a thermal conductivity of 0.039 W/mK to minimise heat losses to and from the environment.



**Fig. 3.2: Schematic of the experimental set-up and test section (inclined tube).**

Two sight glasses were installed at the inlet and outlet of the test section. The sight glasses had the same inner diameter as the test section and were made from borosilicate. The purposes of the sight glasses were twofold. First, they were used to prevent axial conduction from the test section inner tube to the connecting tubes at the inlet and outlet, as the thermal conductivities (1.2 W/mK) of the sight glasses were much lower than those of the copper tubes in the test section line. Second, they were used for visual observations, and to capture the flow patterns with video cameras. Videos were taken in grey levels. However, it was found that without a light emitting diode (LED), the flow could not be visualised properly as evidenced by a black cloud seen around the glass tube. Hence, to improve the image quality and ensure uniformity in the distribution of the light, a uniform (LED) backlight was used. This LED backlight was a 99% uniform, 50 by 50 mm red light. Furthermore, it was chosen to have a low energy output so that it did not thermally affect the passing flow. The flow regimes were captured with two different cameras. The camera at the inlet could capture videos at 200 frames per second, while the camera at the outlet was limited to 100 frames per second. Owing to the frames per

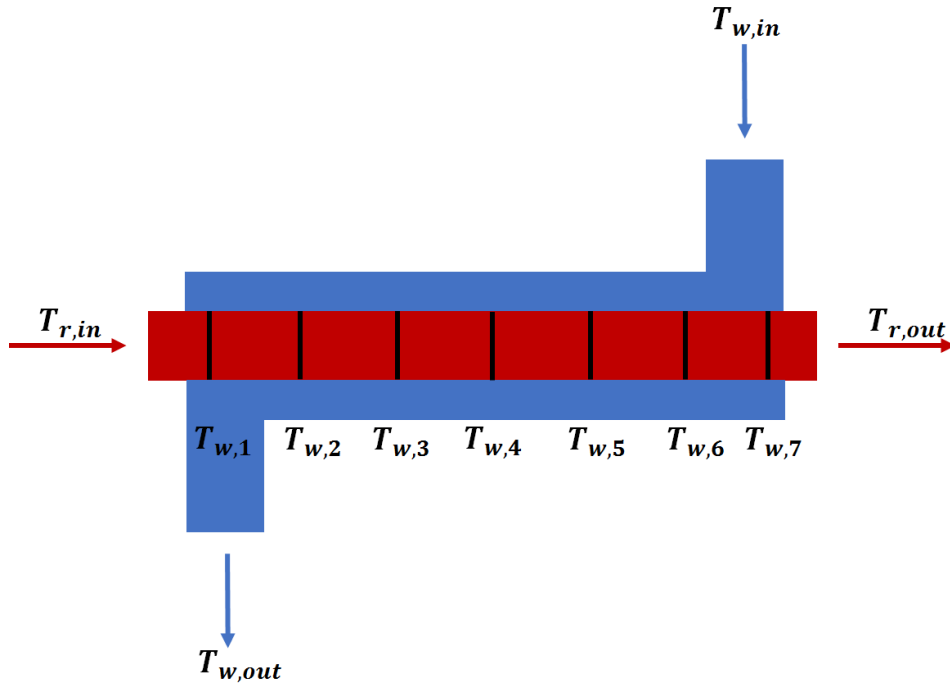
second limitation of the video camera at the outlet, the quality of the outlet videos was not as good as that of the inlet.

To ensure that the flow through the test condenser was fully developed, a straight calming section, 500 mm in length, and of the same diameter as the test section, was positioned upstream of the entrance to the test section (after the sight glasses). Another calming section which was 400 mm long and of the same diameter as the test section was positioned at the exit of the test condenser to minimise the disturbance at the exit sight glass.

The absolute pressures at the inlet and outlet of the test sections were measured with absolute pressure transducers that were connected to pressure taps at the inlet and outlet of the test section. The inaccuracies of the absolute pressure measurements were  $\pm 2$  kPa. The pressure drop over the test section was measured with a calibrated differential pressure drop transducer, which was also connected to two different pressure taps at the inlet and outlet of the test section.

On the outside surface of the test section tube, 28 shallow holes were drilled at seven stations marked A to G, as shown in Figure 3.1. The first station at A was at a distance of 70 mm from the inlet, and the subsequent spacing between all the other stations was 225 mm. Each station had four shallow drilled holes at equal distances around the circumference. In each hole, a 1.3 mm diameter, T-type thermocouple used for outside wall temperature measurements was attached by soldering. The cooling water inlet and outlet temperatures were also measured as the average of three thermocouples mounted on the wall of the inlet and outlet of the annulus that surrounded the test section tube. The same was done with the average inlet and outlet water temperatures at the pre- and post-condensers. Care was taken to ensure that the mass flow rates of all cooling water channels were operated in the turbulent flow regime to ensure that the wall temperature measurement represented the average water temperatures. Fig. 3.3 shows a schematic of the measurement points in the test section.

The refrigerant temperatures were measured at four stations on the outside walls of the tubes. These were at the inlet and outlet of the test section, and at the inlet of the pre-condenser and outlet of the post condenser. These measurements were continuously correlated with the saturation temperatures indirectly obtained from the pressure measurements of the two absolute pressure transducers. These differences were never more than 0.1 °C. All the thermocouples used were calibrated before the start of the experimental programme against a calibrated PT100 to an accuracy of  $\pm 0.1$  °C.



**Fig. 3.3: Schematic of the measurement points in the test section.**

The refrigerant pressure at the inlet to the test condenser was measured with a strain gauge pressure transducer to an accuracy of  $\pm 2$  kPa for mass fluxes between  $50 - 200$  kg/m<sup>2</sup>s. To determine its accuracy, the measured pressure value was cross-checked with the corresponding saturation temperature on the condensation saturation curve provided by REFPROP [249]. The variation in the two values was found to be less than  $0.1^\circ\text{C}$  at high mass fluxes ( $300$  kg/m<sup>2</sup>s and above) and high vapour qualities while a higher difference was observed at mass fluxes lower than  $200$  kg/m<sup>2</sup>s and low vapour qualities. This, however, might be caused by the nature of the prevailing flow pattern at low mass fluxes.

Two calibrated differential pressure transducers with diaphragm capacities of  $0.86$  kPa and  $14$  kPa connected in parallel between the entrance and the exit of the test condenser were used to measure the pressure drops. The sizes of the diaphragms were carefully chosen and were calibrated to an error of  $\pm 0.05$  kPa. The distance between the two pressure taps was  $L_{\Delta P} = 1710$  mm  $\pm 2$  mm. Electrical heating wires were wrapped around the pressure tap lines and heated to approximately  $5^\circ\text{C}$  above the condensation temperature to prevent condensation in the lines. This was similar to the method of Cavallini *et al.* [83], Lips and Meyer [7, 18, 71, 72] and Adelaja *et al.* [8, 9, 33, 92].

All measurements of temperatures, pressures, and mass flow rates were taken at steady state conditions. These measurements were taken when no more fluctuations of these measured values occurred for a period of five minutes, and the energy balance (*EB*), as determined was less than  $5\%$  and also constant for a period of five minutes. A summary of the operating conditions and average

energy balances of all experiments are shown in Table 3.1. The energy balances of all experiments varied between a minimum of 0.2% and a maximum of 5.2%. The average energy balance was 2.1% with a standard deviation of 1.2%.

**Table 3.1: Operating conditions and average energy balances for the experimental matrix**

<b>Parameter</b>	<b>Average</b>	<b>Minimum</b>	<b>Maximum</b>	<b>Standard deviation</b>
Condensation temperature	40.0 °C	39.6 °C	40.5 °C	0.28 °C
Saturation pressure	1 052 kPa	1 031 kPa	1 074 kPa	9.8 kPa
Energy balance	2.1%	0.2%	5.2%	1.2%

All measurements were collected with a data acquisition arrangement which comprised of a desktop computer with LabVIEW software. Furthermore, embedded in the data acquisition system were terminal blocks, channel multiplexers, termination units, transducer multiplexers, an interface card, and signal-conditioning extensions for instrumentation. The readings were captured for 360 s (201 points) at 0.56 Hz, and the averages of all 201 measurement points were used. The standard deviations of these points were monitored continuously. A detailed list of the equipment used by the LabVIEW software in the experimental set-up is given in Table 3.2.

At low refrigerant mass fluxes, the heat transfer rates were very low, and it was, therefore, very challenging to take a large number of measurements, as it took at least 90 minutes before steady-state conditions were reached once a small adjustment was made to obtain data at another experimental point. Furthermore, the required temperature differences between the condensing wall and refrigeration saturation temperature that varied between 3–10°C, was carefully adjusted with errors of less than  $\pm 0.1^\circ\text{C}$ . The required inlet qualities were also carefully adjusted so that the errors in inlet qualities were less than 5%. When the system was shut down and restarted, it took approximately two hours before steady-state conditions were reached for the first time and the first experiment of the day could be conducted.

The oil concentration in the refrigerant was measured by Suliman *et al.* [81] in a previous study using the ASHRAE Standard [250] and was determined to be 1.8% on average. The maximum measured was 2.3% and only occurred at much higher mass fluxes of 700 kg/m<sup>2</sup>s, which was much higher than the range considered in this study. In these studies, it was shown that the presence of oil had a negligible effect on the results presented.

**Table 3.2: Equipment used by LabVIEW in the experimental test rig**

Measurable	Equipment	Range of applicability
Temperature	T-type thermocouple wire <i>Omega</i> , UK, 30-gauge	-30 – 300 °C
Pressure Sensors		
Low	<i>Gems Sensor</i> , UK	0 – 2000 kPa
High	<i>Gems Sensor</i> UK	0 – 2000 kPa
Test	<i>FP Sensotec</i> , USA	0 – 2000 kPa
Differential	<i>Validyne</i> , USA	0 – 14 kPa
Mass flow rate		
Water	Coriolis flow meter: <i>Micro Motion Inc.</i> , USA Flow meter: <i>Bürkert</i> , Germany	CMF 010 (0.4 kg/s) max CMF 025 (0.6 kg/s) max DIN 025 (1.8 kg/s) max DIN 025 (1.8 kg/s) max
Refrigerant	Coriolis flow meter: <i>Micro Motion Inc.</i> , USA	CMF 010 (0.4 kg/s) max
Expansion valves		
Test line	<i>Carel</i> EEV-05 <i>Carel</i> EEV-09	4 –20 mA 4 –20 mA
Bypass line	<i>Carel</i> EEV-014 <i>Carel</i> EEV-024 <i>Carel</i> , Italy	4 –20 mA 4 –20 mA
Data acquisition	<i>National Instruments</i> , USA	
Temperature	SCXI-1102:32-Channel Multiplexer	± 10 V, 4 –20 m A inputs 250 kS/s single channel sampling rate
Pressure and Mass flow	SCXI-1102:32-Channel Multiplexer	± 10 V, 4 –20 m A inputs 250 kS/s single channel sampling rate
Control	SCXI-1124:6- Channel low- bandwidth output module	±10 V, 4 –20 mA outputs
Flow visualization		
Camera	Basler A601f high- speed camera	
Lens	µTron FV 2520	25 mm, f/2 lens
Backlight	<i>Phlox</i> 50 mm x 50mm red 98.7% even lighting LED backlight	99 % even lighting
Capture software	Pylon viewer	

### 3.3. Data reduction

The heat transfer rate,  $\dot{Q}_{r,pre}$ , of the condensing refrigerant was assumed to be equal to the water side heat transfer rate,  $\dot{Q}_{w,pre}$  (Eq. (3.1)). It was determined from the measured water mass flow rate,  $\dot{m}_{w,pre}$ , through the pre-condenser and the measured average water inlet,  $T_{w,pre-in}$ , and outlet temperatures,  $T_{w,pre-out}$ :

$$\dot{Q}_{w,pre} = \dot{Q}_{r,pre} = \dot{m}_{w,pre} C_{p,w} (T_{w,pre-out} - T_{w,pre-in}) \quad (3.1)$$

The specific heat values of the water,  $C_{p,w}$ , were obtained from REFPROP [249] using the average of the measured inlet- and outlet water temperatures through the pre-condenser. The heat transfer rates through the test section and post-condensers were determined similarly:

$$\dot{Q}_{w,test} = \dot{Q}_{r,test} = \dot{m}_{w,test} C_{p,w} (T_{w,test-out} - T_{w,test-in}) \quad (3.2)$$

and

$$\dot{Q}_{w,post} = \dot{Q}_{r,post} = \dot{m}_{w,post} C_{p,w} (T_{w,post-out} - T_{w,post-in}) \quad (3.3)$$

The enthalpy value of the refrigerant at the outlet of the pre-condenser,  $h_{r,pre-out}$ , was determined as

$$\dot{Q}_{w,pre} = \dot{m}_{r,pre} (h_{r,pre-in} - h_{r,pre-out}) \quad (3.4)$$

The value of  $h_{r,pre-out}$  could be determined from Eq. (3.4), as  $\dot{Q}_{w,pre}$  was determined from Eq. (3.1).  $\dot{m}_{r,pre}$  was the measured mass flow rate of the refrigerant through the pre-condenser, and  $h_{r,pre-in}$  was the specific enthalpy of the refrigerant at the inlet to the pre-condenser (acquired from REFPROP [249] using the measured temperature and pressure conditions at the inlet to the pre-condenser).

The enthalpy values of the refrigerant at the outlet of the test-condenser,  $h_{r,test-out}$ , and outlet of post-condenser,  $h_{r,post-out}$ , were determined similarly:

$$\dot{Q}_{w,test} = \dot{m}_{r,test} (h_{r,test-in} - h_{r,test-out}) \quad (3.5)$$

and

$$\dot{Q}_{w,post} = \dot{m}_{r,post} (h_{r,post-in} - h_{r,post-out}) \quad (3.6)$$

As the post condenser was always operated to ensure fully condensed liquid at its outlet, the outlet enthalpy values,  $h_{r,post-out}$ , determined from Eq. (3.6) were cross-checked with enthalpy values obtained from REFPROP [249] using the measured refrigerant pressure and temperatures values at the exit of the pre-condenser.

The total water side heat transfer rate,  $\dot{Q}_{w,tot}$ , was determined as

$$\dot{Q}_{w,tot} = \dot{Q}_{w,pre} + \dot{Q}_{w,test} + \dot{Q}_{w,post} \quad (3.7)$$

while the total condensing refrigerant heat transfer rate,  $\dot{Q}_{r,tot}$ , was determined as

$$\dot{Q}_{r,tot} = \dot{m}_r (h_{r,pre-in} - h_{r,post-out}) \quad (3.8)$$

In Eq. (3.8),  $\dot{m}_r$  was the measured refrigerant mass flow rate through the test line, which was the same refrigerant mass flow rate through the pre-condenser as well as through the post-condenser; thus,  $\dot{m}_r = \dot{m}_{r,pre} = \dot{m}_{r,test} = \dot{m}_{r,post}$

The relative differences in heat transfer rates between the water and refrigerant sides were then compared in the format of an energy balance (*EB*) as follows:

$$EB = \frac{|\dot{Q}_{r,tot} - \dot{Q}_{w,tot}|}{\dot{Q}_{r,tot}} \quad (3.9)$$

The inlet vapour qualities,  $x_{in}$ , of the refrigerant at the test section inlet were determined as:

$$x_{in} = \frac{h_{r,test-in} - h_l}{h_v - h_l} \quad (3.10)$$

The saturated vapour and liquid values of the specific enthalpies,  $h_v$  and  $h_l$ , respectively, were obtained from REFPROP using the average of the measured test section inlet and outlet refrigerant temperatures, and/or average of the measured inlet and outlet refrigerant absolute pressures. It was found that the values obtained from either the measured pressures and temperatures correlated to saturation temperature differences of less than 0.1 °C from each other.

The outlet vapour qualities,  $x_{out}$ , of the refrigerant at the test section outlet were determined similarly as:

$$x_{out} = \frac{h_{r,test-out} - h_l}{h_v - h_l} \quad (3.11)$$

With the inlet and outlet qualities of the test section known, the mean qualities,  $x_m$ , were taken as the average between the inlet and outlet qualities:

$$x_m = \frac{x_{out} + x_{in}}{2} \quad (3.12)$$

For all experiments, while the enthalpies and qualities were determined, the outside wall temperatures,  $\bar{T}_{w,o}$ , were determined as the average measured wall temperatures obtained from the trapezium



integration technique of the 28 thermocouple measurements at seven different stations (Fig. 3.3) on the outside of the tube.

$$\bar{T}_{w,o} = \frac{1}{L} \sum_{j=1}^7 [(T_{w,o}^j + T_{w,o}^{j+1})(z_{j+1} - z_j)] \quad (3.13)$$

At each of the seven stations, the average station temperatures were taken as the average of the four thermocouple measurements around the perimeter of the test section tube.

The average temperatures on the inside of the test section wall,  $\bar{T}_{w,i}$ , were determined by using the outside wall tube temperature measurements,  $\bar{T}_{w,o}$ , and taking into consideration the heat transfer rate through the wall,  $\dot{Q}_{w,test}$ , and the thermal wall resistance,  $R_w$ , of the wall:

$$\bar{T}_{w,i} = \bar{T}_{w,o} + |\dot{Q}_{w,test} R_w| \quad (3.14)$$

The thermal wall resistance was determined as:

$$R_w = \frac{\ln(d_o/d_i)}{2\pi k_{cu} L} \quad (3.15)$$

where  $d_o$  and  $d_i$  were respectively the measured outside and inside diameters of the test section,  $k_{cu}$  was the thermal conductivity of the test section which was made from copper, and the measured length,  $L$ , of the test section tube.

It was found that the wall thermal resistances were negligible in all cases, as the differences between the inside and outside tube walls were all less than the errors ( $0.1^\circ\text{C}$ ) of the temperature measurements. Therefore, it was found that the average wall temperature measurements in Eq. (3.13) on the outside of the wall were equal to the inside wall temperatures required in Eq. (3.14).

The “*temperature differences*” referred to in this paper used for the heat transfer coefficient calculations were:

$$\Delta T = T_{sat} - \bar{T}_{w,i} \quad (3.16)$$

They referred to the temperature difference between the refrigerant saturation temperatures,  $T_{sat}$ , and average wall inner temperatures,  $\bar{T}_{w,i}$ , of the test section determined by Eq. (3.14). The saturation temperatures were taken as the average between the measured inlet,  $T_{r,in}$  and outlet refrigerant temperature  $T_{r,out}$ , measurements of the test section (Fig. 3.3). This saturation temperature also corresponded to within  $0.1^\circ\text{C}$  of the saturation temperature that was implicitly determined from REFPROP when the measured absolute saturation pressure measurements taken from the average of the inlet and outlet test section pressure measurements were used.

With the heat transfer rates known, the average heat transfer coefficients,  $\alpha$ , of the condensing refrigerant in the test section were determined as:

$$\alpha = \frac{\dot{Q}_{w,test}}{A_i \Delta T} \quad (3.17)$$

The heat transfer rates,  $\dot{Q}_{w,test}$ , of the water side of the test section were used to determine the heat transfer coefficients, not the refrigerant heat transfer rates,  $\dot{Q}_{r,test}$ . The uncertainties of the refrigerant rate depended on the uncertainties of the inlet and outlet enthalpies whose uncertainties further depended on the uncertainties of the inlet and outlet vapour qualities which were approximately 5%. However, the uncertainties of the heat transfer rate on the water side,  $\dot{Q}_{w,test}$ , was 3%. The internal surface area ( $A_i = \pi d_i L$ ) of the test section of the test tube was determined from the measured tube inlet diameter  $d_i$ , which was 8.38 mm, and measured test section length over which the heat transfer occurred,  $L$ , which was 1.49 m.

Lastly, since the heat transfer coefficients were mass flux dependent, the corresponding mass fluxes were determined as:

$$G = \frac{\dot{m}_{r,test}}{A_{CS}} \quad (3.18)$$

where the test section cross-sectional area was determined as  $A_{CS} = (\pi/4)d_i^2$ .

The nomenclature used and data reduction for heat transfer in smooth tubes and inclined tubes were practically the same. The only new term introduced is the inclination effect, ( $I_\alpha$ ) defined by Lips and Meyer [72], as:

$$I_\alpha = \frac{\alpha_{max} - \alpha_{min}}{\alpha_{\beta=0}} \quad (3.19)$$

In Eq. 3.19,  $\alpha_{max}$  and  $\alpha_{min}$  are the maximum and minimum heat transfer coefficients obtained for a specific mass flux and mean vapour quality for the various angles of inclination. Furthermore,  $\alpha_{\beta=0}$  is the heat transfer coefficient obtained for the horizontal orientation.

The pressure drops were determined as was done by Adelaja *et al.* [8]. The frictional pressure drops were calculated as:

$$\Delta P_{fri} = \Delta P_{meas} + \Delta P_{line} - \Delta P_{mom} - \Delta P_{stat} \quad (3.20)$$

The measured pressure drops,  $\Delta P_{meas}$ , were obtained directly from the transducer pressure drop measurements.  $\Delta P_{line}$  was the measured line pressure drop difference due to the height difference as a result of varying the angles of inclination. The line pressure drop is important because it measures the

static pressure difference effect due to the vapour that was trapped in the pressure lines. It was calculated as:

$$\Delta P_{line} = \rho_v g L_{\Delta P} \sin \beta \quad (3.21)$$

where,  $\rho_v$  was the refrigerant vapour density obtained from the measured saturation temperature and REFPROP [249]. The gravitational acceleration was taken as  $9.81 \text{ m/s}^2$ .  $L_{\Delta P}$ , was the measured distance (1.71 m) between the two pressure taps and,  $\beta$ , was the measured inclination angle of the test section. The inclination angle was taken from the horizontal. The inclination angle was considered as positive for upward inclinations, zero for horizontal inclinations, and negative for downward inclinations. For horizontal flow ( $\beta = 0^\circ$ ) which implies that  $\sin \beta = 0^\circ$ , which means that  $\Delta P_{line} = 0$ .

The static pressure drops,  $\Delta P_{stat}$ , caused by the difference in height from one side to the other side in the test section were dependent on inclination angle and were calculated as:

$$\Delta P_{stat} = \rho_{tp} g L_{\Delta P} \sin \beta \quad (3.22)$$

From Eq. 3.22, it can be deduced the static pressure drop reduces to zero for horizontal flow ( $\beta=0^\circ$ ) scenarios. In the equation,  $\rho_{tp}$  represents the two-phase density and was determined as recommended by [251-255]. This expression represents a homogenous model and was calculated as:

$$\rho_{tp} = \rho_l (1 - \varepsilon) + \rho_v \varepsilon \quad (3.23)$$

From Eq. 3.24, the surface tension,  $\sigma$ , the liquid phase density,  $\rho_l$ , and the vapour phase density,  $\rho_v$ , were all determined at the measured condensation temperature (which was cross checked against the measured saturation pressure) with REFPROP [249]. The void fraction,  $\varepsilon$ , for horizontal and inclined flows respectively, were calculated using the Steiner versions of the drift-flux model of the Rouhani and Axelsson model [169, 170] as:

$$\varepsilon_{rh} = \frac{x}{\rho_v} \left[ 1 + 0.12(1 - x) \left( \frac{x}{\rho_v} + \frac{1 - x}{\rho_l} \right) + \frac{1.18(1 - x)(g\sigma(\rho_l - \rho_v))^{0.25}}{G^2 \rho_l^{0.5}} \right]^{-1} \quad (3.24)$$

$$\varepsilon_{rh} = \frac{x}{\rho_v} \left[ \left[ 1 + 0.2(1 - x) \left( \frac{gd\rho_l^2}{G^2} \right)^{0.25} \right] \left( \frac{x}{\rho_v} + \frac{1 - x}{\rho_l} \right) + \frac{1.18(1 - x)(g\sigma(\rho_l - \rho_v))^{0.25}}{G^2 \rho_l^{0.5}} \right]^{-1} \quad (3.25)$$

It should be noted that Bhagwat and Ghajar [248] developed a flow pattern independent drift flux model based void fraction correlation for a wide range of gas-liquid two-phase flows suitable for inclined tubes. However, when comparing their void fraction predictions with that of Rouhani

and Axelsson, it was found that the average deviation was less than 3% which translated to a negligible deviation of about 1% in the calculated measured pressure drops. Hence, we opted to use the models listed in Eqs. (3.24 and 3.25) because of its simplicity and longevity.

Finally, the momentum pressure drop was calculated making use of the void fraction calculations as recommended by Carey [256] as:

$$\Delta P_{mom} = G^2 \left[ \left( \frac{(1-x)^2}{\rho_l(1-\varepsilon)} + \frac{x^2}{\rho_v\varepsilon} \right)_{out} - \left( \frac{(1-x)^2}{\rho_l(1-\varepsilon)} + \frac{x^2}{\rho_v\varepsilon} \right)_{in} \right] \quad (3.26)$$

The mass flux,  $G$ , was calculated from the measured refrigerant mass flow rate and the cross-sectional area of the test section. The vapour qualities were determined as described in our previous works [52, 54, 167]. Furthermore, the temperature differences ( $\Delta T$ ) referred to in this paper are the temperature differences between the average refrigerant saturation temperature,  $T_{sat}$ , and the average inner wall temperature,  $\bar{T}_{w,i}$ , as explained in refs. [52, 54, 167]. The operating conditions and average energy balances (as defined in refs [52, 54] for the experimental matrix is given in Table 3.3.

### 3.4. Uncertainty analysis and repeatability

An uncertainty analysis (Appendix A) was conducted as prescribed by Dunn [257], based on the experimental parameters and uncertainties given in Table 3.3. The results showed that, in the range over which experiments were conducted, the uncertainties were 1%, 5%, and 10% for the mass fluxes, qualities, and heat transfer coefficients, respectively, at a specific mean quality. Two challenges were encountered during the generation of results. First, because of the low mass fluxes, the heat transfer rates in the test section were low, and varied as low as 170 W. Second, in many cases, the changes in quality values from the inlet to outlet were significant. This can be solved by using a shorter test section length. However, then the heat transfer rates decrease even further and the uncertainties would increase significantly. For example, decreasing the test section length by 50% would have increased the uncertainties of the heat transfer coefficients to 18%.

**Table 3.3: Experimental parameters, ranges, and uncertainties**

Parameter	Range	Uncertainties
$T_{sat}$	40 °C	± 0.1 °C
$G$	50 – 200 kg/m <sup>2</sup> s	± 1%
$x_m$	0.1 – 0.9	± 5%
$\alpha$	1 300 – 3 300 W/m <sup>2</sup> K	± 10%
$\dot{Q}_w$	170 – 600 W	± 1%
$\Delta P$	0 – 9 kPa	±8%
$\beta$	-90 – 90°	±0.1%

The repeatability of the measured results of the condensation heat transfer coefficients and pressure drops was established by repeating a selection of approximately 60% of the results three months later. The maximum percentage differences in the heat transfer coefficients and pressure drops when the experiments were repeated was about 2%. The maximum differences were found at a vapour mass flux of 50 kg/m<sup>2</sup>s, qualities below 0.25 and inclination angles of +90° and -90°.

### **3.5. Test matrix for smooth tubes**

Table 3.4 shows the test matrix of the experiments that were carried out at mass fluxes of 200, 150, 100, 75 and 50 kg/m<sup>2</sup>s at different temperature differences,  $\Delta T$ , and average qualities,  $x_m$ . A total of 97 experimental data points were produced. The average saturation temperature of all the measurements conducted was at a condensing temperature of 40 °C, with a standard deviation of just less than approximately 0.3 °C.

At a mass flux of 200 kg/m<sup>2</sup>s, 24 measurements were taken at six different qualities of 0.10, 0.25, 0.50, 0.62, 0.75, and 0.9, and at four different temperature differences of 3, 5, 8, and 10 °C. At a mass flux of 150 kg/m<sup>2</sup>s, 24 measurements were taken at the same experimental conditions as those taken at 200 kg/m<sup>2</sup>s. At mass fluxes of 100 kg/m<sup>2</sup>s, 75 kg/m<sup>2</sup>s, and 50 kg/m<sup>2</sup>s, the number of experimental conditions at which experiments were conducted was 31, 11, and 7, respectively. The experimental conditions at which experiments could be conducted therefore decreased with mass flux. This was because the changes in quality from the test section inlet to outlet increased. To prevent this from occurring, the mass flow rate through the water in the annulus and/or water inlet temperature to the annulus can be altered. However, it has been found that the heat transfer rates became too low, and the uncertainties of the heat transfer coefficients became too high.

### **3.6. Test matrix for inclined tubes**

The in-tube condensation heat transfer experiments were carried out at a condensation temperature of 40 °C, and mass fluxes of 50, 75, and 100 kg/m<sup>2</sup>s, at different temperature differences, inclination angles, and mean vapour qualities. The inlet and outlet flow regimes were also captured and all the results are shown in Figs. 6.1 – 6.8. Where relevant, the heat transfer coefficients were the averaged over the test section length.

The approximate mass fluxes, vapour qualities, and temperature differences are presented in an experimental matrix in Table 3.5, which shows that 900 experimental data points were produced. At a mass flux of 100 kg/m<sup>2</sup>s, it was possible to take 375 measurements: 15 different inclination angles of -90°, -60°, -45°, -30°, -15°, -10°, -5°, 0°, 5°, 10°, 15°, 30°, 45°, 60°, and 90° and at five different

**Table 3.4: Summary of experimental test points for smooth tubes**

	<b><math>G = 150</math> and <math>200 \text{ kg/m}^2\text{s}</math></b>				
<b>Mean vapour quality</b>	<b><math>\Delta T = 3 \text{ }^\circ\text{C}</math></b>	<b><math>\Delta T = 5 \text{ }^\circ\text{C}</math></b>	<b><math>\Delta T = 8 \text{ }^\circ\text{C}</math></b>	<b><math>\Delta T = 10 \text{ }^\circ\text{C}</math></b>	
$x_m$	0.1	0.1	0.1	0.1	
$x_m$	0.25	0.25	0.25	0.25	
$x_m$	0.5	0.5	0.5	0.5	
$x_m$	0.62	0.62	0.62	0.62	
$x_m$	0.75	0.75	0.75	0.75	
$x_m$	0.9	0.9	0.9	0.9	
					<b>Sub-total = 48 points</b>
	<b><math>G = 100 \text{ kg/m}^2\text{s}</math></b>				
<b>Mean vapour quality</b>	<b><math>\Delta T = 3 \text{ }^\circ\text{C}</math></b>	<b><math>\Delta T = 5 \text{ }^\circ\text{C}</math></b>	<b><math>\Delta T = 8 \text{ }^\circ\text{C}</math></b>	<b><math>\Delta T = 10 \text{ }^\circ\text{C}</math></b>	
$x_m$	0.1	0.15	0.25	0.3	
$x_m$	0.17	0.22	0.3	0.4	
$x_m$	0.25	0.25	0.35	0.45	
$x_m$	0.41	0.3	0.41	0.52	
$x_m$	0.45	0.35	0.43	0.62	
$x_m$	0.60	0.38	0.5		
$x_m$	0.75	0.41	0.55		
$x_m$	0.82	0.5	0.62		
		0.55			
		0.6			
					<b>Sub-total = 31 points</b>
	<b><math>G = 75 \text{ kg/m}^2\text{s}</math></b>				
<b>Mean vapour quality</b>	<b><math>\Delta T = 3 \text{ }^\circ\text{C}</math></b>	<b><math>\Delta T = 5 \text{ }^\circ\text{C}</math></b>	<b><math>\Delta T = 8 \text{ }^\circ\text{C}</math></b>		
$x_m$	0.25	0.25	0.3		
$x_m$	0.3	0.5	0.5		
$x_m$	0.43	0.62	0.62		
$x_m$	0.5				
$x_m$	0.62				
					<b>Sub-total = 11 points</b>
	<b><math>G = 50 \text{ kg/m}^2\text{s}</math></b>				
<b>Mean vapour quality</b>	<b><math>\Delta T = 3 \text{ }^\circ\text{C}</math></b>	<b><math>\Delta T = 5 \text{ }^\circ\text{C}</math></b>			
$x_m$	0.25	0.35			
$x_m$	0.35	0.5			
$x_m$	0.62	0.62			
$x_m$	0.75				
					<b>Sub-total = 7 points</b>
					<b>Total = 97 points</b>

temperature differences of 1, 3, 5, 8, and 10 °C with mean vapour qualities varying between 0.25 and 0.9. At a mass flux of 75 kg/m<sup>2</sup>s, it was possible to take 300 measurements at 15 different inclination angles between -90° and 90° and four different temperature differences of 1, 3, 5, and 8 °C with mean

vapour qualities varying between 0.10 and 0.9. At a mass flux of 50 kg/m<sup>2</sup>s, it was possible to take 225 measurements at 15 different inclination angles between -90° and 90° and at temperature differences of 1, 3, and 5 °C with mean vapour qualities of 0.10 – 0.90. The measurement points that could not be produced were specifically at lower qualities and the resolution between the different qualities decreased. The challenges at these points were high-temperature differences between the temperatures of the condensing refrigerant at the inlet and outlet of the test section.

**Table 3.5: Summary of experimental test points for inclined tubes**

$G$	$\Delta T$	$x_m$	$\beta$	Points
[kg/m <sup>2</sup> s]	[°C]	[-]	[°]	
50	1, 3, 5	0.10, 0.25, 0.5, 0.62, 0.75, 0.9	-90, -60, -45, -30, -15, -10, -5, 0, 5, 10, 15, 30, 45, 60, 90	<b>225</b>
75	1, 3, 5, 8	0.10, 0.25, 0.5, 0.62, 0.75, 0.9	-90, -60, -45, -30, -15, -10, -5, 0, 5, 10, 15, 30, 45, 60, 90	<b>300</b>
100	1, 3, 5, 8, 10	0.10, 0.25, 0.5, 0.62, 0.75, 0.9	-90, -60, -45, -30, -15, -10, -5, 0, 5, 10, 15, 30, 45, 60, 90	<b>375</b>
				<b>Total = 900</b>

### 3.7. Summary and conclusion

This chapter gave a broad overview of the two-phase experimental setup and all its appendages. It highlighted the system requirements and distinct cycles in the system. It detailed the test section, testing procedure, LabVIEW, instrumentation, control methodology and the data reduction methodology. Experiments were conducted using a smooth and inclined tube condensation of R134a at low mass fluxes in smooth horizontal and inclined tubes with an internal diameter of 8.38 mm and a length of 1.49 m. The refrigerant mass flux was varied between 500 and 200 kg/m<sup>2</sup>s and water was used as the cooling fluid in the annulus of the test section. The wall temperatures were measured at 28 thermocouple stations. Two calibrated differential pressure transducers with diaphragm capacities of 0.86 kPa and 14 kPa connected in parallel between the inlet and the outlet of the test condenser over a length of 1.71 m were used to measure the pressure drops. The flow patterns were captured concurrently with two high-speed video cameras positioned at the entrance and exit of the test section through sight glasses. The test section was adequately insulated and the maximum heat loss was found to be less than 3%.

The experimental set-up was very complex and any change in the system settings affected all other parameters; hence it required skill and patience to manoeuvre the system until the desired testing points were reached. The measurements were only taken once there was no significant increase or decrease in temperatures, pressure drops and mass flow rates, within a period of approximately 120 seconds. It

was necessary to have control over the working pressures, temperature difference, mass flux, saturation temperature, energy balance and mean vapour quality.

To control the test line mass flux, the amount of refrigerant bypassed or entering the test line must be adjusted using the installed electronic expansion values; these adjustments led to changes in the general back pressure in the lines. Adjustments made in the electronic expansion valve settings required enough settling and response time. There was a combination of ways to control the system pressure. For instance, the modification of the bypass line electronic expansion valve setting led to the correct condensation pressure in the system. Hence, when the condensation pressure needed to be increased, the bypass electronic expansion valve was closed. To achieve the same effect, the bypass condenser water could also be used. From experience, the system reacted more to small water flow changes than medium electronic expansion value setting changes. This made the use of the electronic expansion valve as a precision control necessary and the water bypass water for approximate settings. Changes in the system settings were always gradual because substantial changes impinged upon the system pressure. As a last – ditch effort when the system was in danger of tripping off on high pressure, the bypass condenser water supply valve was always opened by a significant amount. This immediately decreased the pressure of the system. If the system was in danger of tripping on low pressure, the bypass electronic expansion valve, as well as the bypass condenser water valves, were closed.

An uncertainty analysis was conducted. It was found that the maximum uncertainties were 1%, 5%, and 1% for the mass fluxes, qualities, and heat transfer rates respectively. It was also found that the maximum uncertainty for the measured pressure drop and heat transfer coefficients were 9% and 10% respectively. Second, in many cases, the changes in quality values from the inlet to outlet were significant. This could have been solved by using a shorter test section length. However, the heat transfer rates would have decreased even further and the uncertainties would have increased significantly. For example, reducing the test section length by 50% would have increased the uncertainties of the heat transfer coefficients to about 18%. To conclude, a repeatability analysis was also carried out wherein a selection of approximately 60% of the experiments were repeated three months later to check possible drift in measurements, and the differences in results were compared. The maximum percentage differences of the measured heat transfer coefficients and pressure drops when the tests were repeated, was about 5%. This maximum difference was found at a vapour mass flux of  $50 \text{ kg/m}^2\text{s}$ , qualities below 0.25 and inclination angles of  $+90^\circ$  and  $-90^\circ$ .



# Chapter 4: Validation

---

## 4.1. Introduction

The purpose of this chapter is to validate the integrity of our experimental set-up. The gains of this chapter will ensure that the results of the experiments to be presented in the succeeding sections will be used with a very high confidence level. Validation for condensation heat transfer coefficients, flow pattern visualisation, and pressure drop experiments conducted for mass fluxes between 100 and 400 kg/m<sup>2</sup>s will be presented.

## 4.2. Validation of heat transfer coefficients in horizontal tubes

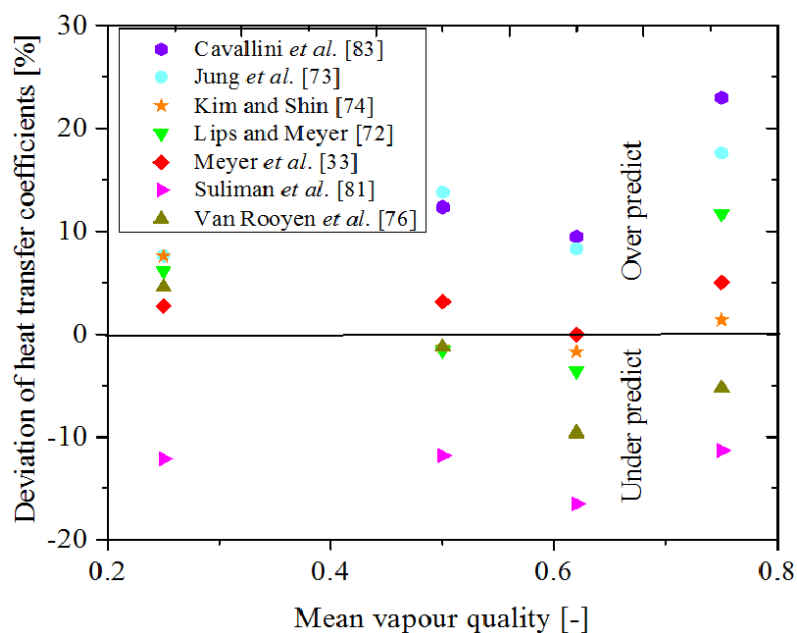
A validation study was carried out to ascertain the functionality and accuracy of the experimental set-up and the data generated from it. A summary of the validation test matrix is shown in Table 4.1, and it identifies the 25 different conditions that were used for experimental comparison purposes. The validation experiments were conducted at a saturation temperature of 40 °C over a mass flux range of 100 – 400 kg/m<sup>2</sup>s at qualities of 0.1 – 0.9. It was found that the heat transfer coefficients compared well to literature and the average deviation of the 25 heat transfer coefficients with the literature was 8%, the maximum deviation was 15%, and a minimum deviation was 1%. The results of a part of the validation experiments are summarised in Figure 4.1.

**Table 4.1: Summary of validation heat transfer coefficient experiments conducted at different qualities**

$G$ [kg/m <sup>2</sup> s]	$x_m$ [-]	$x_m$ [-]	$x_m$ [-]	$x_m$ [-]	$x_m$ [-]	$x_m$ [-]	$x_m$ [-]	Points
100	0.1	0.2	0.35	0.5	0.62	0.75	0.9	7
200	0.1	0.2	-	0.5	0.62	0.75	0.9	6
300	0.1	0.2	-	0.5	0.62	0.75	0.9	6
400	0.1	0.2	-	0.5	0.62	0.75	0.9	6
								<b>Total = 25 points</b>

In Figure 4.1, the results are given at a mass flux of 300 kg/m<sup>2</sup>s, and were compared to the measurements of Cavallini *et al.* [83], Jung *et al.* [73], Kim and Shin [74], Lips and Meyer [72], Meyer *et al.* [33], Suliman *et al.* [81], and Van Rooyen *et al.* [76]. In general, the measurements compared well to measurements from literature. The measurements were lower than the measurements of Cavallini *et al.*, Van Rooyen *et al.*, Jung *et al.*, and Kim and Shin, but higher than those of Suliman *et al.* The mean deviations were 16% lower than the values of Cavallini *et al.*, and 11% higher than those of Suliman *et al.*

A verification at mass fluxes lower than  $100 \text{ kg/m}^2\text{s}$ , which would have been desirable, was not possible, and for that reason, verifications were conducted in this section on mass fluxes of only  $100\text{--}400 \text{ kg/m}^2\text{s}$ . Specific verifications against the work of others at low mass fluxes were not possible because of differences in refrigerants [60, 64-66], tube diameter [86], tube shape [68], orientation (vertical and not horizontal) [75, 77], and temperature differences not specified [81]. Moreover, the other studies [2, 4, 58, 59, 61, 70, 77, 79, 84, 258] were general reviews with no experimental results to show. The only direct comparison that could have been possible against previous work was with the work of Suliman *et al.* [81], in which two heat transfer coefficients at a heat flux of  $75 \text{ kg/m}^2\text{s}$  were determined; however, the temperature differences at which the measurements were made were not specified.



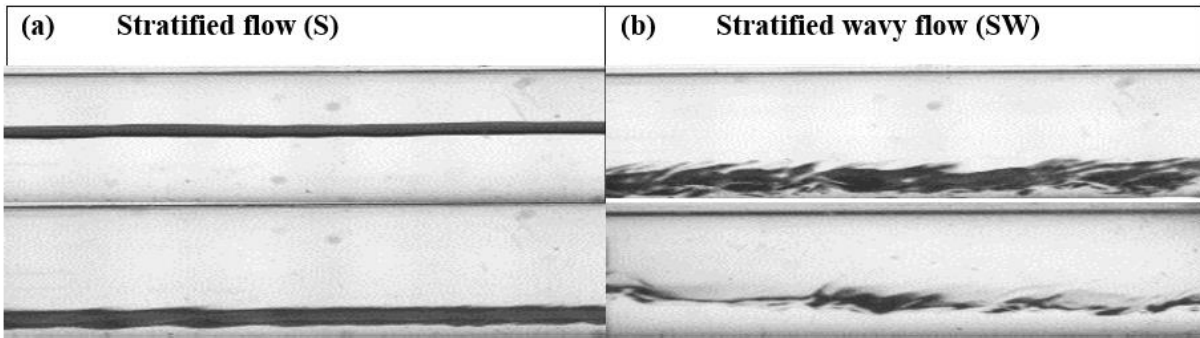
**Fig. 4.1: Validation results of experimental heat transfer coefficients as functions of quality at a mass flux of  $300 \text{ kg/m}^2\text{s}$  compared to experimental data at a saturation temperature of  $40 \text{ }^\circ\text{C}$ .**

### 4.3. Validation of flow pattern in horizontal tubes

Figure 4.2 summarises the only two flow patterns observed for horizontal flow. These flow patterns, which were smooth stratified (S) flow and stratified wavy (SW) flow, were adopted using the definitions and descriptions of flow regimes prescribed by Thome [62]. All the experimental data points summarized in Table 4.1 were also compared to the Thome [97] flow regime map. It was found that the observed flow regimes were in all cases correctly predicted and thus validated.

In general, although extensive verification experiments at mass fluxes lower than  $100 \text{ kg/m}^2\text{s}$  were not possible, the agreement of heat transfer coefficients and flow regime observations at mass fluxes from  $100\text{--}400 \text{ kg/m}^2\text{s}$  were satisfactory, and at least verifications were conducted at a mass flux of

100 kg/m<sup>2</sup>s, which was on the upper boundary of the range of mass fluxes considered in the following section.



**Fig. 4.2: General description of flow patterns found at mass fluxes of 50, 75, and 100 kg/m<sup>2</sup>s (horizontal flow).**

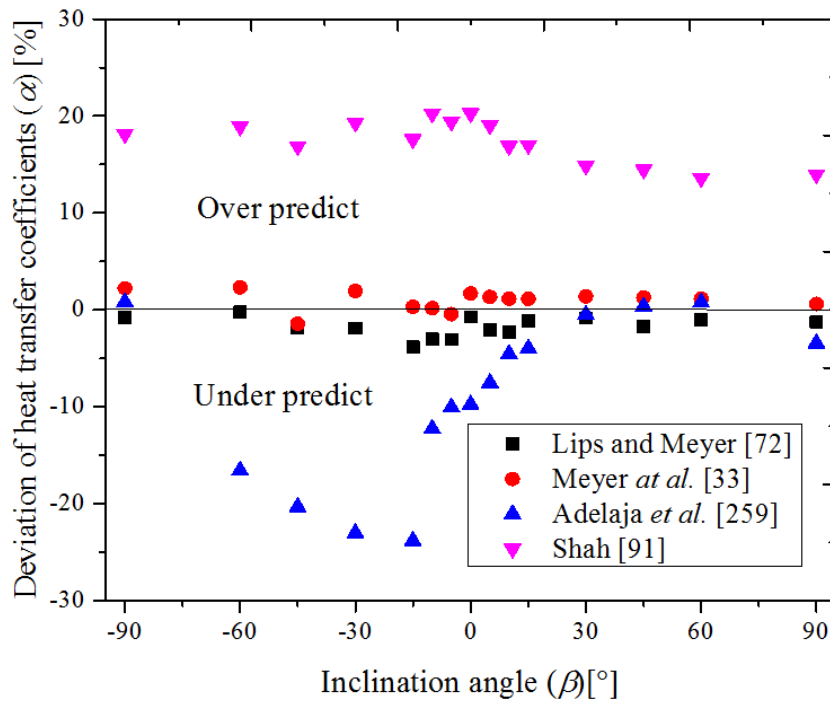
#### 4.4. Validation of heat transfer coefficients in inclined tubes

Validation experiments for the heat transfer coefficients were conducted at different inclination angles, as summarized in Table 4.2, which identifies the 45 different conditions that were used for experimental comparison purposes. The validation experiments were conducted at a saturation temperature of 40 °C, over a mass flux range of 200 – 400 kg/m<sup>2</sup>s, at a mean vapour quality of 0.5, at inclination angles of  $-90^\circ \leq \beta \leq 90^\circ$ , and with heat transfer rates of approximately 200 W, as were done by Lips and Meyer [72] and Meyer *et al.* [33]. The results of a part of the validation experiments are summarized in Figure 4.3

In this figure, the results are given for a mass flux of 300 kg/m<sup>2</sup>s and vapour quality of 0.5 for 15 different inclination angles from  $-90^\circ$  to  $90^\circ$ , and are compared to the measurements of Lips and Meyer [72], Meyer *et al.* [33] and the correlations of Adelaja *et al.* [259], and Shah [91]. In general, the measurements compared well and were on average, 5% higher than the measurements of Lips and Meyer [72] but 3% lower than those of Meyer *et al.* [33]. The measurements were also 10% higher than the correlation of Adelaja *et al.* [259] with most of the deviation occurring during downward flow. Finally, the measurements were generally lower than the correlation of Shah [91] by an average value of 17%.

**Table 4.2: Summary of validation test points**

$G$ [kg/m <sup>2</sup> s]	$x_m$ [-]	$\beta$ [°]	Points
200	0.5	-90, -60, -45, -30, -15, -10, -5, 0, 5, 10, 15, 30, 45, 60, 90	15
300	0.5	-90, -60, -45, -30, -15, -10, -5, 0, 5, 10, 15, 30, 45, 60, 90	15
400	0.5	-90, -60, -45, -30, -15, -10, -5, 0, 5, 10, 15, 30, 45, 60, 90	15
			<b>45 points</b>



**Fig. 4.3: Validation results of experimental heat transfer coefficients as a function of inclination angle at a mass flux of 300 kg/m<sup>2</sup>s and mean vapour quality of 0.5.**

#### 4.5. Validation of pressure drop results

A validation study was conducted to establish the integrity of our test rig and the results emanating from it. The validation experiments were summarised in Table 4.2 and identified 45 different conditions that were considered for experimental comparison purposes. The validation experiments were conducted at a saturation temperature of 40 °C. The mass fluxes range of 200 - 400 kg/m<sup>2</sup>s, at a mean vapour quality of 0.5 for inclination angles of  $-90^\circ \leq \beta \leq +90^\circ$  and with heat transfer rates of about 250 W. This was done to repeat the experimental conditions of Lips and Meyer [7, 18] and Adelaja *et al.* [8, 33]. The measurements compared very well and were within the pressure drop uncertainties. Furthermore, the pressure drop results for horizontal flow were compared to the

correlation of Moreno Quibén and Thome [21] and the homogeneous model [62]. It was found that they compared well and on the average, were 6% lower and 20% higher respectively.

#### **4.6. Summary and conclusion**

The experimental set-up and data reduction method for heat transfer coefficients and pressure drops were validated in this chapter. The results were presented in the order of heat transfer in smooth tubes, flow pattern in smooth tubes, heat transfer in inclined tubes and pressure drops in smooth and inclined tubes. It was very challenging to validate for low mass fluxes as there limited studies. Hence, the validations were done for the mass fluxes that had substantial experimental data published in the open literature.

For smooth tubes, the heat transfer coefficients compared well to experimental data from the literature: the average deviation of the 25 heat transfer coefficients with the literature was 8%, the maximum deviation was 15%, and the minimum deviation was 1%. For flow visualisation, it was found that at a mass flux of 300 kg/m<sup>2</sup>s, the observed flow regimes for horizontal flow were in all cases correctly predicted using the Thome flow pattern map and thus validated. For inclined tubes, the heat transfer validation measurements compared well and were on average, 5% higher than the measurements of Lips and Meyer, but 3% lower than those of Meyer *et al.* The measurements were also 10% higher than the correlation of Adelaja *et al.* with most of the deviation occurring during downward flow. Finally, the measurements were generally lower than the correlation of Shah [91] by an average value of 17%.

For pressure drops, the validation measurements compared well and were within the pressure drop uncertainties of the experimental conditions of Lips and Meyer and Adelaja *et al.* Furthermore, the validation experiments compared well with the Moreno Quibén and Thome correlation and the homogenous model.

To conclude, the integrity of our experimental set-up and the data emanating from it was established. Therefore, the results could be considered as valid and reliable.

# Chapter 5: Heat Transfer Coefficients in Smooth Tubes

---

## 5.1. Introduction

It was the purpose of this chapter to experimentally determine the heat transfer coefficients in a smooth horizontal tube at low mass fluxes and different quality values. During experimentation, the flow regimes were also captured at the inlet and outlet of the test section, and these results are also presented here. The experimental data were also compared to literature, and existing literature was modified to generate an equation that could be used to more accurately estimate the heat transfer coefficients at low mass fluxes.

## 5.2. Flow patterns

In Figs. 5.1 to 5.3, the captured flow patterns at the test section inlet and outlet at different mean qualities (average between the inlet and outlet qualities) are given at three different mass fluxes 100 kg/m<sup>2</sup>s (Fig. 5.1), 75 kg/m<sup>2</sup>s (Fig. 5.2), and 50 kg/m<sup>2</sup>s (Fig. 5.3).

In Fig. 5.1, at a mass flux of 100 kg/m<sup>2</sup>s, a mean vapour quality of 0.15, and temperature difference of 3 °C, the inlet vapour quality was 0.27 and the outlet vapour quality was 0.03. The flow pattern visualisation showed that, at the test section inlet, the flow pattern was stratified wavy (SW), and at the tests section outlet, the flow pattern was stratified (S). As the flow pattern changed from the test section inlet to outlet, an “averaged” phenomenon that corresponds to an average quality of 0.15 was observed (hereafter referred to in this paper as an “SW-S” flow pattern). Although this SW-S flow pattern occurred only at an average quality of 0.15 for a 3 °C temperature difference, it also occurred at temperature differences of 5 °C, 8 °C, and 10 °C. Moreover, it was not only observed at an average quality of 0.15 but also at average qualities of 0.25 and 0.35. Except for the SW-S flow patterns that were identified, all the other flow patterns in Fig. 5.1 at a mass flux of 100 kg/m<sup>2</sup>s were stratified wavy.

At a lower mass flux of 75 kg/m<sup>2</sup>s (Fig. 5.2), stratified flow occurred at both the inlet and outlet for the case of a temperature difference of 3 °C and an average quality of 0.15, while all the other flow regimes were stratified wavy. The exceptions were SW-S regimes that occurred at the following temperatures and average qualities: (a) a temperature difference of 3°C and average qualities of 0.25 and 0.35; (b) a temperature difference of 5 °C and average qualities of 0.15 and 0.25; and (c) a temperature difference of 8 °C and average qualities of 0.15, 0.25, and 0.35.

In Fig. 5.3, at a mass flux of 50 kg/m<sup>2</sup>s, all the flow regimes for temperature differences of 1 °C, 3 °C, and 5 °C were found to be in general SW-S. The exceptions were at qualities of 0.25 and 0.35, where

the flow regimes were stratified. A debatable point occurred at 1°C at an inlet quality of 0.30. Although it was observed to be closer to stratified than stratified wavy, the general tendency of results indicates that it should be stratified.

The different flow regimes observed at the determined inlet and outlet qualities were plotted onto the relevant part of the El-Hajal *et al.* map [97], as shown in Fig. 5.4. The effects of temperature differences are also shown. This excludes the SW-S points, as the “averaging” of these points that specifically correspond to the average qualities listed in Figs. 5.1–5.3 are not accurate. The reason is that the transition from the stratified wavy regimes to the stratified regimes could have occurred anywhere between the inlet and outlet quality values.

For mass fluxes of 50 kg/m<sup>2</sup>s, 75 kg/m<sup>2</sup>s, and 100 kg/m<sup>2</sup>s, the map predicts that the transition vapour quality from stratified to stratified wavy flow should be 0.29, 0.17, and 0.11, respectively. At a mass flux of 100 kg/m<sup>2</sup>s, all the flow regimes were predicted correctly.

However, at a mass flux of 75 kg/m<sup>2</sup>s, two points were incorrectly predicted. The first was at a temperature difference of 3 °C and inlet vapour quality of 0.25. According to the flow pattern map, the flow regime should have been stratified wavy flow; however, stratified flow was observed. Secondly, at a temperature difference of 8°C and outlet vapour quality of 0.17, stratified flow was observed although the flow regime predicted stratified wavy flow.

At a mass flux of 50 kg/m<sup>2</sup>s, the flow regimes of 4 points were incorrectly predicted in Fig. 5.4. At a temperature difference of 1 °C and quality of 0.58, the flow regime was observed to be stratified, although the map predicted stratified wavy. At a temperature difference of 5 °C and qualities of 0.28, 0.31, and 0.4, the flow regimes were observed to be stratified wavy, although the map predicted that the flow regimes should be stratified flow.

	$\Delta T=3^{\circ}\text{C}$		$\Delta T=5^{\circ}\text{C}$		$\Delta T=8^{\circ}\text{C}$		$\Delta T=10^{\circ}\text{C}$	
	$x_{in}=0.27$	$x_{out}=0.03$	$x_{in}=0.29$	$x_{out}=0.01$	$x_{in}=0.31$	$x_{out}=0.00$	$x_{in}=0.31$	$x_{out}=0.00$
$x_m=0.15$	SW	S	SW	S	SW	S	SW	S
	$x_{in}=0.35$	$x_{out}=0.15$	$x_{in}=0.39$	$x_{out}=0.11$	$x_{in}=0.49$	$x_{out}=0.01$	$x_{in}=0.50$	$x_{out}=0.00$
$x_m=0.25$	SW	SW	SW	S	SW	S	SW	S
	$x_{in}=0.44$	$x_{out}=0.25$	$x_{in}=0.53$	$x_{out}=0.17$	$x_{in}=0.64$	$x_{out}=0.01$	$x_{in}=0.65$	$x_{out}=0.05$
$x_m=0.35$	SW	SW	SW	S	SW	S	SW	S
	$x_{in}=0.62$	$x_{out}=0.38$	$x_{in}=0.71$	$x_{out}=0.29$	$x=0.77$	$x_{out}=0.21$	$x_{in}=0.85$	$x_{out}=0.15$
$x_m=0.5$	SW	SW	SW	SW	SW	SW	SW	SW
	$x_{in}=0.73$	$x_{out}=0.5$	$x_{in}=0.81$	$x_{out}=0.39$	$x_{in}=0.91$	$x_{out}=0.31$	$x_{in}=0.99$	$x_{out}=0.23$
$x_m=0.62$	SW	SW	SW	SW	SW	SW	SW	SW
	$x_{in}=0.86$	$x_{out}=0.63$	$x_{in}=0.93$	$x_{out}=0.51$				
$x_m=0.75$	SW	SW	SW	SW				

Fig. 5.1: Flow regimes at different temperature differences and vapour qualities at a mass flux of  $100 \text{ kg/m}^2\text{s}$ .



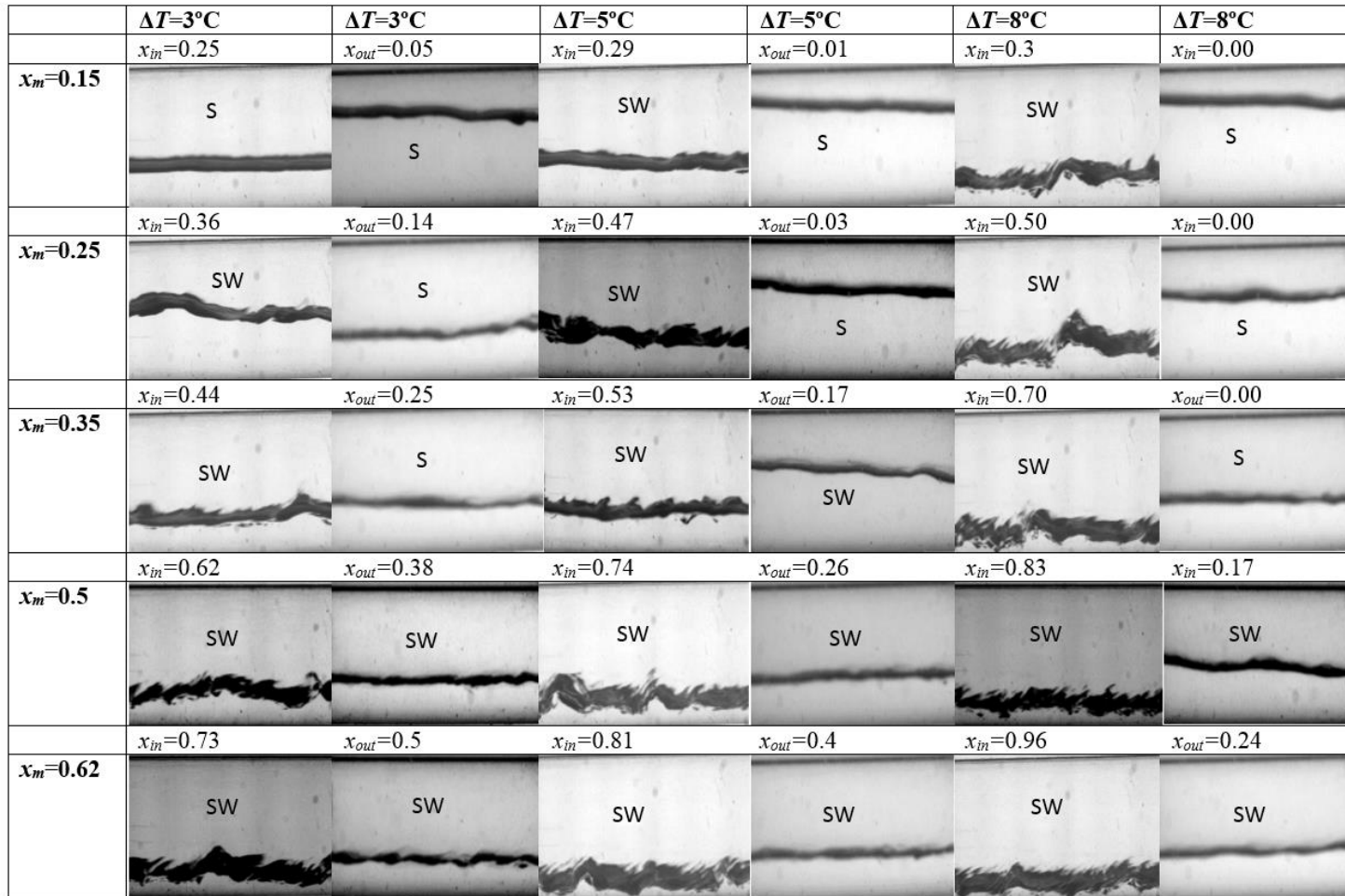


Fig. 5.2: Flow regimes at different temperature differences and vapour qualities at a mass flux of  $75 \text{ kg/m}^2\text{s}$ .

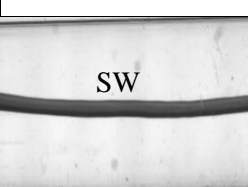
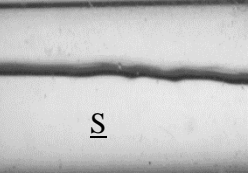
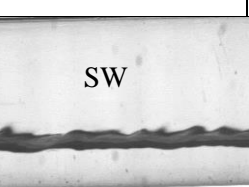
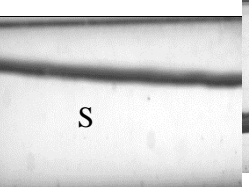
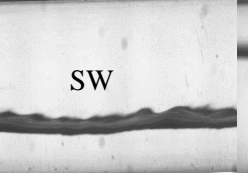
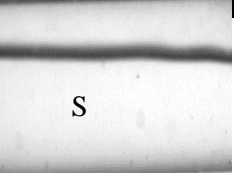
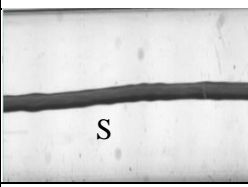
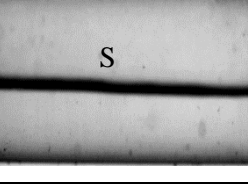
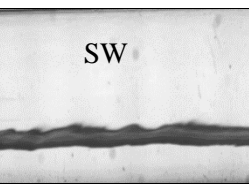
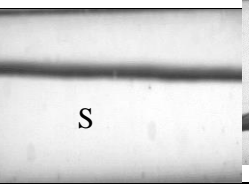
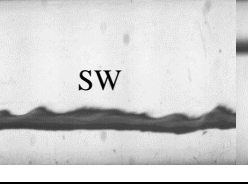
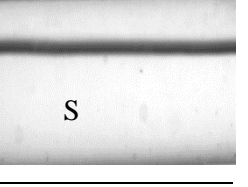
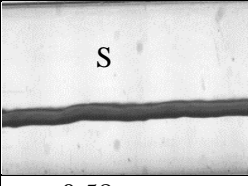
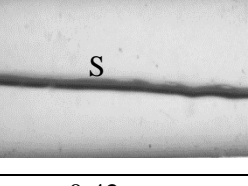
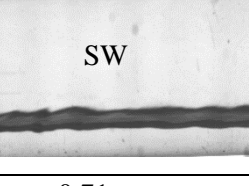
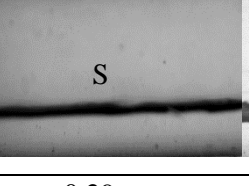
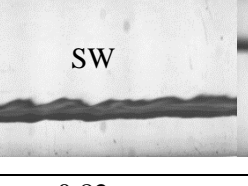
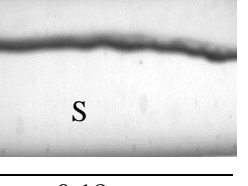
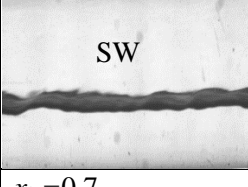
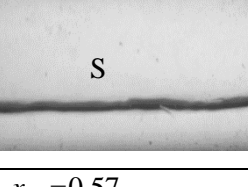
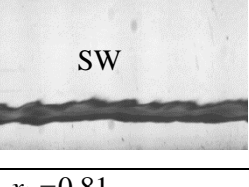
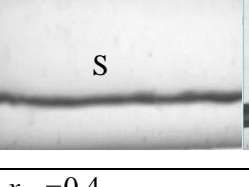
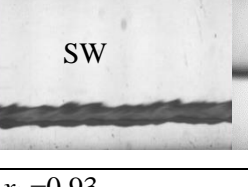
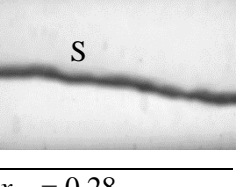

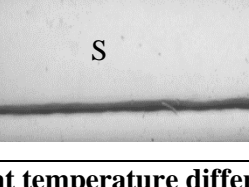
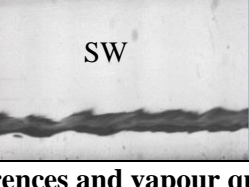
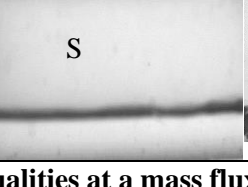
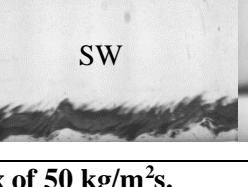
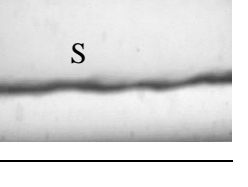
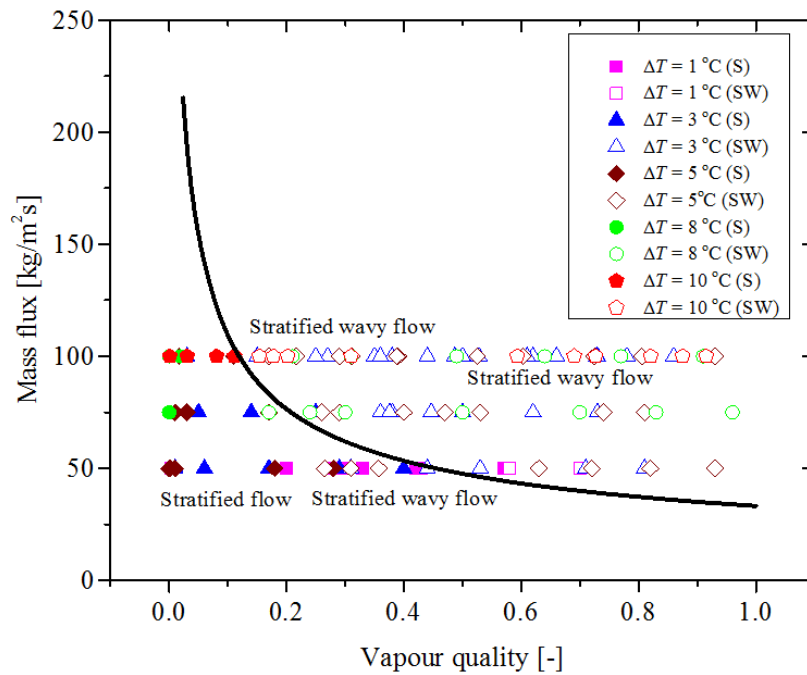
	$\Delta T=1\text{ }^{\circ}\text{C}$	$\Delta T=1\text{ }^{\circ}\text{C}$	$\Delta T=3\text{ }^{\circ}\text{C}$	$\Delta T=3\text{ }^{\circ}\text{C}$	$\Delta T=5\text{ }^{\circ}\text{C}$	$\Delta T=5\text{ }^{\circ}\text{C}$
	$x_{in}=0.30$	$x_{out}=0.03$	$x_{in}=0.31$	$x_{out}=0.01$	$x_{in}=0.31$	$x_{out}=0.01$
$x_m=0.15$						
	$x_{in}=0.33$	$x_{out}=0.20$	$x_{in}=0.44$	$x_{out}=0.06$	$x_{in}=0.5$	$x_{out}=0.00$
$x_m=0.25$						
	$x_{in}=0.43$	$x_{out}=0.28$	$x_{in}=0.53$	$x_{out}=0.17$	$x_{in}=0.63$	$x_{out}=0.02$
$x_m=0.35$						
	$x_{in}=0.58$	$x_{out}=0.42$	$x_{in}=0.71$	$x_{out}=0.29$	$x_{in}=0.82$	$x_{out}=0.18$
$x_m=0.5$						
	$x_{in}=0.7$	$x_{out}=0.57$	$x_{in}=0.81$	$x_{out}=0.4$	$x_{in}=0.93$	$x_{out}=0.28$
$x_m=0.62$						

Fig. 5.3: Flow regimes at different temperature differences and vapour qualities at a mass flux of  $50\text{ kg/m}^2\text{s}$ .



**Fig. 5.4: Verification experimental data points generated in this study plotted on the El Hajal *et al.* [97] map.**

In general, if all three mass fluxes of 100 kg/m<sup>2</sup>s, 75 kg/m<sup>2</sup>s, and 50 kg/m<sup>2</sup>s are considered, the map predicted 85% of the experimental data points correctly. In general, it seems as if the map inaccurately predicted the flow regimes as the mass flux decreased and the temperature differences increased.

### 5.3. Heat transfer coefficients

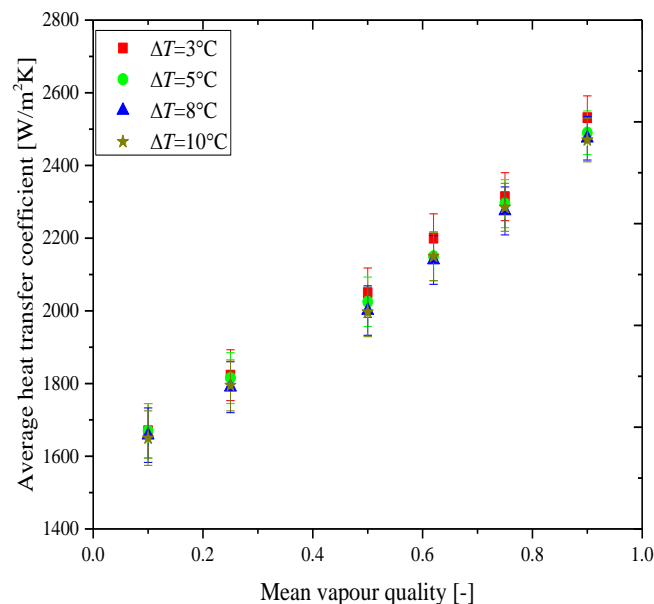
The heat transfer coefficients at mass fluxes of 200, 150, 100, 75, and 50 kg/m<sup>2</sup>s at different mean qualities are given in Figs. 5.5–5.9 for different temperature differences. The heat transfer coefficients are the average heat transfer coefficients over the test section lengths and the mean quality values were the average qualities between the inlet and outlet qualities are given in Figs. 5.1–5.3. The results show the expected trend of heat transfer coefficients as a function of vapour qualities that has been shown in previous work. Thus, the heat transfer coefficients increase with increasing values of mean vapour quality and mass flux. Fig. 5.5 shows the effect of temperature difference at a mass flux of 200 kg/m<sup>2</sup>s. The heat transfer coefficients at different temperature differences were all within the uncertainties of the measurements. It was, therefore, concluded that the heat transfer coefficients at a mass flux of 200 kg/m<sup>2</sup>s were independent of temperature difference and remained approximately constant. This can be attributed to the dominance of shear forces over gravity forces at this mass flux.

At a mass flux of 150 kg/m<sup>2</sup>s (Fig. 5.6), the effect of temperature difference was only detected noticeably at a low vapour quality of 0.1, which was observed to be stratified flow, while all the other

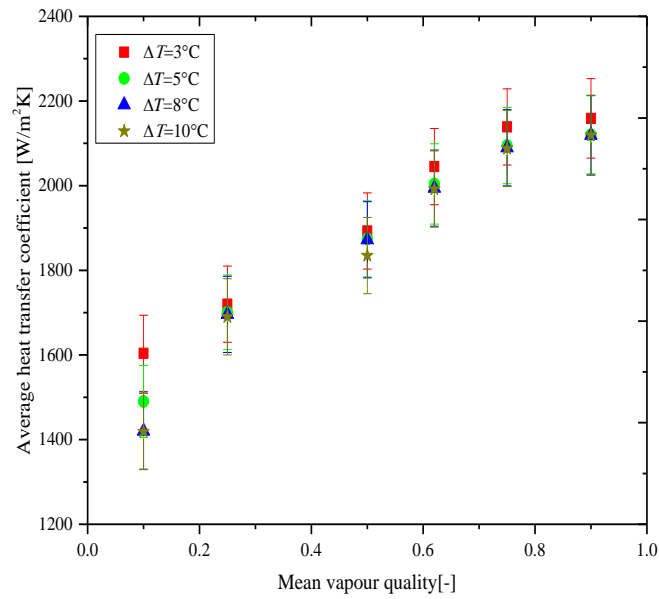
flow regimes were stratified wavy flow. The percentage difference between the measured heat transfer coefficients for the extremes of temperature differences (3 and 10 °C) at a quality of 0.1 was 12%. However, at vapour qualities greater than 0.25, the temperature difference had a negligible effect on the value of the heat transfer coefficients.

Fig. 5.7 shows the effect of temperature difference at a mass flux of 100 kg/m<sup>2</sup>s. Except for the one point at a quality of 0.15 which is in the stratified flow regime, all the other experimental conditions were taken in the stratified wavy flow regime. The results show that, in general, the heat transfer coefficients increase as the temperature difference decreases. The effect of the temperature difference is more dominant at higher qualities. For example, if the heat transfer coefficients at temperature differences of 3 and 10 °C are compared, the increase in the heat transfer coefficient is 10% at a vapour quality of 0.25, while at a vapour quality of 0.62, the increase is 13%. At a mass flux of 75 kg/m<sup>2</sup>s (Fig. 5.8), the same conclusion can be made about the effect of temperature difference: the heat transfer coefficients are dependent on temperature difference and increase as the temperature difference decrease.

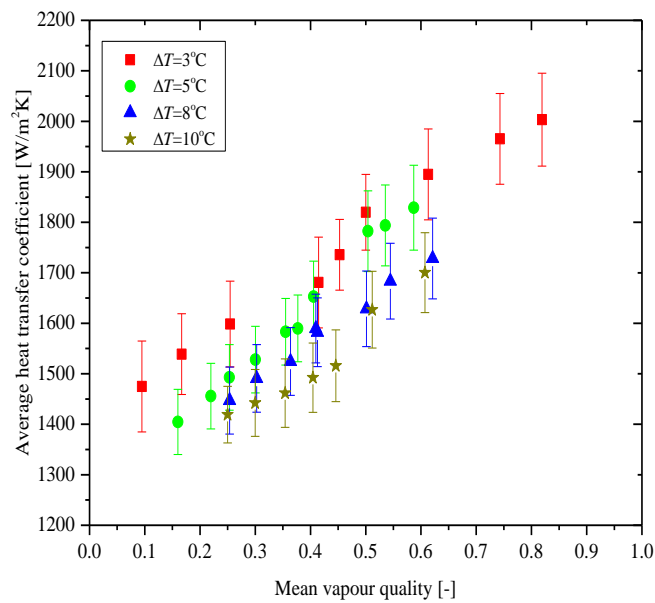
Fig. 5.9 shows the effect of temperature difference at a mass flux of 50 kg/m<sup>2</sup>s. Again, the conclusion about temperature difference made for mass fluxes of 150 – 75kg/m<sup>2</sup>s can be made for the mass flux of 50 kg/m<sup>2</sup>s. However, the data points were not sufficient enough for any conclusions about the influence of quality to be made.



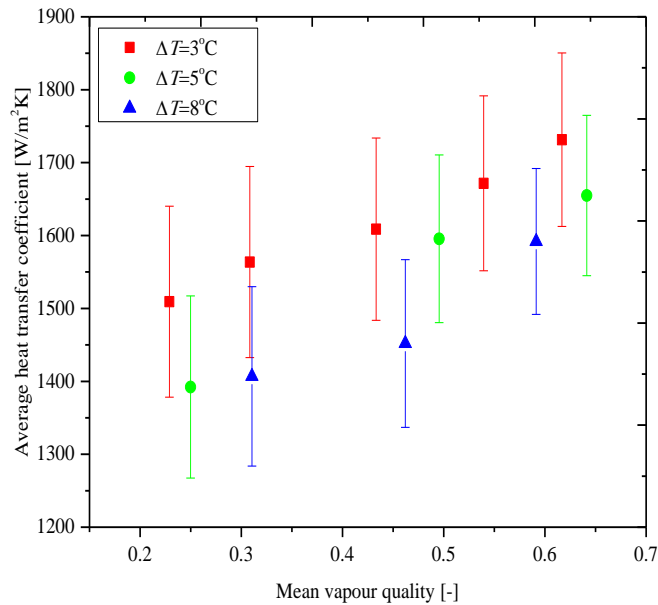
**Fig. 5.5: Heat transfer coefficients as a function of different wall and refrigerant saturation temperature differences,  $\Delta T$ , at different mean qualities during condensation at a mass flux of 200 kg/m<sup>2</sup>s.**



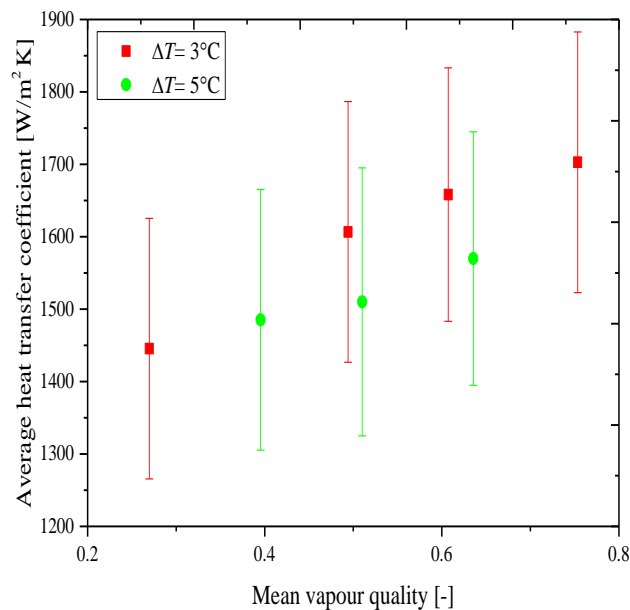
**Fig. 5.6:** Heat transfer coefficients as a function of different wall and refrigerant saturation temperature differences,  $\Delta T$ , at different mean qualities during condensation at a mass flux of  $150 \text{ kg/m}^2\text{s}$ .



**Fig. 5.7:** Heat transfer coefficients as a function of different wall and refrigerant saturation temperature differences,  $\Delta T$ , at different mean qualities during condensation at a mass flux of  $100 \text{ kg/m}^2\text{s}$ .



**Fig. 5.8:** Heat transfer coefficients as functions of different wall and refrigerant temperature differences,  $\Delta T$ , at different mean qualities during condensation at a mass flux of  $75 \text{ kg/m}^2\text{s}$ .



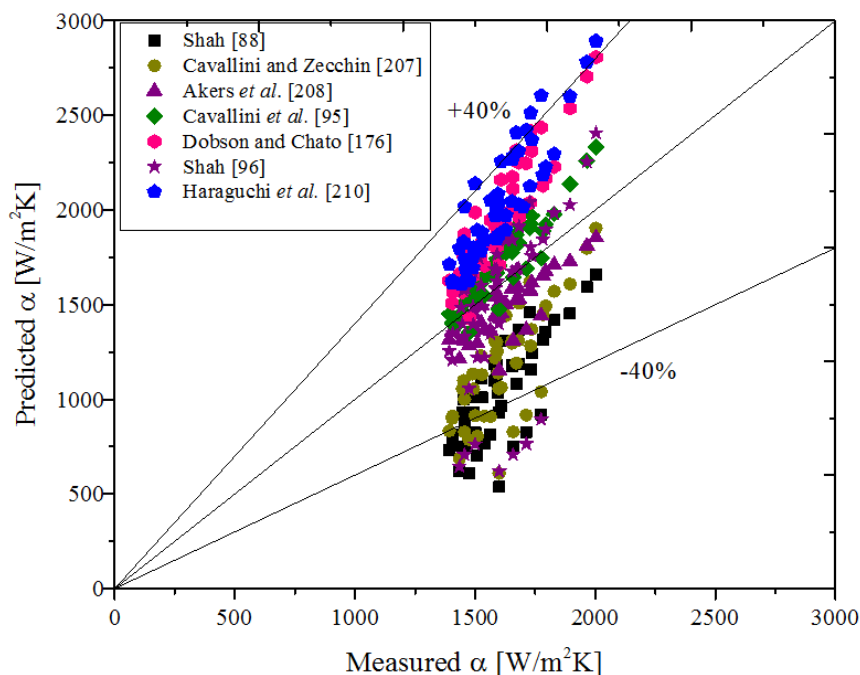
**Fig. 5.9:** Heat transfer coefficients as functions of different wall and refrigerant temperature differences,  $\Delta T$ , at different mean qualities during condensation at a mass flux of  $50 \text{ kg/m}^2\text{s}$ .

The general conclusions that can be made when comparing Figs. 5.5 – 5.9 were that at mass fluxes of  $50 - 100 \text{ kg/m}^2\text{s}$ , the condensing heat transfer coefficients were temperature dependent. The heat transfer coefficients increased as the temperature differences decreased. It can thus be concluded that the effect of  $\Delta T$  was more significant at lower mass fluxes due to the existence of gravity-dominated flow like stratified or stratified-wavy flow. In these types of flow patterns, the conduction resistance through the liquid film played a more significant role. With an increase in film thickness with  $\Delta T$ , the

thermal resistance of heat transfer increased and resulted in lower heat transfer coefficients. At higher mass fluxes the flow regimes were almost annular and shear stresses played the main role in the total thermal resistance or heat transfer coefficients, therefore the increase in film thickness with respect to  $\Delta T$  had a negligible effect on the heat transfer coefficients. Furthermore, at a mass flux of  $100 \text{ kg/m}^2\text{s}$ , it was found that the effect of the temperature difference was more dominant at higher qualities. This effect was only observed at this specific mass flow rate.

#### 5.4. Comparison with literature

The results of this study at mass fluxes of  $50$ ,  $75$ , and  $100 \text{ kg/m}^2\text{s}$  are compared in Fig. 5.10 to the theoretical models of Shah [88], Cavallini and Zecchin [207], Akers *et al.* [208], Cavallini *et al.* [95], Dobson and Chato [176], Shah [96] and Haraguchi *et al.* [210] The comparison was only conducted with the mass fluxes that were found to be temperature dependent.



**Fig. 5.10: Comparison of experimental data with several theoretical models from literature.**

The comparison shows that the experimental results of this study were lower than the predicted values of Cavallini *et al.*, Haraguchi *et al.*, and Dobson and Chato, but higher than the predicted values of Akers *et al.* and Cavallini and Zecchin. With respect to the newest model of Shah [96], some of the results of our experiments were higher while others were lower. The absolute mean deviations in comparison to the theoretical models of Shah, Cavallini and Zecchin, Akers *et al.*, Cavallini *et al.*, Haraguchi *et al.*, Dobson and Chato, and the newest method of Shah correlations were 42%, 29%, 21%, 19%, 31%, 27%, and 25%, respectively. The maximum deviations per data point were generally

recorded at the lowest mass flux of 50 kg/m<sup>2</sup>s. This showed that the theoretical models became error-prone with decreasing mass fluxes. In general, it was also found that as the temperature difference increased, the absolute mean deviation decreased.

With respect to the Cavallini *et al.* [95] correlation, the experimental results compared well only at vapour qualities below 0.2. It was also found that, for the new Shah [96] correlation, the experimental data correlated to within 17% for mass fluxes of 75 and 100 kg/m<sup>2</sup>s. However, at a mass flux of 50 kg/m<sup>2</sup>s, the absolute mean deviation was 54%.

Following the instructions of Shah, our data points at this mass flux fell on the “Shah Regime III”, which represented stratified flows. In that regime, Shah neglected the heat transfer from the condensate in the liquid pool at low mass velocities and this ultimately lowered the heat transfer coefficients. If the “Shah Regime II” equation (representing stratified wavy flow) had been used for all the mass fluxes (50, 75, and 100 kg/m<sup>2</sup>s) at which experiments in this study were conducted, the absolute mean deviation would have decreased from 17% to 12%. Although this modification can be considered for implementation, there is no theoretical justification for the model proposed by Shah [96], as our experimental observations show that only 65% of our measurements were conducted in the stratified wavy flow regime.

### 5.5. Revised theoretical model

From the previous section, it was deduced that the heat transfer models of Akers *et al.* [208] and Cavallini *et al.* [95] predicted the results of our experiments with the lowest absolute mean deviations. The Akers *et al.* model is a semi-empirical, two-phase multiplier-based correlation which defines the all-liquid mass flow rate. It also provides the same heat transfer coefficient as for an annular condensing flow. The general limitation of this correlation and others of its type is that it does not include sufficient variables to accurately describe condensation in tube flow. On the other hand, the Cavallini *et al.* model is based on the physical description of the actual flow structure, and it predicts and identifies the local two-phase flow pattern based on localised flow conditions. This model also requires a reliable two-phase flow pattern map. We have, therefore, selected the Cavallini *et al.* correlation [95] for our revised model, which takes into consideration several heat transfer coefficients that contribute to the total heat transfer coefficient. The total heat transfer coefficient is given as:

$$\alpha_D = [\alpha_A (J_v^T / J_v)^{0.8} - \alpha_{strat}] (J_v / J_v^T) + \alpha_{strat} \quad (5.1)$$

with  $\alpha_A$ , the annular flow heat transfer coefficient, given as



$$\alpha_A = \alpha_{lo} [1 + 1.128x^{0.8170}(\rho_l/\rho_v)^{0.3685}(\mu_l/\mu_v)^{0.2363}(1 - \mu_v/\mu_l)^{2.144}Pr_l^{-0.1}] \quad (5.2)$$

and the liquid only heat transfer coefficient,  $\alpha_{lo}$ , given as:

$$\alpha_{lo} = 0.023Re_{lo}^{0.8}Pr_l^{0.4}k_l/d \quad (5.3)$$

where  $\alpha_{strat}$  is the fully-stratified flow heat transfer coefficient. In the dimensionless vapour velocity term,  $J_v^T$ , a value of  $C_T = 2.6$  was used as prescribed by Cavallini *et al.*, as we have used R134a as the condensing fluid. An analysis of the Cavallini *et al.* equation showed that it has only the fully-stratified flow heat transfer coefficient term which is dependent on the temperature difference,  $\Delta T$  which drives the heat transfer at low mass fluxes. It then lent credence to the fact that the Cavallini *et al.* model may not be predicting this parameter accurately as evidenced by the discrepancy noticed during comparison where it over-predicted the measured heat transfer coefficients. This discrepancy was attributed to the varying temperature differences. Having established that the  $\alpha_{strat}$  component of the total heat transfer component ( $\alpha$ ), was responsible for the over prediction of the Cavallini *et al.* correlation by about 20%, a parametric study was done on the  $\alpha_{strat}$  to quantify the effects and sensitivity of both the exponents of the temperature difference,  $\Delta T$  and the vapour quality on its value. It was then found that the exponent of  $\Delta T$  ( $T_1$ ) was more sensitive to a change in the value of  $\alpha_{strat}$  as compared to a large change in the value of the exponent of vapour quality ( $x$ ) ( $T_2$ ) on the liquid only heat transfer coefficient term, ( $\alpha_{lo}$ ) component of the ( $\alpha_{strat}$ ). This then led to the modification of the existing correlation as shown in Eq. 5.4.

$$\alpha_{strat} = 0.725[1 + 0.741[(1 - x)/x]^{0.3321}]^{-1}[k_l^3\rho_l(\rho_l - \rho_v)gh_{lv}/(\mu_l d_i \Delta T)]^{T_1} + (1 - x^{T_2})\alpha_{lo} \quad (5.4)$$

In Eq. (5.4), the exponents  $T_1$  and  $T_2$  proposed by Cavallini *et al.* were 0.25 and 0.087, respectively. It has been found that by using the values  $T_1 = 0.245$  and  $T_2 = 0.25$  for low mass fluxes ( $G \leq 100 \text{ kg/m}^2.\text{s}$ ), the mass fluxes can be estimated more accurately, as shown in Fig. 5.11-5.12 The measured and predicted heat transfer coefficients with the original Cavallini *et al.* equation for different mass fluxes are shown in Fig. 5.11. The figure shows that 53% of the heat transfer coefficients outside the  $\pm 10\%$  range were for mass fluxes lower than  $100 \text{ kg/m}^2.\text{s}$ . In Fig. 5.12, the Cavallini *et al.* equation was used to determine the heat transfer coefficients, but with  $T_1 = 0.245$ , and  $T_2 = 0.25$ . These values were only used for mass fluxes lower or equal than  $100 \text{ kg/m}^2.\text{s}$ , while the originally proposed values of 0.25 and 0.087 were used for all the mass fluxes larger than  $100 \text{ kg/m}^2.\text{s}$ . This adjustment resulted in 90% of the data at low mass fluxes ( $G \leq 100 \text{ kg/m}^2.\text{s}$ ), with errors smaller than  $\pm 10\%$ . The results show that, for the 48 experimental points at low mass fluxes ( $G \leq 100 \text{ kg/m}^2.\text{s}$ ), the average errors improved from 25% (Fig. 5.11) to 6% (Fig. 5.12).

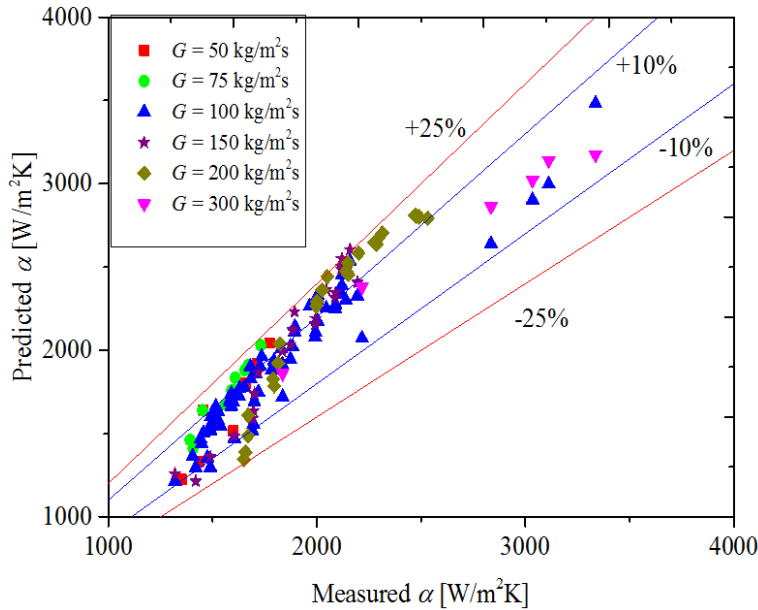
As discontinuities in the  $T_1$  and  $T_2$  values as proposed by Cavallini *et al.* occurred in this study, we investigated several curve fittings techniques that would produce equations without discontinuities. The equations were of the following format:  $T_1 = f_1(G)$  and  $T_2 = f_2(G)$ ; thus, two different functions ( $f_1$  and  $f_2$ ) of mass flux,  $G$ , were obtained. At mass fluxes higher than  $100 \text{ kg/m}^2\text{s}$ , the  $T_1$  and  $T_2$  values should be 0.5 and 0.087, respectively. However, at mass fluxes lower than  $100 \text{ kg/m}^2\text{s}$ , the  $T_1$  and  $T_2$  values should be 0.245 and 0.25, respectively. The combination of the best and most simple equations were the third order polynomial equations given in Eqs. (5.5) and (5.6).

$$T_1 = -1 * 10^{-9}G^3 + 4 * 10^{-7}G^2 - 6 * 10^{-6}G + 0.2449 \quad (5.5)$$

and

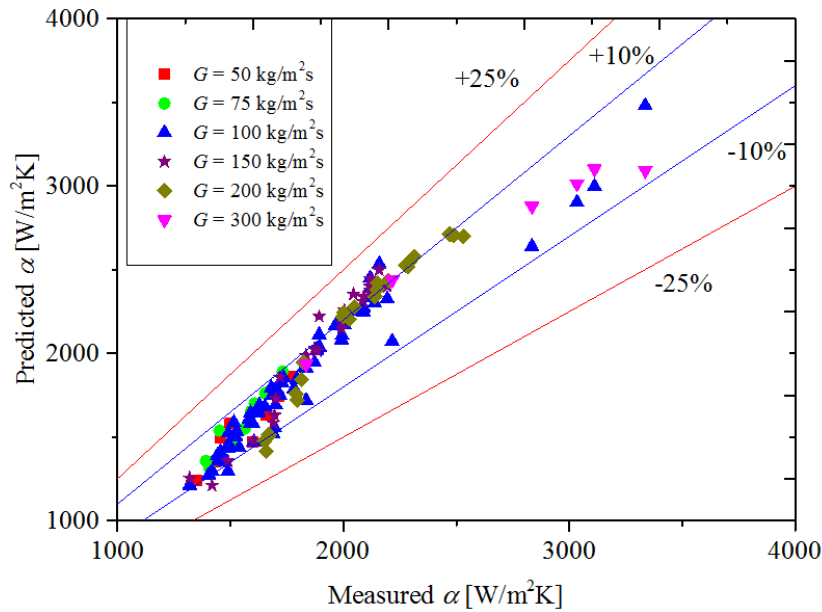
$$T_2 = -1 * 10^{-8}G^3 + 1 * 10^{-6}G^2 - 0.0012G + 0.2698 \quad (5.6)$$

However, both these equations show that the first three terms contribute very little to the values of  $T_1$  and  $T_2$ , and that the last terms of 0.245 and 0.25 contribute the most. Thus, if the third order polynomial equations are used rather than the values of 0.245 and 0.25, then it will have an insignificant effect on the results in Fig. 5.12.



**Fig. 5.11: Measured heat transfer coefficients compared to the Cavallini *et al.* [48] equation as functions of mass flux using the original values of  $T_1$  and  $T_2$ , i.e., 0.25 and 0.087, respectively as proposed by Cavallini *et al.* [48].**

The proposed correlation may be used as a universal model because it is a modification of an already existing universal flow pattern based heat transfer model. The experimental and test conditions (besides the low mass fluxes) used in arriving at this modification were similar to many previous studies.



**Fig. 5.12: Measured heat transfer coefficients compared to the modified Cavallini *et al.* [48] using the revised values of  $T_1$  and  $T_2$ , i.e., 0.245 and 0.25, respectively, (which take into consideration the temperature differences at low mass fluxes) as suggested.**

## 5.6. Summary and conclusion

There have been many experimental and theoretical studies on condensation inside smooth horizontal tubes. However, limited studies have been conducted on the effect of the temperature difference between the wall temperature on which the condensation occurred and the refrigerant saturation temperature on the heat transfer coefficients. It was, therefore, the purpose of this study to investigate the effect of this temperature difference on heat transfer coefficients at low mass fluxes during condensation. This was done with experiments conducted at five different mass fluxes of 50, 75, 100, 150, and 200  $\text{kg/m}^2\text{s}$  during the convective condensation of R134a in a smooth horizontal tube with an internal diameter of 8.38 mm. Experiments were conducted with temperature differences from 3 °C to 10 °C at a condensing temperature of 40 °C. The inlet and outlet qualities of the condensing refrigerant were determined, and videos of both the inlet and outlet flow regimes were captured.

The observed flow patterns were compared to a flow regime map, and it was found that the map predicted most of the experimental data points correctly. In general, however, the map inaccurately predicted the flow regimes as the mass flux decreased and the temperature differences increased. It was found that the effect of the temperature difference on the heat transfer coefficients began to show at a mass flux of 150  $\text{kg/m}^2\text{s}$ , but only at a vapour quality of 0.1. However, the dependency of heat transfer coefficients on temperature difference increased at all vapour qualities when the mass fluxes were lower or equal to 100  $\text{kg/m}^2\text{s}$ . In all cases, for a specific mass flux lower than 100  $\text{kg/m}^2\text{s}$  and a

specific mean quality, the maximum heat transfer coefficients were found at the lowest temperature difference, while the minimum heat transfer coefficients were found at the maximum temperature difference. Finally, as the mass flux decreased, the heat transfer coefficients became more dependent on the temperature difference.

The heat transfer coefficients from this study were also compared to six correlations from literature, and it was found that the literature did not accurately predict the heat transfer coefficients at low mass fluxes. In general, as the temperature difference increased, the errors between measurements and predictions increased. Two minor revisions to one of these correlations were suggested in a term that is influenced by the temperature difference. It was found that, when these two revisions to the correlations were introduced, the heat transfer coefficients could be predicted more accurately at low mass fluxes.

# Chapter 6: Heat Transfer Coefficients in Inclined Tubes

---

## 6.1. Introduction

It was the purpose of this chapter to present the flow regimes and heat transfer coefficients at different inclination angles at low mass fluxes and different temperature differences,  $\Delta T$ . This study is a continuation of the previous chapter which was limited to condensation in horizontal tubes. This chapter concentrates on the effect of different inclination angles on the heat transfer coefficients.

## 6.2. Flow patterns

Figure 6.1 summarizes the six flow patterns observed in this study. These flow patterns are smooth stratified (S), stratified wavy (SW) (also observed in Meyer and Ewim [52]), annular (A), annular wavy (AW), intermittent (I), and churns flows (C). These flow patterns were adopted using the descriptions of flow regimes as prescribed by Thome [52, 260]. The bubbly flow was not observed on its own but was observed during intermittent flows. The flow pattern abbreviations S, SW, A, AW, I, and C are used to identify the flow patterns in Figs. 6.2 and 6.3. In these figures, the flow patterns are given for two different mass fluxes  $100 \text{ kg/m}^2\text{s}$  (Fig. 6.2) and  $50 \text{ kg/m}^2\text{s}$  (Fig. 6.3) as a function of temperature differences and inclination angles for mean qualities of 0.5 and 0.25, respectively. These were chosen to reflect most of the flow pattern descriptions observed during the experiments.

In Fig. 6.2, at a mass flux of  $100 \text{ kg/m}^2\text{s}$ , and mean vapour quality of 0.5, the flow patterns are given for temperature differences of 3, 5, and  $10 \text{ }^\circ\text{C}$ , and inclination angles of  $-90^\circ$ ,  $-60^\circ$ ,  $-30^\circ$ ,  $0^\circ$ ,  $30^\circ$ ,  $60^\circ$ , and  $90^\circ$ . At an inclination angle of  $-90^\circ$ , it was found that both the inlet and outlet flow regimes were either annular or annular wavy for all the temperature differences. At inclination angles of  $-60^\circ$ ,  $-30^\circ$ , and  $0^\circ$ , it was found that both the inlet and outlet flow regimes were stratified wavy at all the temperature differences. The only exception was at a temperature difference of  $10 \text{ }^\circ\text{C}$  and an inclination of  $0^\circ$ , for which stratified flow was observed. At inclination angles of  $30^\circ$  and  $60^\circ$ , it was found that both the inlet and outlet flow regimes were frequently changing from churn to stratified wavy for all the temperature differences. At an inclination angle of  $90^\circ$ , both the inlet and outlet flow regimes were churn flow.

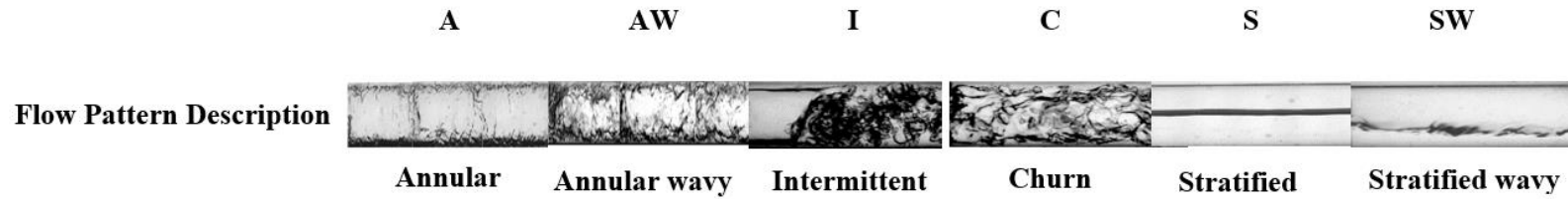


Fig. 6.1: Description of flow patterns found in the study.

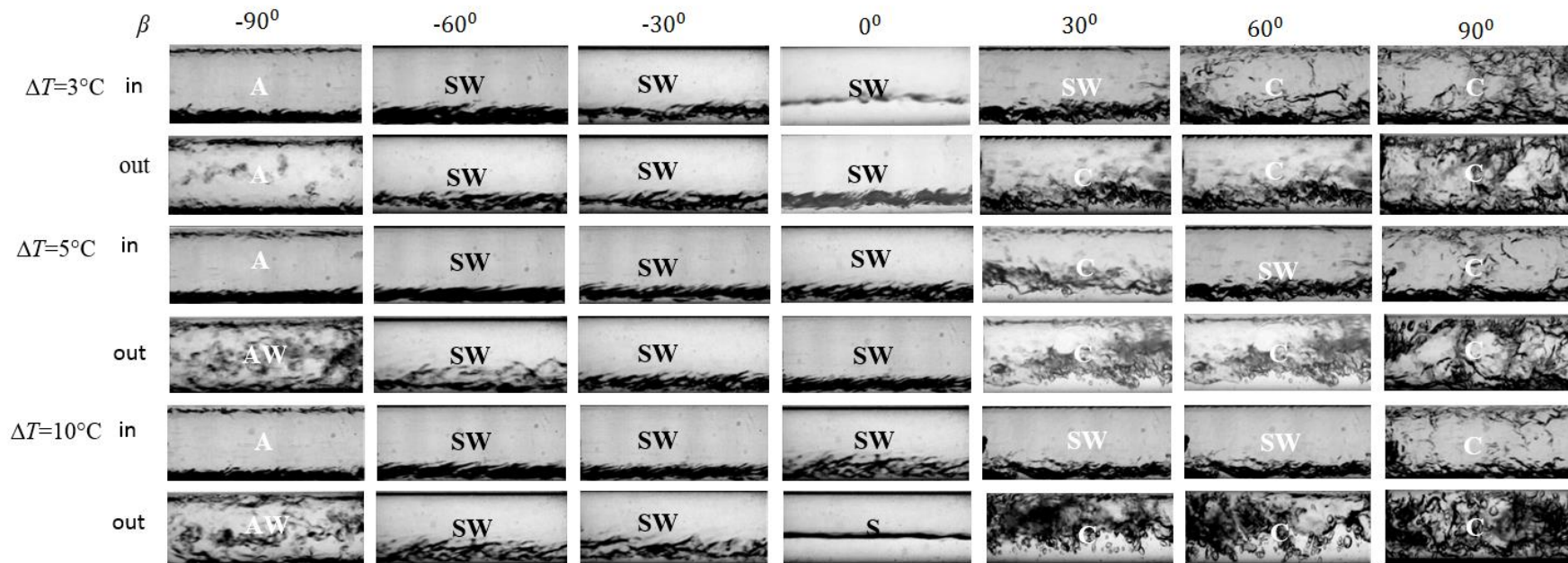
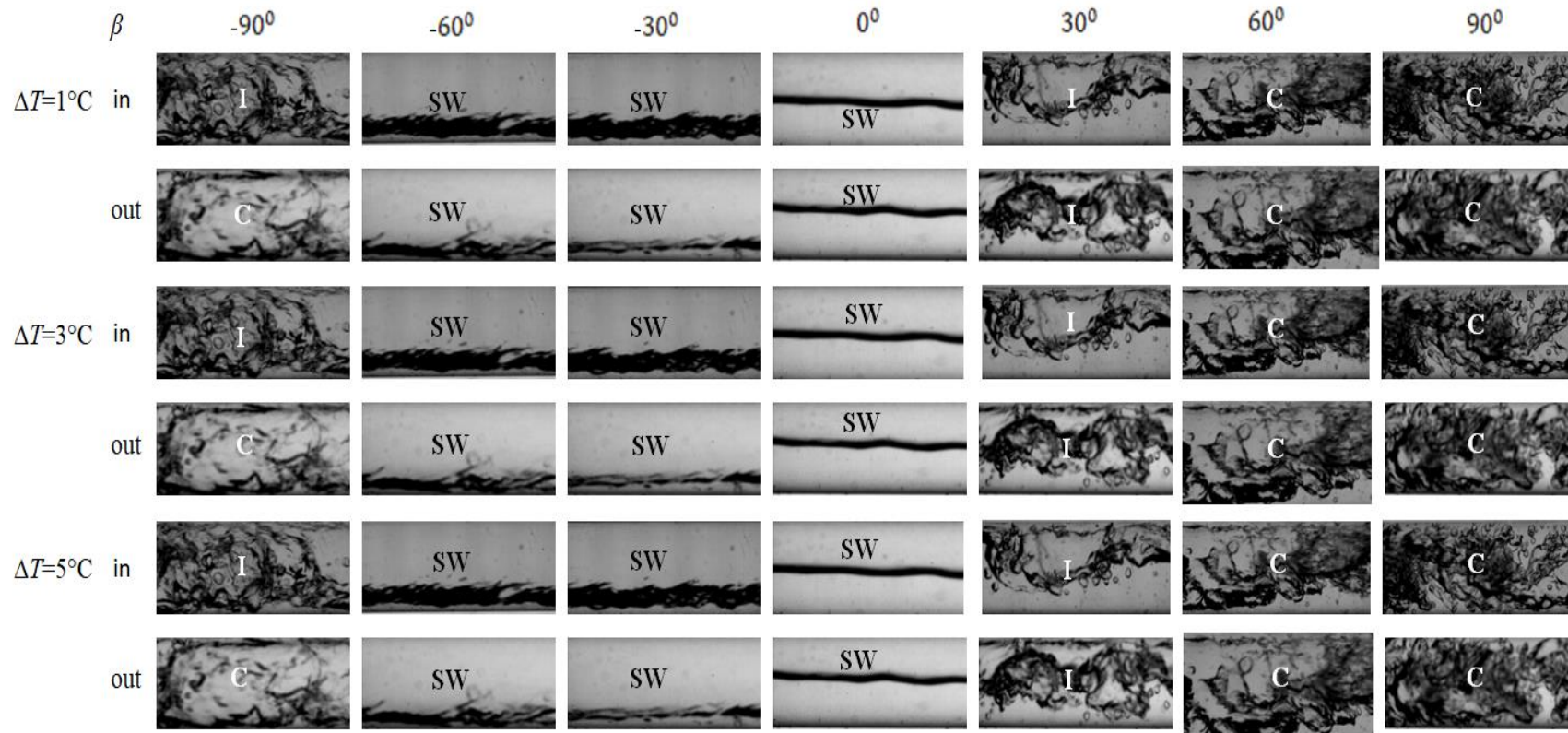


Fig. 6.2: Flow regimes at different temperature differences for a vapour quality of 0.5 at a mass flux of  $G = 100 \text{ kg/m}^2\text{s}$ .



**Fig. 6.3: Flow regimes at different temperature differences for a vapour quality of 0.25 at a mass flux of  $G = 50 \text{ kg/m}^2\text{s}$ .**

In Fig. 6.3, at a mass flux of  $50 \text{ kg/m}^2\text{s}$  and mean vapour quality of 0.25, the flow patterns are given for temperature differences of 1, 3, and 5 °C, and inclination angles of  $-90^\circ$ ,  $-60^\circ$ ,  $-30^\circ$ ,  $0^\circ$ ,  $30^\circ$ ,  $60^\circ$ , and  $90^\circ$ . At an inclination angle of  $-90^\circ$ , both the inlet and outlet flow regimes were intermittent and churn, respectively, for the three temperature differences. At inclination angles of  $-60^\circ$ ,  $-30^\circ$  and  $0^\circ$ , both the inlet and outlet flow regimes were stratified wavy for all temperature differences. At inclination angles of  $30^\circ$  and  $60^\circ$ , both the inlet and outlet flow regimes were intermittent for the three temperature differences. At an inclination of  $90^\circ$ , all the flow patterns were churn flow at both the inlet and outlet.

### 6.3. Heat transfer coefficients

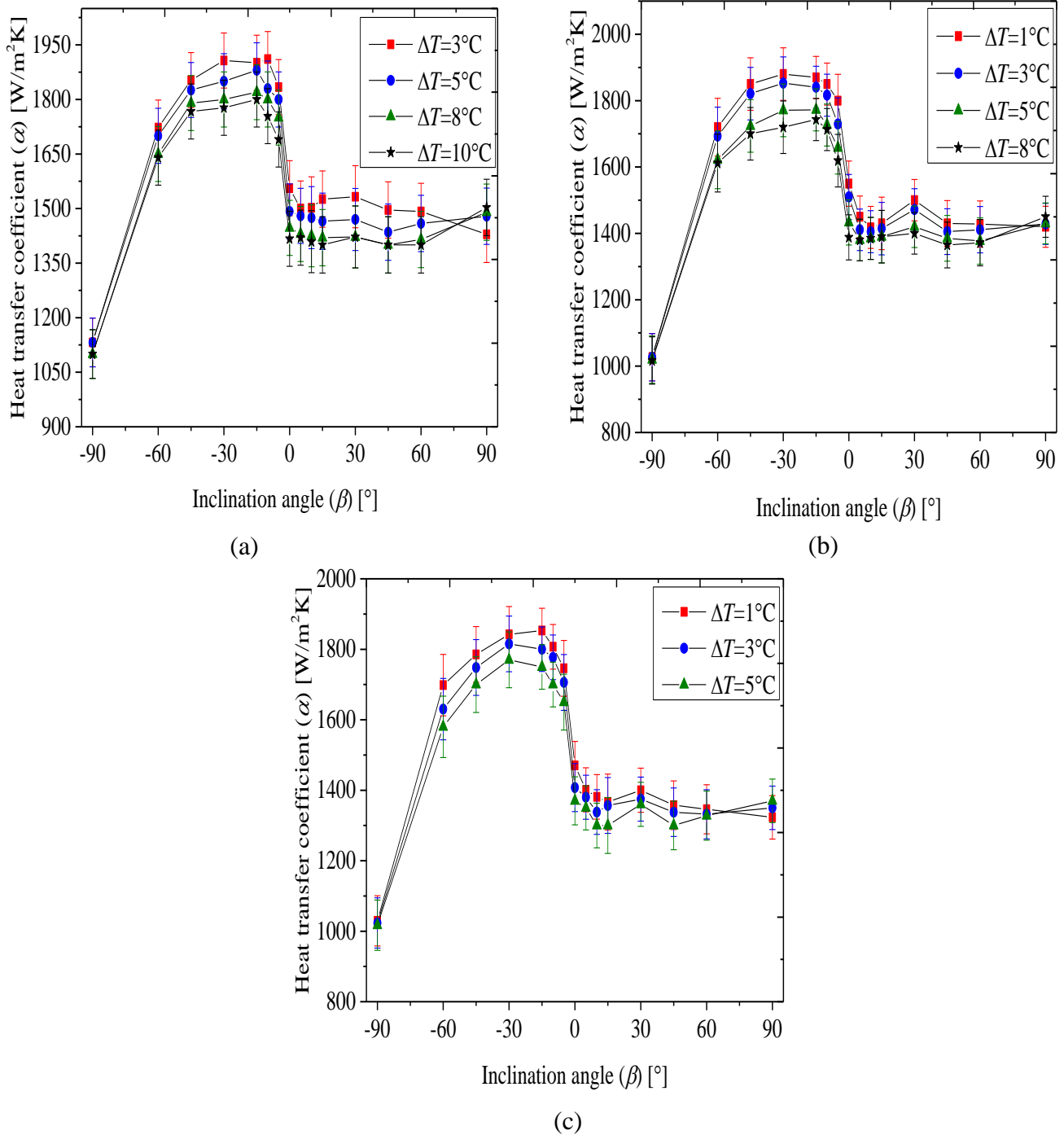
The heat transfer coefficients at mass fluxes of 100, 75, and  $50 \text{ kg/m}^2\text{s}$  are plotted as functions of different inclination angles with varying temperature differences at different mean vapour qualities of 0.25, 0.5, 0.62, and 0.75 in Figs. 6.4–6.6 Furthermore, the heat transfer coefficients at mass fluxes of 100 and  $50 \text{ kg/m}^2\text{s}$  are plotted as functions of temperature differences of 1, 3, 5, 8, and 10 °C with varying inclination angles in Fig 6.7 In general, the results showed the same general trends of heat transfer coefficients as a function of mass flux, temperature differences, and vapour qualities that have been shown in previous work [52, 167]. Thus, the heat transfer coefficients increased with decreasing values of temperature differences and increased with increasing values of vapour quality and mass flux.

Fig. 6.4 shows that at a mean vapour quality of 0.25, the maximum heat transfer coefficients were found at the minimum temperature differences in each case; i.e., 3 °C (Fig. 6.4a), 1 °C (Fig. 6.4b), and 1 °C (Fig. 6.4c) for mass fluxes of 100, 75, and  $50 \text{ kg/m}^2\text{s}$ , respectively. These occurred at inclination angles of  $-15^\circ$ ,  $-30^\circ$ , and  $-15^\circ$ . Furthermore, it was found that the minimum heat transfer coefficients for all the temperature differences were found at an inclination of  $-90^\circ$  (downwards flow) and the corresponding maximum temperature differences were 10, 8, and 5 °C for mass fluxes of 100, 75, and  $50 \text{ kg/m}^2\text{s}$ , respectively.

It was also found that the inclination effect was more dominant for downwards flows than upwards flows. For downwards flows, the flow regimes were, in general, all stratified wavy (Figs. 6.2 and 6.3) with the gravity forces collecting the condensing liquid on the bottom part of the tube with a very thin condensing liquid layer around the circumference on the top part of the tube. As this layer is thin, the heat transfer resistance is small and therefore, the heat transfer coefficients are large. Furthermore, the condensing liquid did not only flow downwards to the bottom part of the tube but also in an axial



direction to the tube outlet. The results show that in general, the optimal downwards angle is between  $-30^\circ$  and  $-15^\circ$ .



**Fig. 6.4: Condensation heat transfer coefficients,  $\alpha$ , as a function of inclination angle,  $\beta$ , at different wall and refrigerant temperature differences,  $\Delta T$ , at a mean quality of 0.25 during condensation: (a) Mass flux of  $100 \text{ kg}/\text{m}^2\text{s}$ , (b) mass flux of  $75 \text{ kg}/\text{m}^2\text{s}$ , and (c) mass flux of  $50 \text{ kg}/\text{m}^2\text{s}$ .**

The trend of variations in heat transfer coefficient may be related to the prevailing flow regime. At  $\beta = -90^\circ$ , the flow regime is churn which generally corresponds to low heat transfer coefficients. With

an increase in the inclination angle to the optimum, the flow regime becomes stratified and as a result, the heat transfer coefficient increases. With further increase in the inclination angle, the liquid film thickness seems to increase, which results in an increase in the heat transfer resistance and consequently, a decrease in the heat transfer coefficient. For the upwards flow direction, the flow regimes are almost churn and therefore, the heat transfer coefficients decrease and the inclination effect is negligible.

For upwards flows, it was found that there seemed not to be any major effect of inclination on the heat transfer coefficients of different temperature differences. Furthermore, it was deduced that the effect of temperature difference was different for the vertically upwards ( $+90^\circ$ ) flow in comparison to the vertically downwards ( $-90^\circ$ ) flow. The temperature differences had a negligible effect on the heat transfer coefficients during both vertically downwards flows and vertically upwards flows.

When comparing the heat transfer coefficients of the horizontal tube ( $\beta = 0^\circ$ ) orientation to that of downwards vertical ( $\beta = -90^\circ$ ) orientation, it was found that the heat transfer coefficients of the horizontal orientation were greater. This could be attributed to the stratification due to gravity, which enhanced the heat transfer by keeping the condensate thickness low in the upper region of the tube as compared to the vertically downwards flow. In this case, even though the heat transfer coefficient at the bottom was reduced, the heat transfer enhancement in the upper region prevailed and the mean cross-sectional heat transfer coefficient was increased as compared to the vertically downwards flow orientation. It can also be deduced that condensation heat transfer coefficients were more sensitive to changes in the inclination angles near the horizontal position. In these slightly inclined positions (either upwards or downwards) the flow patterns were mainly stratified smooth flow and stratified wavy.

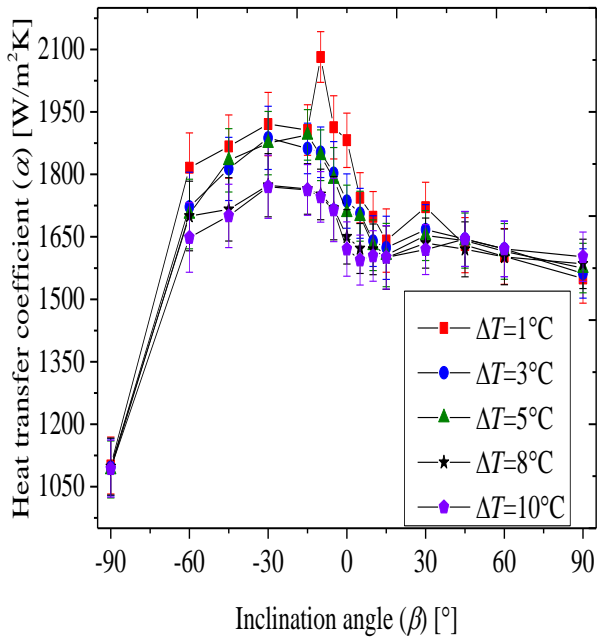
When stratified smooth flow and stratified wavy flow occurred, the inclination angles had a heat transfer enhancement effect. As the inclination angles (Figs. 6.2 and 6.3) decreased from  $0^\circ$  to  $-30^\circ$ , the liquid film thickness decreased because of gravity and consequently led to an increase in the convection effect. As a result, the thermal resistance decreased, and therefore, the heat transfer coefficient increased. Furthermore, the flow regimes were almost the same for this region (stratified wavy or stratified.) With a further decrease of the inclination angle from  $-30^\circ$  to  $-60^\circ$ , the flow regime remained stratified wavy and the liquid film thickness did not change significantly; therefore, the heat transfer coefficient remained almost unchanged between these two inclination angles. This can be seen in Figs. 6.4 – 6.6. However, with the decrease in the inclination angle from  $-60^\circ$  to  $-90^\circ$ , there was a change in the flow regime from stratified wavy to either churn, intermittent or annular flows. When the flow regime changed to churn or intermittent flows, the liquid phase covered the tube surface sporadically, which caused an increase in thermal resistance and consequently a decrease in the heat

transfer coefficients. However, when the flow regime changed to annular flow, the liquid film always covered the entire tube surface, which also caused a significant decrease in the heat transfer coefficients. This considerable decrease can be observed in Figs. 6.4–6.6 at an inclination angle is  $-90^\circ$ . The same interpretation is valid for the upwards flow directions, but the difference is that in those regions, the flow regimes were always intermittent or churn, for which the inclination had no significant effect on the heat transfer coefficients. In summary, the variations of heat transfer coefficients with respect to the tube inclination angle can be attributed to the change of flow regime and liquid film thickness on the tube surface.

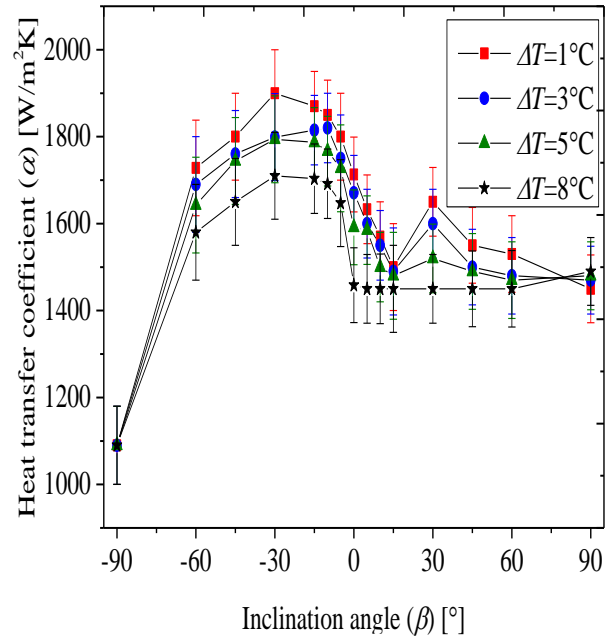
Comparing the heat transfer coefficients between the mass fluxes in Figs. 6.4 (a), (b), and (c), it was found that in general, there was an increase in heat transfer coefficient as the mass flux increased. This increase could be expressly attributed to an increase in shear forces because, for each comparison, the temperature differences and inclination angle was kept constant. This same trend was observed in our previous study [52] on horizontal tubes, where in general, the heat transfer coefficients increased with mass flux. In that study, the effect of the temperature difference on the heat transfer coefficients was found to be the main driving force of the heat transfer process. In the current study, the prevailing flow regime and inclination angles also played roles in the heat transfer process.

Fig. 6.5 shows the effect of inclination on the heat transfer coefficients at different temperature differences at a vapour quality of 50%. In general, the results are the same as for a vapour quality of 25% (Fig. 6.4), except that the maximum heat transfer coefficients were found to be at a slightly lower inclination angle of  $-15^\circ$  or  $-30^\circ$  (downwards flow).

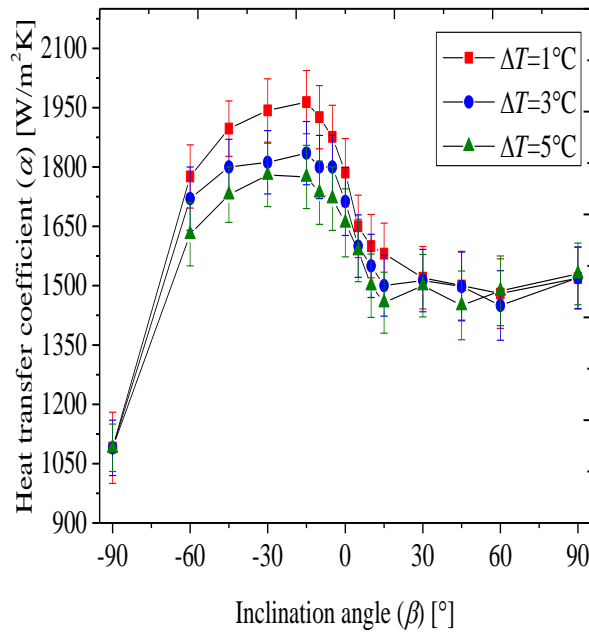
At this vapour quality of 50%, complicated by the role of interfacial waves and inclination angles, there was increased shear stress on the vapour–liquid interface causing a more unstable interface, thereby enhancing the condensation heat transfer. With respect to the minimum heat transfer coefficient, it was also found that the heat transfer coefficient was more sensitive to the combined effect of inclination angles and temperature difference for downwards flows than for upwards flows. In general, it can be deduced that because the heat transfer coefficient is closely related to the liquid film thickness on the tube wall, the higher heat transfer coefficient was found when there was the thinner liquid film thickness and the converse was true for lower heat transfer coefficients. Finally, it was found that the phenomenon of the vertically upwards flow, where higher heat transfer coefficients were found for the maximum temperature difference, was also experienced.



(a)

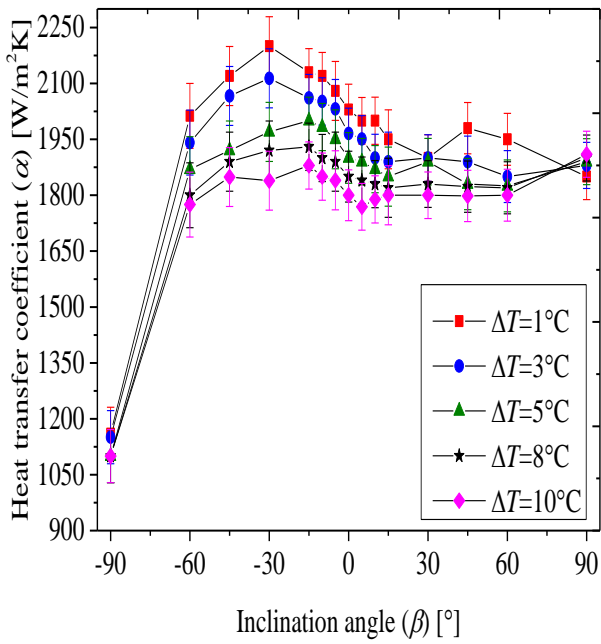


(b)

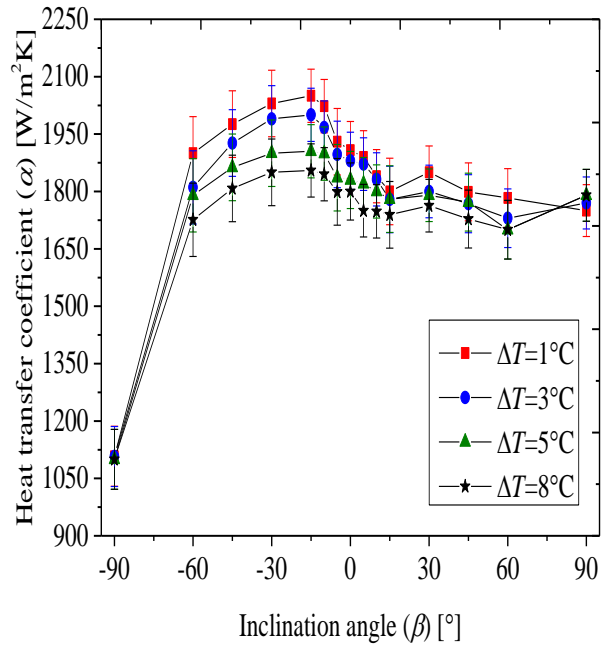


(c)

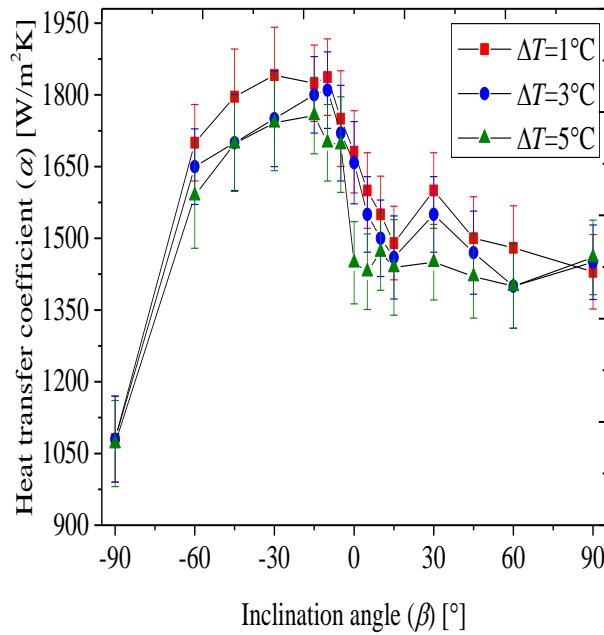
**Fig. 6.5: Condensation heat transfer coefficients,  $\alpha$ , as a function of inclination angle,  $\beta$ , at different wall and refrigerant temperature differences,  $\Delta T$ , at a mean quality of 0.50 during condensation: (a) Mass flux of 100 kg/m<sup>2</sup>s, (b) mass flux of 75 kg/m<sup>2</sup>s, and (c) mass flux of 50kg/m<sup>2</sup>s.**



(a)



(b)



(c)

**Fig. 6.6: Condensation heat transfer coefficients,  $\alpha$ , as a function of inclination angle,  $\beta$ , at different wall and refrigerant temperature differences,  $\Delta T$ , at a mean quality of 0.75 during condensation: (a) Mass flux of 100 kg/m<sup>2</sup>s, (b) mass flux of 75 kg/m<sup>2</sup>s, and (c) mass flux of 50kg/m<sup>2</sup>s.**

Fig. 6.6 shows the effect of inclination on the heat transfer coefficients at different temperature differences but at a higher vapour quality of 75%. These results do not differ significantly from the results in Figs. 6.4 and 6.5, which were for qualities of 25% and 50%. However, for upwards inclination angles at this vapour quality, there is an increase in the vapour shear forces exerted on the

liquid film interface, which slows down the downwards motion of the liquid film and subsequently causes the interfacial portion of the film to be carried upwards instead downwards to the drain at the bottom of the tube. This condition leads to the onset of flooding.

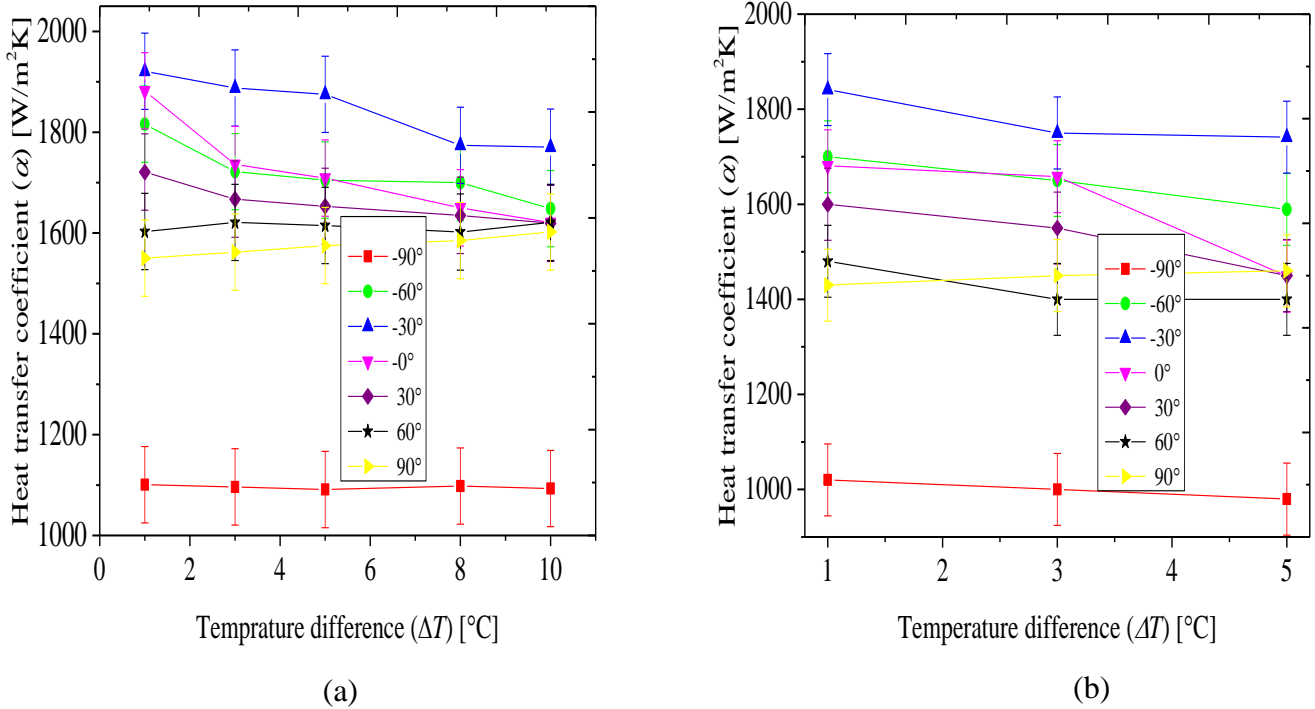
For downwards inclination angles, analogous to Figs. 6.4 and 6.5, it was found that the maximum heat transfer coefficients were obtained at the minimum temperature difference tested for and an inclination angle of either  $-15^\circ$  or  $-30^\circ$ , whereas the minimum heat transfer coefficient was at an inclination of  $-90^\circ$  at the maximum temperature difference.

Consistent with previous figures, it can also be deduced that there was practically no effect of temperature difference at both the upwards and downwards vertical orientations, even though there was a minimal increase in heat transfer coefficient as temperature difference was increased in the vertically downwards orientation. The converse was true for the vertically upwards orientation.

Fig. 6.7 more clearly shows the effect of the temperature differences and inclination angles at a mass flux of  $100 \text{ kg/m}^2\text{s}$  (Fig. 6.7a) and  $50 \text{ kg/m}^2\text{s}$  (Fig. 6.7b) for a mean vapour quality of 50%. The results show that the maximum heat transfer coefficients were at an inclination angle of  $-30^\circ$  for all the temperature differences. Furthermore, they show that the minimum heat transfer coefficients occurred at an inclination angle of  $-90^\circ$  for all the temperature differences. It was also found that the percentage difference of the maximum heat transfer coefficient and the minimum heat transfer coefficient for a mass flux of  $100 \text{ kg/m}^2\text{s}$  in Fig 6.7a was 73%, whereas that at a mass flux of  $50 \text{ kg/m}^2\text{s}$  in Fig. 6.7b was 81%. This further lends credence to the fact that the heat transfer enhancement effect decreased with an increase in mass flux. In addition, the figure clearly shows that although the heat transfer slightly decreased for the vertically downwards flow as the temperature increased, this decrease was less than 2% (negligible). The converse was true for vertically upwards flow and the increase was also 2%. The figure also shows that the effect of temperature difference was more dominant for downwards flows.

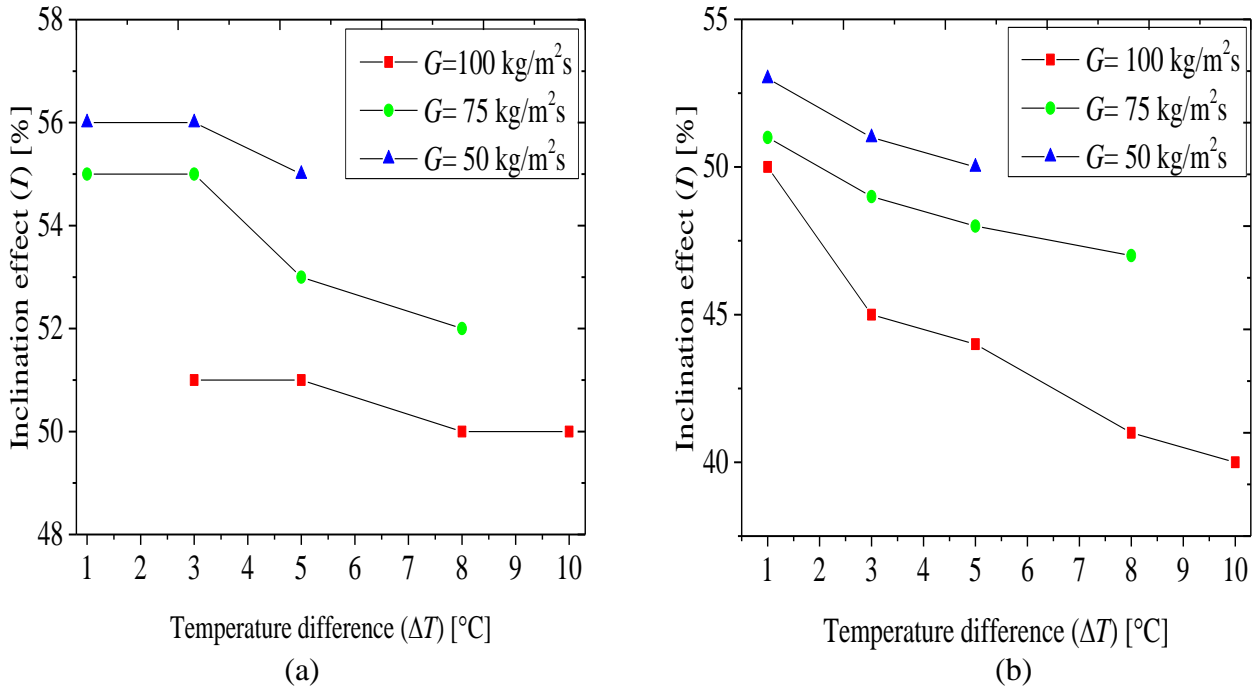
Fig. 6.8 shows the effect of inclination on temperature differences and mass fluxes. In the figure, the inclination effect at mass fluxes of 100, 75, and  $50 \text{ kg/m}^2\text{s}$  for mean vapour qualities of 0.25 and 0.5 are plotted against the different temperature differences. This figure shows that the inclination effect was inversely proportional to the mass fluxes. Hence, as the mass flux decreased, the inclination effect increased. It was also found that between the minimum and maximum temperature differences, there was a decrease in the inclination effect. For instance, at a mass flux of  $75 \text{ kg/m}^2\text{s}$  and quality of 0.5, the inclination effect of 55% was found at a temperature difference of  $1^\circ\text{C}$  and an inclination angle of  $-30^\circ$ . This was greater than the inclination effect of 52%, which was observed at a temperature difference of  $3^\circ\text{C}$  and an inclination angle of  $-15^\circ$  for a mass flux of  $100 \text{ kg/m}^2\text{s}$ . Furthermore, at a

mass flux of 50 kg/m<sup>2</sup>s and quality of 0.25, the average inclination effect across the temperature differences of 1, 3, and 5 °C was 50%, which was higher than at the average inclination effect of 75 kg/m<sup>2</sup>s at the same quality.



**Fig. 6.7: Condensing heat transfer coefficients as a function of temperature differences,  $\Delta T$ , and different inclination angles,  $\beta$ , at a mean quality of 0.50: (a) Mass flux of 100 kg/m<sup>2</sup>s and (b) mass flux of 50 kg/m<sup>2</sup>s.**

Overall, it was found that the average inclination effect at a mean vapour quality of 0.50 was lower than the inclination effect at a mean vapour quality of 0.25. This lends credence to the fact that the inclination effect was more significant at lower vapour qualities. In general, the inclination effect increased with a decrease in mass flux and increased with a decrease in vapour quality.



**Fig. 6.8: Inclination effect as a function of temperature differences,  $\Delta T$ , at different mass fluxes during condensation: (a) Vapour quality of 0.25 and (b) Vapour quality of 0.50.**

#### 6.4. Summary and conclusion

Experiments were carried out during the condensation of R134a in a smooth inclined tube at mass fluxes of 50, 75, and 100 kg/m<sup>2</sup>s. The mean vapour qualities ranged from 0.1 to 0.9 at temperature differences of 1, 3, 5, 8, and 10 °C. In total, 945 data points were obtained for the validation and actual experiments. The flow patterns were visualised using two high-speed cameras installed at the inlet and outlet of the test section. It was observed that an annular flow pattern is prevalent for vertically downwards inclination ( $-90^\circ$ ). In contrast, churn was common for the vertically upwards inclination ( $+90^\circ$ ), with wavy annular being observed at higher qualities and intermittent at lower qualities.

In all cases, the maximum heat transfer coefficients were found at the minimum temperature difference tested per data point and at inclination angles alternating between  $-15^\circ$  and  $-30^\circ$ . However, the minimum heat transfer coefficients were consistently found at the maximum temperature difference tested per data point and at an inclination angle of  $-90^\circ$  (vertically downwards flow). It was found that even though the heat transfer coefficients for vertically downwards flow decreased with an increase in temperature difference, the percentage differences were approximately 2% (negligible). The converse was true for vertically upwards flows.

With respect to the inclination effect, it was found that it decreased with an increase in temperature difference. It was also found that at low qualities (below 0.35), the inclination effect was more



noticeable. On the contrary, at high vapour qualities (above 0.5), no significant additional effect of vapour quality was found on the inclination effect. In general, the maximum inclination effect was found at the lowest mass flux tested for and the converse was true for the maximum mass flux investigated for. For annular flows, it was found that the heat transfer coefficients were independent of the inclination angle. In such cases, the heat transfer coefficient increased with increasing mass flux and this could be attributed to thinning of the liquid film by the increasing effect of vapour shear forces. However, for flows found to be stratified and intermittent, the effect of inclination angles was significant. Beyond a certain downwards inclination angle, it was found that the heat transfer coefficient decreased and this could be attributed to the decrease in the perimeter occupied by the thin film of condensation at the top of the tube, where most of the condensation occurs.

In general, the heat transfer coefficient mainly depends on the perimeter occupied by the condensation film and its thickness, which were primarily a function of inclination and temperature difference. In conclusion, it is recommended that future inclined condensers be inclined at angles between  $-15^\circ$  and  $-30^\circ$ . Furthermore, it is required that more flow-pattern-dependent mechanistic models be developed to assist with the prediction of the heat transfer coefficients for condensing flows in inclined tubes.

## Chapter 7: Pressure Drops in Smooth and Inclined Tubes

---

### 7.1. Introduction

It was the purpose of this chapter to present the results for both measured and frictional pressure drops in smooth and inclined tubes. The results of the 900 pressure drop measurements with test conditions as given in Table 3.5 are presented in three sections covering flow visualisation (7.2), measured pressure drops (7.3) and the frictional pressure drops (7.4).

### 7.2. Flow pattern visualisation results

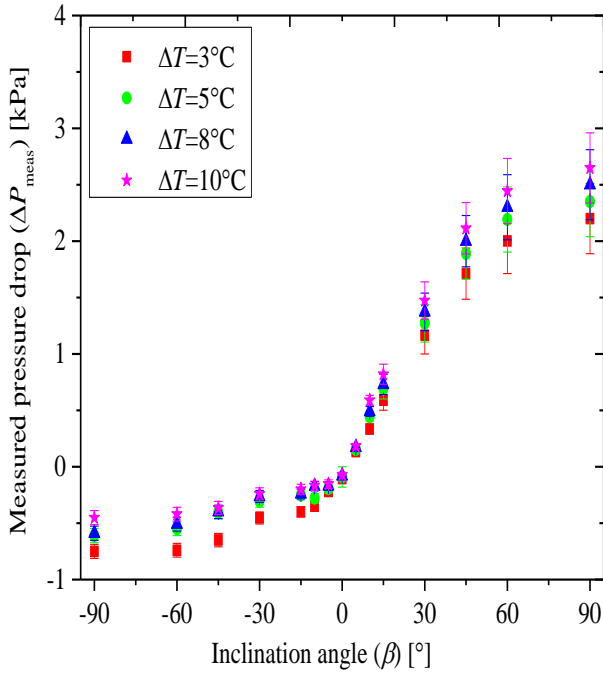
It is recommended that the photos with flow patterns identified and described in Figs. 6.1 – 6.3 which are not repeated in this chapter are read in conjunction with the discussion below.

### 7.3. Measured pressure drops

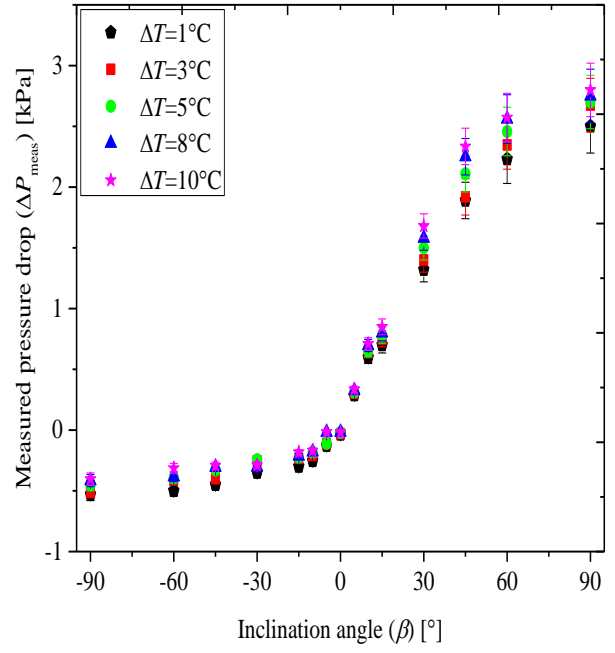
The measured pressure drops for mass fluxes of 100, 75, and 50 kg/m<sup>2</sup>s are plotted as functions of the different inclination angles with varying temperature differences at various mean vapour qualities of 0.25, 0.5, and 0.75 as shown in Figs. 7.1 – 7.3. In general, the results showed the same trends of measured pressure drops as a function of mass flux, and vapour qualities that have been established in previous works. Thus, in general, the measured pressure drops increased with increasing values of vapour quality and mass flux. Other trends that have been experienced will be divided based on contributing parameters such as inclination angle, temperature differences, mass fluxes and vapour qualities.

#### 7.3.1. Effect of inclination angles

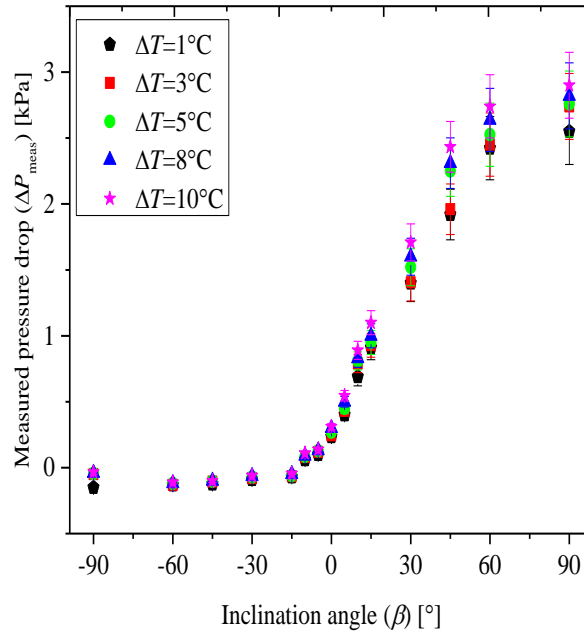
The inclination angle had a significant effect on the measured pressure drop ( $\Delta P_{\text{meas}}$ ) as shown in Figs. 7.1 – 7.3. The trend of variations in measured pressure drop may be attributed to the gravitational force which acts in the opposite direction when the tube is gradually tilted to the vertical upward directions. The maximum measured pressure drops were obtained during the upward flows ( $+60^\circ \leq \beta \leq +90^\circ$ ), while the minimums were found during the downward flows between ( $-90^\circ \leq \beta \leq -60^\circ$ ). The results wherein higher measured pressure drops were found during the upward inclination can further be explained by the fact that as the tube is inclined upwards, the mean flow velocity reduced which subsequently increased the liquid film thickness as can be deduced from the flow patterns in Figs 6.2 and 6.3.



(a)



(b)



(c)

**Fig. 7.1: Measured pressure drop,  $\Delta P_{\text{meas}}$  as a function of inclination angle,  $\beta$ , at different wall and refrigerant temperature differences,  $\Delta T$ , at a mass flux of  $100 \text{ kg/m}^2\text{s}$  during condensation: (a) at a mean quality of 0.25, (b) at a mean quality of 0.50 and (c) at a mean quality of 0.62.**

The results wherein lower measured values were found during the downward inclination was as a result of the reduction of pressure drop due to gravity-assisted drainage of condensate. Consistent with the findings in Ewim and Meyer [54], at an inclination angle ( $\beta$ ) =  $-90^\circ$  and vapour quality of 0.25, the

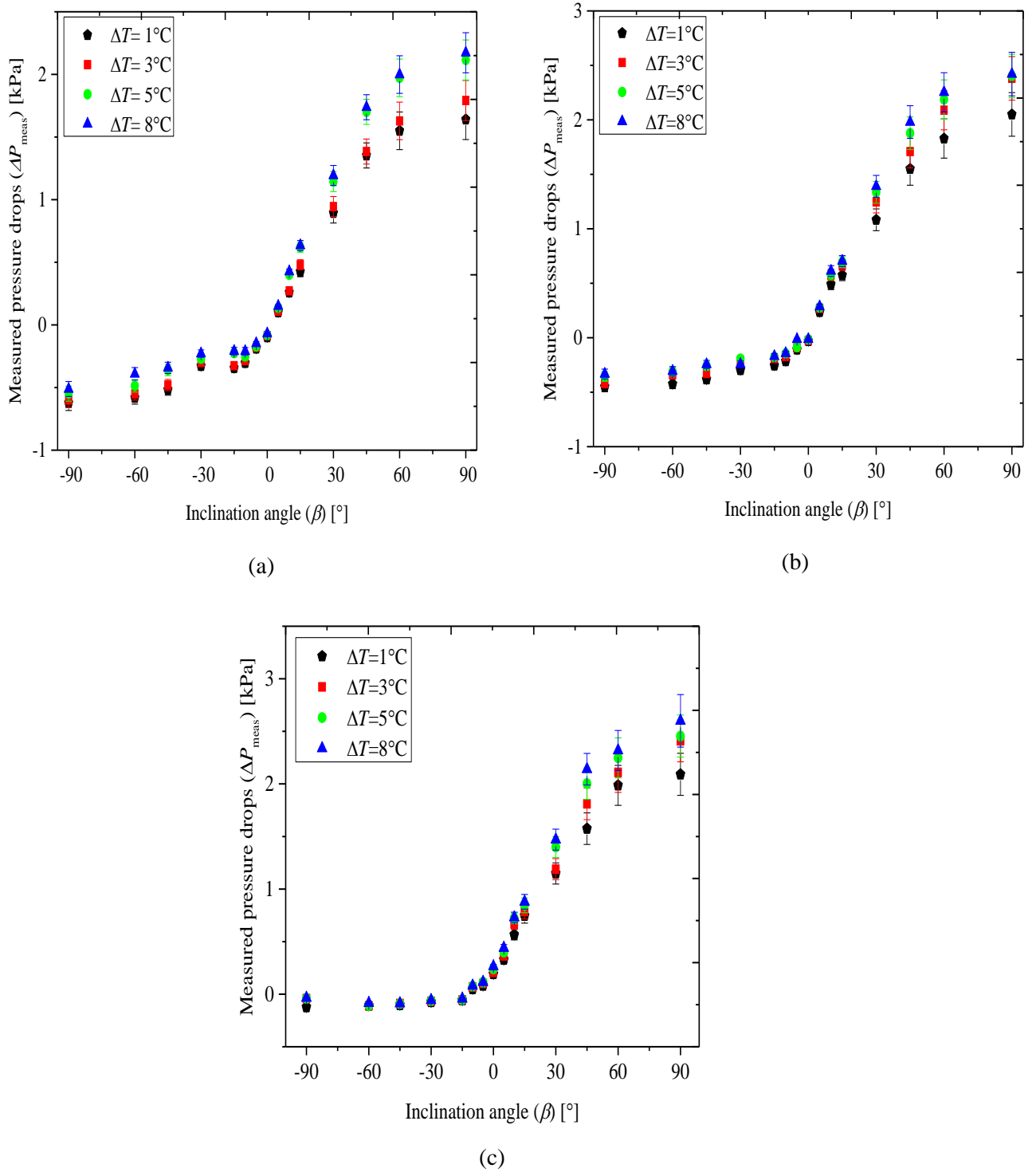
outlet flow regime was churn which is characterised by the presence of Taylor bubbles within the core of the tube.

With an increase in the inclination angle to  $-30^\circ \leq \beta \leq -15^\circ$  (Figs. 6.2 and 6.3), the vapour flowed at the top of the tube, while the liquid film remained at the bottom due to the effect of the gravity force and thus a stratified wavy flow regime. In this flow regime, there was direct contact between the vapour and tube wall, and as a result, there was an increase in the measured pressure drop. With an additional increase in the inclination angle, the liquid film thickness increased which further led to a rise in the measured pressure drop. We can also relate the increase in the measured drop as the inclination angle increased to a rise in the static pressure drop.

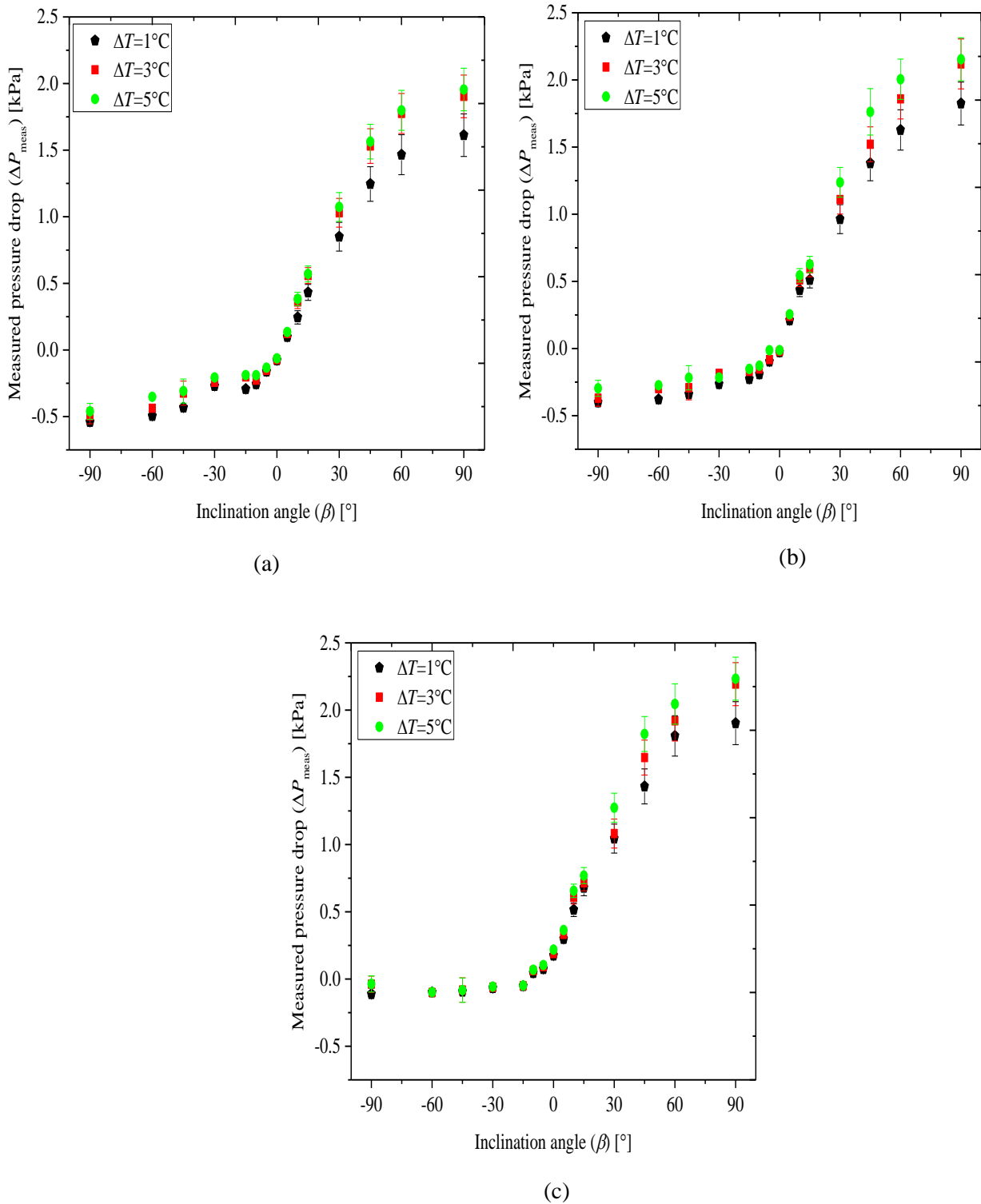
The upward flows generally led to a positive static pressure drop ( $\Delta P_{stat}$ ) and the opposite was true for downward flows. This is due to the fact that the sinus of the angle of inclination ( $\beta$ ) was negative for downward flows but positive for upward flows. In essence, the static pressure drop was higher during upward flows, zero during horizontal flow and minimum during downward flows. To summarise, the variations of measured pressure drop with respect to the inclination angles may be ascribed to the variation of flow regime, the liquid film thickness on the tube surface, and the static pressure drop.

### **7.3.2. Effect of temperature differences**

The effect of the temperature difference on the measured pressure drops is shown in Figs. 7.1 – 7.3. It was found from our earlier work [52, 54] that during the smooth stratified and stratified wavy flow regimes which was typically characterised by low mass fluxes, an increment in the temperature difference ( $\Delta T$ ) led to a rise in the liquid film thickness. This increase in film thickness and consequent greater flow resistance best explains why there was an increase in the measured pressure drops as the temperature difference increased. This can be seen from Figs. 3 and 4 when comparing the flow patterns at a temperature difference of 10 °C and inclination angle of 0° to the flow pattern at a temperature difference of 3 °C at the same inclination angle. However, it seems as if the effect of temperature difference competed with the inclination effect on the measured pressure drops for this two-phase flow process. Also, at low mass fluxes, the low-velocity vapour flow and gravity forces caused downward flow of the condensate that formed at the bottom portion of the tube into the liquid pool during condensation. As the condensation occurred, the thickness of the film increased and this thick layer of liquid at the bottom of the tube increased with temperature difference leading to higher measure pressure drops.



**Fig. 7.2:** Measured pressure drop,  $\Delta P_{\text{meas}}$  as a function of inclination angle,  $\beta$ , at different wall and refrigerant temperature differences,  $\Delta T$ , at a mass flux of  $75 \text{ kg/m}^2\text{s}$  during condensation: (a) at a mean quality of 0.25, (b) at a mean quality of 0.50 and (c) at a mean quality of 0.62.



**Fig. 7.3:** Measured pressure drop,  $\Delta P_{\text{meas}}$  as a function of inclination angle,  $\beta$ , at different wall and refrigerant temperature differences,  $\Delta T$ , at a mass flux of  $50 \text{ kg/m}^2\text{s}$  during condensation: (a) at a mean quality of 0.25, (b) at a mean quality of 0.50 and (c) at a mean quality of 0.62.

### 7.3.3. Effect of mass flux and vapour quality

In general, Figs. 7.1 – 7.3, show that there was an increase in the measured pressure drops with an increase in vapour qualities and mass fluxes. The increases in vapour qualities and mass fluxes

increased the shear forces on the vapour–liquid interface causing a more unstable interface, thereby increasing the pressure drops. This can be deduced when comparing the flow pattern for a mass flux of 100 kg/m<sup>2</sup>s (Fig. 6.2) and mass flux of 75 kg/m<sup>2</sup>s (Fig. 6.3). It can also be deduced that with a further increase of the vapour qualities and inclination angles, the shear forces caused the liquid film to be evenly distributed around the perimeter as the vapour travelled through the core of the tube. In general, since the effect of shear force began to manifest with increasing mass fluxes and quality, there was an expected increase in the measured pressure drops as mass fluxes, and vapour quality was increased.

#### **7.4. Frictional pressure drops**

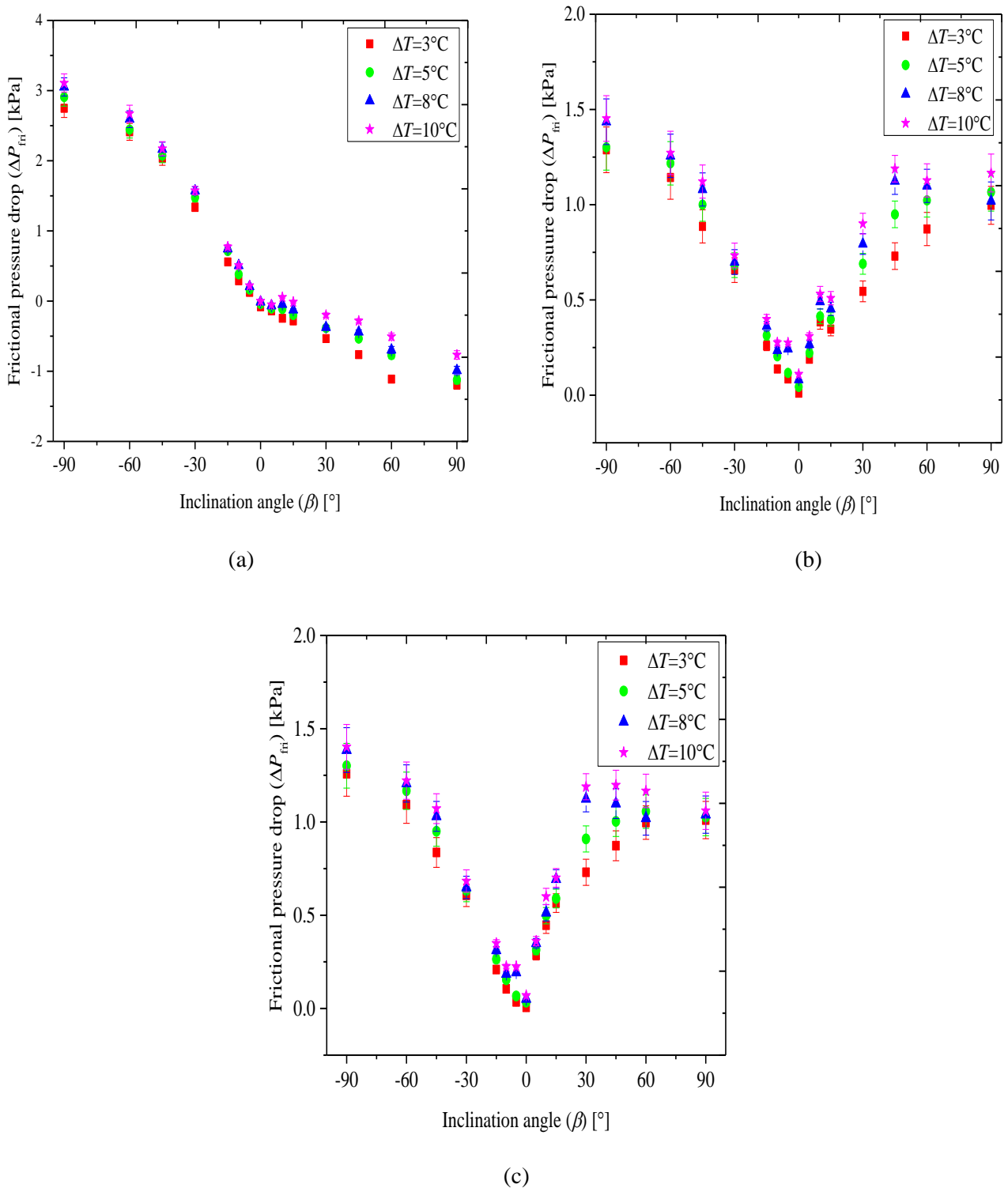
The frictional pressure drops at mass fluxes of 100, 75, and 50 kg/m<sup>2</sup>s are plotted as functions of different inclination angles with varying temperature differences at various mean vapour qualities of 0.25, 0.5, and 0.62 in Figs. 7.4 – 7.6. In general, the results showed some general trends of the frictional pressure drop as a function of mass flux and vapour qualities that have been shown in previous work. Thus, in general, the frictional pressure drops increased with increasing values of vapour quality and mass flux. Other trends that have been found will be divided based on new contributing parameters such as inclination angles and temperature differences.

##### **7.4.1. Effect of inclination angles**

From Figs. 7.4 – 7.6, it follows that the inclination angle had a significant effect on the frictional pressure drops. The trend of variations in frictional pressure drop may be attributed to the prevailing flow pattern and other parameters. The maximum frictional pressure drops were obtained during the downward flows, while the minimum was typically obtained during horizontal and vertical flows. The results wherein higher measured pressure drops were found during upward inclination angles is because the mean flow velocity reduced which subsequently caused higher static pressure drops and consequently lower frictional pressure drops. This reduction in the flow velocity during upward flow weakened the wall-fluid, and the liquid-vapour shear stresses which produced a decrease in the frictional pressure drops.

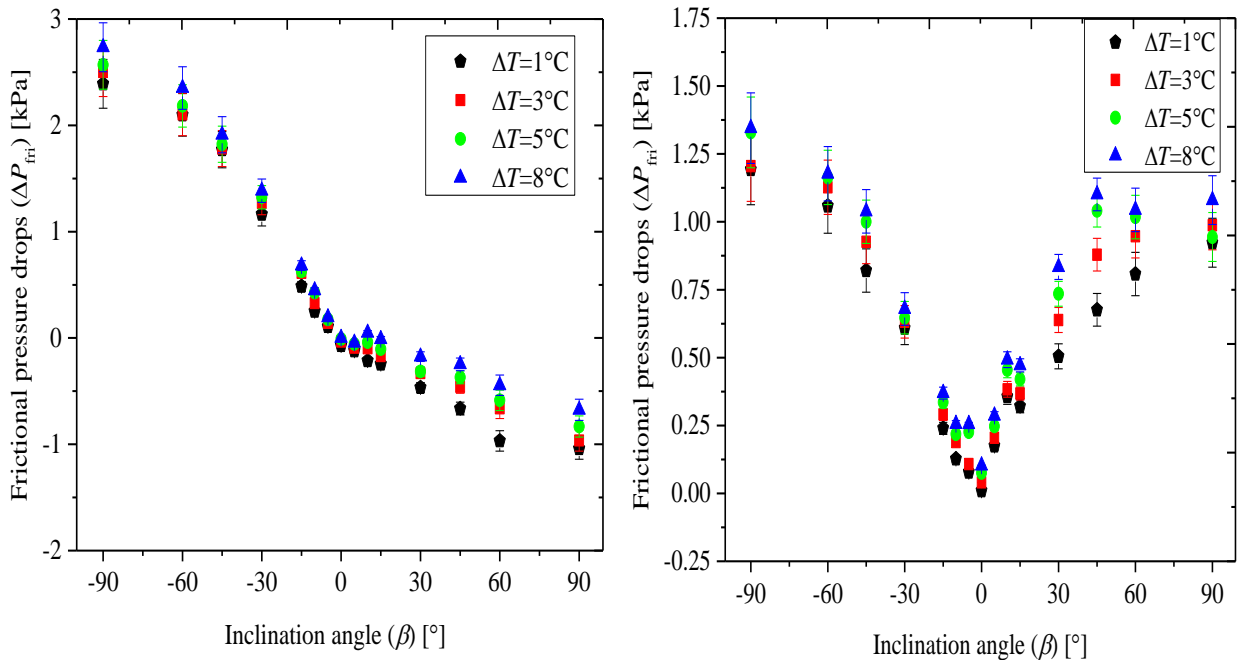
Typically, at a mass flux of 100 and quality of 0.5, it was found that for downward flows, the flow pattern changed from mainly stratified-wavy at the near horizontal positions to annular at the vertical downward tube orientation. However, during the upward tube orientation, the flow pattern changes from stratified-wavy to churn at the vertical upward tube orientation. This variation of flow pattern with inclination angle was explicitly captured during the flow pattern analysis [52, 54, 167]. The change of frictional pressure drops with inclination angle can also be attributed to higher liquid holds during upward flows; hence predominant static pressure drops which adversely affected the frictional

pressure drops. The opposite was true during downward flow where the liquid film decreased, resulting in a decrease in the wall-fluid and vapour-liquid interfacial stresses hence an increase in the frictional



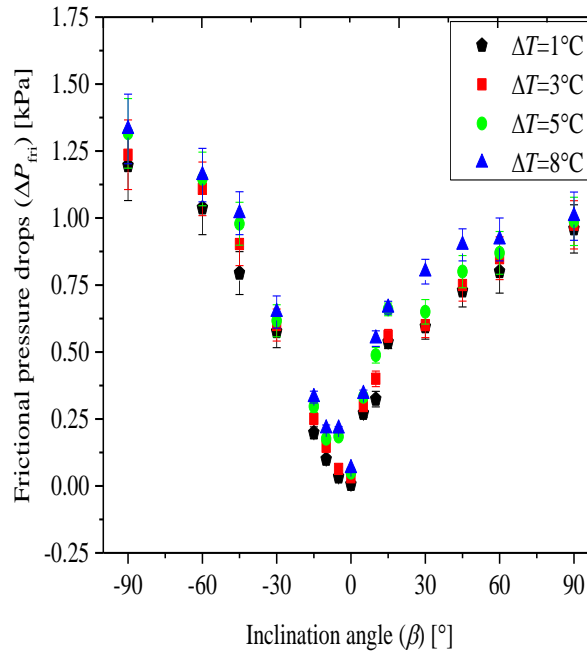
**Fig. 7.4:** Frictional pressure drop,  $\Delta P_{\text{fri}}$  as a function of inclination angle,  $\beta$ , at different wall and refrigerant temperature differences,  $\Delta T$ , at a mass flux of  $100 \text{ kg/m}^2\text{s}$  during condensation: (a) at a mean quality of 0.25, (b) at a mean quality of 0.50 and (c) at a mean quality of 0.62.





(a)

(b)



(c)

**Fig. 7.5: Frictional pressure drop,  $\Delta P_{\text{fri}}$  as a function of inclination angle,  $\beta$ , at different wall and refrigerant temperature differences,  $\Delta T$ , at a mass flux of  $75 \text{ kg/m}^2\text{s}$  during condensation: (a) at a mean quality of 0.25, (b) at a mean quality of 0.50 and (c) at a mean quality of 0.62.**

pressure drop. To summarise, the inclination angle affected the flow patterns, and this manifested in the frictional pressure drop results.

#### **7.4.2. Effect of temperature differences**

The effect of the temperature difference on the frictional pressure drops is also shown in Figs. 7.4 – 7.6. In general, it was found that the frictional pressure drops increased with increasing values of the temperature differences for all angles of inclination. It has been shown from our previous works that as the liquid film thickness increased, the temperature difference increased, causing more resistance which leads to an increase in the frictional pressure drops. This can be seen from Figs. 6.2 and 6.3 when comparing the flow patterns at a temperature difference of 10 °C and inclination angle of 15° to the flow pattern at a temperature difference of 3 °C at the same inclination angle. The interaction between the fluid and the tube wall is intimately linked to the frictional pressure drop. The frictional pressure drops were found to be related to properties of the liquid film which was affected by the temperature differences. With an increase in temperature differences, the densities of the liquid film increased so increasing the wall – fluid and vapour-liquid interfacial shear forces leading to an increase in the frictional pressure drops.

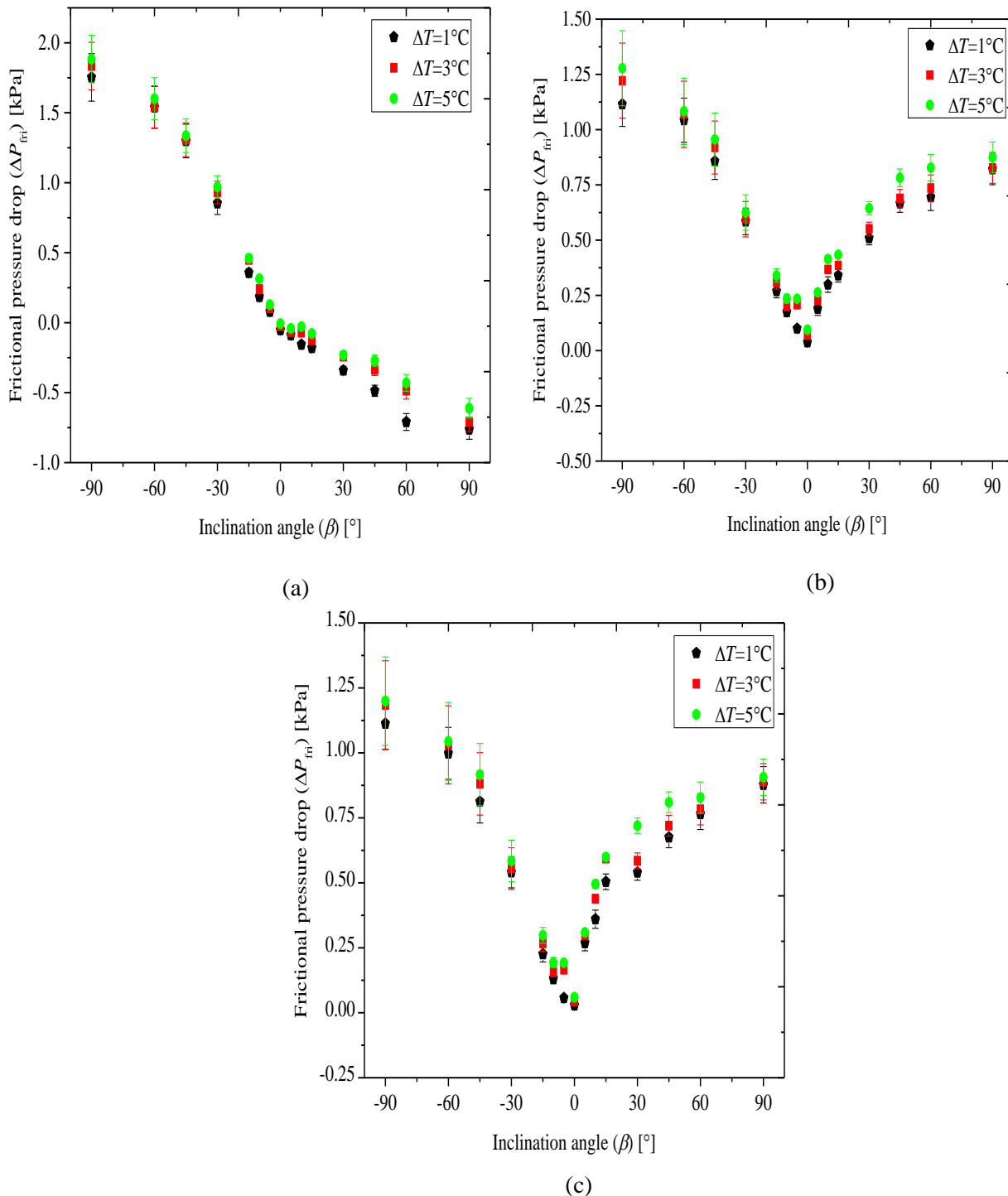
#### **7.4.3. Effect of vapour qualities**

From Figs. 7.4 – 7.6. it followed that the qualities and mass fluxes affected the frictional pressure drops. For the horizontal flows, there was an increase in the frictional pressure drops as the vapour quality was increased. However, for upward flows, the effect of inclination led to higher frictional pressure drops for lower vapour qualities ( $x_m = 0.25$ ). The converse was true for downward flows. Furthermore, it was found that the frictional pressure drops were higher for upward flows and horizontal flows but lower for downward flows as the vapour qualities increased. At high vapour qualities ( $x_m = 0.5$  and above), the frictional pressure drops increased with vapour quality for all orientations. This may be attributed to the fact that the same pattern was prevalent at those high vapour qualities. To summarise, the frictional pressure drops increased with an increase in vapour quality at 0.25 (Fig 7.4a). However, as the vapour quality was increased (Fig 7.4b) and (Fig 7.4c), the frictional drop decreased with decreasing vapour qualities (for all downward flows) until a horizontal inclination angle when it began to rise again. Similarly, increasing qualities resulted in increasing vapour phase velocities and decreasing liquid phase velocities, which increases the slip between the two phases and resulted in increased frictional pressure drops.

#### **7.4.4. Effect of mass fluxes**

In general, it can be deduced from Figs 7.4 – 7.6, that the frictional pressure drops increased with mass fluxes for all vapour qualities and inclination angles. This can be attributed to the fact that the mass

flux is closely linked with the fluid friction against the wall of the test section. Furthermore, since the interfacial shear stress on the tube depends on the mass fluxes and vapour velocities, the frictional pressure drops were affected by the increase in mass fluxes. Furthermore, an increase in mass flux resulted in an increase in the vapour and liquid velocities of the fluid.



**Fig. 7.6: Frictional pressure drop,  $\Delta P_{\text{fri}}$  as a function of inclination angle,  $\beta$ , at different wall and refrigerant temperature differences,  $\Delta T$ , at a mass flux of  $50 \text{ kg/m}^2\text{s}$  during condensation: (a) at a mean quality of 0.25, (b) at a mean quality of 0.50 and (c) at a mean quality of 0.62.**

This increase caused higher wall shear stresses resulting in greater frictional pressure drops. This can be deduced when comparing the flow patterns for a mass flux of  $100 \text{ kg/m}^2\text{s}$  (Fig. 6.2) and mass flux of  $75 \text{ kg/m}^2\text{s}$  (Fig. 6.3). Also, at low mass fluxes, the liquid films were typically asymmetric similar to stratified flow. However, increasing the mass fluxes led to a highly disturbed interface. In such conditions, the friction factor ratios appeared to be mainly a function of the liquid Reynolds number which also depended on mass fluxes. Hence, an increment in the mass flux will lead to an intensification of the turbulence of the flow consequently affecting the frictional pressure drop.

## 7.5. Summary and conclusion

Limited studies have been conducted during the condensation at low mass fluxes where the pressure drops are a function of temperature differences. Therefore, pressure drop experiments were conducted during the convective condensation of R134a in a smooth horizontal and inclined tube at mass fluxes of 50, 75, and  $100 \text{ kg/m}^2\text{s}$ . The mean vapour qualities were varied from 0.1 to 0.9 at temperature differences of 1, 3, 5, 8, and  $10 \text{ }^\circ\text{C}$ . In total, 945 experimental data points were collected for both the validation and low mass flux results.

The flow regimes were captured using two high-speed cameras installed at the entrance and exit of the test condenser. The effects of mass fluxes, inclination angles, temperature differences, vapour qualities and mass fluxes were investigated on the measured and frictional pressure drops and were found to be significant. In all cases, the maximum measured pressure drops were found at the maximum temperature differences and inclinations angles between  $+60^\circ$  and  $90^\circ$  (vertically upward). On the other hand, the maximum frictional pressure drops were found at the maximum temperature differences tested per data point and at an inclinations angle of  $-90^\circ$  (vertical downward flow cases). Furthermore, the minimum measured pressure drops were always found at the lowest temperature differences tested per data point and at an inclination angle of  $-90^\circ$  (vertically downwards flow).

The frictional pressure drops were found to decrease with a decrease in temperature differences. Also, for horizontal and upward flows, the frictional pressure drops increased with an increase in vapour quality. However, for downward flows, it was higher at a vapour quality of 0.25 (low vapour qualities). On the contrary, at high vapour qualities ( $x_m = 0.5$  and above), no significant additional impact of vapour quality was found on the inclination effect.

It was also found that increasing the mass fluxes and vapour qualities, led to a rise in both frictional and measured pressure drops, and this can be attributed to the effects of the interfacial shear forces. With an increase in temperature differences, the densities of the liquid film increased. This increased the wall-fluid and vapour-liquid interfacial shear forces that increased the frictional pressure drops.

Finally, both the measured and frictional pressure drops increased with an increase in temperature difference.

# Chapter 8: Summary, Conclusions and Recommendations

---

## 8.1. Summary

Condensers have a wide range of applications and are found in the process, petrochemical, petroleum, transport, sewage treatment, manufacturing and heating, ventilation and air-conditioning (HVAC) industries. In essence, the applications of condensation are multifarious, consume energy and cover our everyday lives. In addition, condensers are essential components in the cycles of fossil fuel, refrigeration, nuclear and solar power plants. Thus, it is critical that sufficient design information is available for condenser effectiveness and optimization. In general, the aim is to maximize the heat transfer coefficients and minimize the pressure drops through the use of accurate and unified predictive methods. (Although pressure drop and heat transfer are usually investigated independently, there exists a direct relationship that is often overlooked. We need to maximize heat transfer and minimise pressure drops).

In the design process, a selection can be made between low and high mass flow rates. However, little design information is available for heat transfer and pressure drop at low mass fluxes. Although in tube condensation has been extensively investigated, previous studies focused on either horizontal or vertical tubes at high mass fluxes. What further complicates the local heat transfer and pressure drop characteristics in tube condensation is the effect of inclination. However, little work has been published in the open literature which justifies the angles being used or which gives performance data at different inclination angles. Furthermore, most of the design correlations presently in use are either limited or deficient in terms of the conditions which were used to formulate them (i.e. diameter size, working fluid, saturation temperature, mass flux, and tube orientation). All these highlights the gap in the open literature.

To summarise, no study that systematically investigates the influence of temperature difference, vapour quality, and inclination on condensation heat transfer coefficients and pressure drops during the in-tube condensation of low mass fluxes has been conducted. The lack of experimental data at low mass fluxes and inclined angles is most probably the main reason for the limited understanding of and little design information that is available. Thus, the purpose of this study was to experimentally investigate the heat transfer and pressure drop characteristics during the condensation of low mass fluxes in smooth horizontal and inclined tubes. An experimental set-up was modified to accommodate the low mass flux needs of the study and the results were validated against literature. A smooth circular test section with inner tube 1.49 m long, a measured inner diameter of 8.38 mm and an outer diameter of 9.54 mm was used. The annulus outer tube had an inner diameter of 14.5 mm and an outer diameter

of 15.88 mm. Heat transfer and pressure drop measurements were conducted for mass fluxes of 50, 75, and 100, 150 and 200 kg/m<sup>2</sup>s, at different inclination angles from -90° (vertically downwards) to +90° (vertically upwards). The temperature differences (differences between the refrigeration saturation temperature and wall temperature) were varied from 1 °C to 10 °C while the average saturation temperature was maintained at 40 °C. The mean vapour qualities were varied between 0.1 to 0.9. R134a was used as the test fluid while water was used in the annulus to cool the test section. A total of 912 mass flow rate measurements, 56 301 temperature measurements and 1 536 pressure drop measurements were taken. The flow patterns were recorded with a high-speed video camera installed at the inlet and outlet of the test section through sight glasses. An uncertainty analysis showed that the maximum uncertainty of the heat transfer coefficients and vapour qualities of the data presented in this study was 12% and 5%, respectively.

## **8.2. Conclusions**

For horizontal flows, the observed flow patterns were compared to the Thome flow regime map, and it was found that the map predicted most of the experimental data points correctly. In general, however, the map inaccurately predicted the flow regimes as the mass flux decreased and the temperature differences increased. It was found that the effect of the temperature difference on the heat transfer coefficients began to show at a mass flux of 150 kg/m<sup>2</sup>s, but only at a vapour quality of 0.1. However, the dependency of heat transfer coefficients on temperature difference increased at all vapour qualities when the mass fluxes were lower or equal to 100 kg/m<sup>2</sup>s. In all cases, for a specific mass flux lower than 100 kg/m<sup>2</sup>s and a specific mean quality, the maximum heat transfer coefficients were found at the lowest temperature difference, while the minimum heat transfer coefficients were found at the maximum temperature difference.

Finally, as the mass flux decreased, the heat transfer coefficients became more dependent on the temperature difference. The heat transfer coefficients for horizontal flows from this study were also compared to six correlations in the literature, and it was found that the literature did not accurately predict the heat transfer coefficients at low mass fluxes. In general, as the temperature difference increased, the errors between measurements and predictions increased. Two minor revisions to the Cavallini (2006) correlations were suggested in a term that is influenced by the temperature difference. It was found that, when these two revisions to the correlations were introduced, the heat transfer coefficients could be predicted more accurately at low mass fluxes. The correlation that was modified in this study will not only enable designers to optimize the design of heat exchangers but also improve the fundamental understanding of condensation at low mass fluxes.

For inclined flows, it was observed that an annular flow pattern was prevalent for vertically downwards inclination ( $-90^\circ$ ). In contrast, churn was common for the vertically upwards inclination ( $+90^\circ$ ), with wavy annular being observed at higher qualities and intermittent at lower qualities. In all cases, the maximum heat transfer coefficients were found at the minimum temperature difference tested per data point and at inclination angles between  $-15^\circ$  and  $-30^\circ$ . However, the minimum heat transfer coefficients were consistently found at the maximum temperature difference tested per data point and at an inclination angle of  $-90^\circ$  (vertically downwards flow). It was found that even though the heat transfer coefficients for vertically downwards flow decreased with an increase in temperature difference, the percentage differences were approximately 2% (negligible). The converse was true for vertically upwards flows.

With respect to the inclination effect, it was found that it decreased with an increase in temperature difference. It was also found that at low qualities (below 0.35), the inclination effect was more noticeable. On the contrary, at high vapour qualities (above 0.5), no additional significant effect of vapour quality was found on the inclination effect. In general, the maximum inclination effect was found at the lowest mass flux tested for, and the converse was true for the maximum mass flux investigated for.

For annular flows, it was found that the heat transfer coefficients were independent of the inclination angle. In such cases, the heat transfer coefficient increased with increasing mass flux, and this could be attributed to thinning of the liquid film by the increasing effect of vapour shear forces. However, for flows found to be stratified and intermittent, the effect of inclination angles was significant. Beyond a certain downwards inclination angle, it was found that the heat transfer coefficient decreased, and this could be attributed to the decrease in the perimeter occupied by the thin film of condensation at the top of the tube, where most of the condensation occurred.

In general, the heat transfer coefficient mainly depended on the perimeter occupied by the condensation film and its thickness, which were primarily a function of inclination and temperature difference. In conclusion, it is recommended that future inclined condensers be inclined at angles between  $-15^\circ$  and  $-30^\circ$ . Furthermore, it is required that more flow-pattern-dependent mechanistic models be developed to assist with the prediction of the heat transfer coefficients for condensing flows in inclined tubes.

For pressure drops, in all cases, the maximum measured pressure drops were found at the maximum temperature differences and inclination angles between  $+60^\circ$  and  $90^\circ$  (vertically upward). On the other hand, the maximum frictional pressure drops were found at the maximum temperature differences tested per data point and at an inclination angle of  $-90^\circ$  (vertical downward flow cases).



Furthermore, the minimum measured pressure drops were always found at the lowest temperature differences tested per data point and at an inclination angle of  $-90^\circ$  (vertically downwards flow). The frictional pressure drops were found to decrease with a decrease in temperature differences. Also, for horizontal and upward flows, the frictional pressure drops increased with an increase in vapour quality. However, for downward flows, it was higher at a vapour quality of 0.25 (low vapour qualities). On the contrary, at high vapour qualities (above 0.5), no significant additional impact of vapour quality was found on the inclination effect. It was found that increasing the mass fluxes and vapour qualities, led to a rise in both frictional and measured pressure drops, and this can be attributed to the effects of the interfacial shear forces.

With an increase in temperature differences, the densities of the liquid film increased. This increased the wall-fluid and vapour-liquid interfacial shear forces that increased the frictional pressure drops. Finally, both the measured and frictional pressure drops increased with an increase in temperature difference.

### **8.3. Recommendations**

The following future work is recommended:

- It is required that more flow-pattern-dependent mechanistic models be developed to assist with the prediction of the heat transfer coefficients for condensing flows in inclined tubes.
- Similar studies can be carried out using steam and new environmentally friendly refrigerants e.g. R1234yf to expand the existing experimental data.
- Similar studies can be carried out at different saturation temperatures to ascertain if the effect of temperature differences vary with saturation temperature.
- Void fraction measurements should be considered to increase the accuracy of the frictional pressure drop predictions.
- Advanced “non-intrusive” measurement techniques should be explored to measure the liquid film thickness.
- Development of correlations that will cater for temperature difference effect in pressure drops at low mass fluxes should be considered.
- Similar studies should also be conducted in microchannels where the Bond number and surface tension are known to have an effect on the heat transfer process.
- Because of the complex nature of this experimental work, it is also recommended that numerical and analytical work be explored.

## References

---

- [1] A.S. Dalkilic, S. Wongwises, Validation of void fraction models and correlations using a flow pattern transition mechanism model in relation to the identification of annular vertical downflow in-tube condensation of R134a, *International Communications in Heat and Mass Transfer* 37(7) (2010) 827-834.
- [2] A.S. Dalkilic, S. Wongwises, Intensive literature review of condensation inside smooth and enhanced tubes, *International Journal of Heat and Mass Transfer* 52(15-16) (2009) 3409-3426.
- [3] A.S. Dalkilic, O. Agra, I. Teke, S. Wongwises, Comparison of frictional pressure drop models during annular flow condensation of R600a in a horizontal tube at low mass flux and of R134a in a vertical tube at high mass flux, *International Journal of Heat and Mass Transfer* 53(9-10) (2010) 2052-2064.
- [4] S. Lips, J.P. Meyer, Two-phase flow in inclined tubes with specific reference to condensation: A review, *International Journal of Multiphase Flow* 37(8) (2011) 845-859.
- [5] J.A. Olivier, L. Liebenberg, M.A. Kedzierski, J.P. Meyer, Pressure drop during refrigerant condensation inside horizontal smooth, helical microfin, and herringbone microfin tubes, *Journal of Heat Transfer* 126(5) (2004) 687-687.
- [6] J.A. Olivier, L. Liebenberg, J.R. Thome, J.P. Meyer, Heat transfer, pressure drop, and flow pattern recognition during condensation inside smooth, helical micro-fin, and herringbone tubes, *International Journal of Refrigeration* 30(4) (2007) 609-623.
- [7] S. Lips, J.P. Meyer, Effect of gravity forces on heat transfer and pressure drop during condensation of R134a, *Microgravity Science and Technology* 24(3) (2012) 157-164.
- [8] A.O. Adelaja, J. Dirker, J.P. Meyer, Experimental study of the pressure drop during condensation in an inclined smooth tube at different saturation temperatures, *International Journal of Heat and Mass Transfer* 105 (2017) 237-251.
- [9] A.O. Adelaja, J. Dirker, J.P. Meyer, Experimental investigation of frictional pressure drop in inclined tubes, 11th International Conference on Heat Transfer, Fluid Mechanics and Thermodynamics (HEFAT 2015), Kruger National Park, South Africa, 2015.
- [10] T. Bohdal, H. Charun, S. Malgorzata, Pressure drop during condensation of refrigerants in pipe minichannels, *Archives of Thermodynamics* 33(1) (2012) 87-106.
- [11] A. Cavallini, G. Censi, D.D. Col, L. Doretto, G.A. Longo, L. Rossetto, Experimental investigation on condensation heat transfer and pressure drop of new HFC refrigerants in a horizontal smooth tube, *International Journal of Refrigeration* 24 (2001) 73-87.

- [12] A. Cavallini, D. Del Col, L. Doretti, G.A. Longo, L. Rossetto, Heat transfer and pressure drop during condensation of refrigerants inside horizontal enhanced tubes, *International Journal of Refrigeration* 23(1) (2000) 4-25.
- [13] Y. Chen, K.-S. Yang, Y.-J. Chang, C.-C. Wang, Two-phase pressure drop of air–water and R-410A in small horizontal tubes, *International journal of multiphase flow* 27(7) (2001) 1293-1299.
- [14] D. Chisholm, Pressure gradients due to friction during the flow of evaporating two-phase mixtures in smooth tubes and channels, *International Journal of Heat and Mass Transfer* 16(2) (1973) 347-358.
- [15] M.O. Didi, N. Kattan, J. Thome, Prediction of two-phase pressure gradients of refrigerants in horizontal tubes, *International Journal of refrigeration* 25(7) (2002) 935-947.
- [16] L. Friedel, Improved friction pressure drop correlations for horizontal and vertical two-phase pipe flow, *European two-phase flow group meeting*, Paper E, 1979, p. 1979.
- [17] C. Guo, T. Wang, X. Hu, D. Tang, Experimental and theoretical investigation on two-phase flow characteristics and pressure drop during flow condensation in heat transport pipeline, *Applied Thermal Engineering* 66(1-2) (2014) 365-374.
- [18] S. Lips, J.P. Meyer, Experimental study of convective condensation in an inclined smooth tube. Part II: Inclination effect on pressure drops and void fractions, *International Journal of Heat and Mass Transfer* 55(1) (2012) 405-412.
- [19] A. López-Belchí, F. Illán-Gómez, F. Vera-García, J.R. García-Cascales, Experimental condensing two-phase frictional pressure drop inside mini-channels. Comparisons and new model development, *International Journal of Heat and Mass Transfer* 75 (2014) 581-591.
- [20] M. Matkovič, A. Cavallini, S. Bortolin, D.D. Col, L. Rossetto, Heat transfer coefficient during condensation of a high pressure refrigerant inside a circular minichannel, *5th European Thermal-Sciences Conference* (2008) 1-8.
- [21] J. Moreno Quibén, J.R. Thome, Flow pattern based two-phase frictional pressure drop model for horizontal tubes, Part II: New phenomenological model, *International Journal of Heat and Fluid Flow* 28(5) (2007) 1060-1072.
- [22] H. Müller-Steinhagen, K. Heck, A simple friction pressure drop correlation for two-phase flow in pipes, *Chemical Engineering and Processing: Process Intensification* 20(6) (1986) 297-308.
- [23] C.-H. Son, H.-K. Oh, Condensation pressure drop of R22, R134a and R410A in a single circular microtube, *Heat and Mass Transfer* 48(8) (2012) 1437-1450.
- [24] H.S. Wang, J. Sun, J.W. Rose, Pressure drop during condensation in microchannels, *Journal of Heat Transfer* 135(9) (2013) 091602-091605.
- [25] Y. Xu, X. Fang, X. Su, Z. Zhou, W. Chen, Evaluation of frictional pressure drop correlations for two-phase flow in pipes, *Nuclear Engineering and Design* 253 (2012) 86-97.

- [26] U.C. Andresen, S. Garimella, B. Mitra, Y. Jiang, B.M. Fronk, Pressure drop during near-critical-pressure condensation of refrigerant blends, *International Journal of Refrigeration* 59 (2015) 1-13.
- [27] L.M. Chamra, R.L. Webb, M.R. Randlett, Advanced micro-fin tubes for evaporation, *International Journal of Heat and Mass Transfer* 39(9) (1996) 1827-1838.
- [28] H.-S. Lee, C.-H. Son, Condensation heat transfer and pressure drop characteristics of R-290, R-600a, R-134a and R-22 in horizontal tubes, *Heat and Mass Transfer* 46(5) (2010) 571-584.
- [29] A. Souza, J. Chato, J. Jabardo, J. Wattlelet, J. Panek, B. Christoffersen, N. Rhines, Pressure drop during two-phase flow of refrigerants in horizontal smooth tubes, ACRC Project 01 Refrigerant-Side Evaporation and Condensation Studies, Air Conditioning and Refrigeration Center. College of Engineering. University of Illinois at Urbana-Champaign., 1992.
- [30] S. Mancin, A. Diani, L. Rossetto, R134a flow boiling heat transfer and pressure drop inside a 3.4mm ID microfin tube, *Energy Procedia* 45 (2014) 608-615.
- [31] Y. Kang, W.A. Davies III, P. Hrnjak, A.M. Jacobi, Effect of inclination on pressure drop and flow regimes in large flattened-tube steam condensers, *Applied Thermal Engineering* 123 (2017) 498-513.
- [32] S.P. Olivier, J.P. Meyer, M. De Paepe, K. De Kerpel, The influence of inclination angle on void fraction and heat transfer during condensation inside a smooth tube, *International Journal of Multiphase Flow* 80 (2016) 1-14.
- [33] J.P. Meyer, J. Dirker, A.O. Adelaja, Condensation heat transfer in smooth inclined tubes for R134a at different saturation temperatures, *International Journal of Heat and Mass Transfer* 70 (2014) 515-525.
- [34] D. Jung, R. Radermacher, Prediction of pressure drop during horizontal annular flow boiling of pure and mixed refrigerants, *International Journal of Heat and Mass Transfer* 32(12) (1989) 2435-2446.
- [35] Y.-Y. Yan, T.-F. Lin, Condensation heat transfer and pressure drop of refrigerant R-134a in a small pipe, *International Journal of Heat and Mass Transfer* 42(4) (1999) 697-708.
- [36] R. Sánta, Pressure drop during condensation of refrigerant R134a inside horizontal tubes, *Exploitation of Renewable Energy Sources (EXPRES)*, 2011 IEEE 3rd International Symposium on, IEEE, 2011, pp. 117-122.
- [37] Y. Wang, S. Shen, D. Yuan, Frictional pressure drop during steam stratified condensation flow in vacuum horizontal tube, *International Journal of Heat and Mass Transfer* 115 (2017) 979-990.
- [38] S.M. Bhagwat, A.J. Ghajar, Experimental investigation of non-boiling gas-liquid two phase flow in downward inclined pipes, *Experimental Thermal and Fluid Science* 89 (2017) 219-237.
- [39] G. Goss, J. Oliveira, J. Passos, Pressure drop during condensation of R-134a inside parallel microchannels, *International Journal of Refrigeration* 56 (2015) 114-125.

- [40] W. Kuo, Y. Lie, Y. Hsieh, T. Lin, Condensation heat transfer and pressure drop of refrigerant R-410A flow in a vertical plate heat exchanger, *International Journal of Heat and Mass Transfer* 48(25) (2005) 5205-5220.
- [41] S. Garimella, Condensation flow mechanisms in microchannels: basis for pressure drop and heat transfer models, *Heat Transfer Engineering* 25(3) (2004) 104-116.
- [42] D.A.L. Belchí, Characterisation of heat transfer and pressure drop in condensation processes within mini-channel tubes with last generation of refrigerant fluids, Universidad Politecnica de Cartagena (Spain), 2014.
- [43] A. O'Donovan, R. Grimes, Pressure drop analysis of steam condensation in air-cooled circular tube bundles, *Applied Thermal Engineering* 87 (2015) 106-116.
- [44] D. Del Col, M. Bortolato, S. Bortolin, Comprehensive experimental investigation of two-phase heat transfer and pressure drop with propane in a minichannel, *International Journal of Refrigeration* 47 (2014) 66-84.
- [45] S.-P. Guo, Z. Wu, W. Li, D. Kukulka, B. Sundén, X.-p. Zhou, J.-J. Wei, T. Simon, Condensation and evaporation heat transfer characteristics in horizontal smooth, herringbone and enhanced surface EHT tubes, *International Journal of Heat and Mass Transfer* 85 (2015) 281-291.
- [46] D.H. Beggs, J.P. Brill, A study of two-phase flow in inclined pipes, *Journal of Petroleum Technology* 25(05) (1973) 607-617.
- [47] H.-Y. Zhang, J.-M. Li, N. Liu, B.-X. Wang, Experimental investigation of condensation heat transfer and pressure drop of R22, R410A and R407C in mini-tubes, *International Journal of Heat and Mass Transfer* 55(13) (2012) 3522-3532.
- [48] G.A. Longo, S. Mancin, G. Righetti, C. Zilio, Saturated vapour condensation of R410A inside a 4 mm ID horizontal smooth tube: Comparison with the low GWP substitute R32, *International Journal of Heat and Mass Transfer* 125 (2018) 702-709.
- [49] S.M.A. Noori Rahim Abadi, M. Mehrabi, J.P. Meyer, Prediction and optimization of condensation heat transfer coefficients and pressure drops of R134a inside an inclined smooth tube, *International Journal of Heat and Mass Transfer* 124 (2018) 953-966.
- [50] S.M.A. Noori Rahim Abadi, M. Mehrabi, J.P. Meyer, Numerical study of steam condensation inside a long, inclined, smooth tube at different saturation temperatures, *International Journal of Heat and Mass Transfer* 126 (2018) 15-25.
- [51] A. Diani, M. Campanale, A. Cavallini, L. Rossetto, Low GWP refrigerants condensation inside a 2.4 mm ID microfin tube, *International Journal of Refrigeration* 86 (2018) 312-321.
- [52] J.P. Meyer, D.R.E. Ewim, Heat transfer coefficients during the condensation of low mass fluxes in smooth horizontal tubes, *International Journal of Multiphase Flow* 99 (2018) 485-499.

- [53] S.M.A. Noori Rahim Abadi, J.P. Meyer, J. Dirker, Effect of inclination angle on the condensation of R134a inside an inclined smooth tube, *Chemical Engineering Research and Design* 132 (2018) 346-357.
- [54] D.R.E. Ewim, J.P. Meyer, S.M.A. Noori Rahim Abadi, Condensation heat transfer coefficients in an inclined smooth tube at low mass fluxes, *International Journal of Heat and Mass Transfer* 123 (2018) 455-467.
- [55] B. Ren, L. Zhang, J. Cao, H. Xu, Z. Tao, Experimental and theoretical investigation on condensation inside a horizontal tube with noncondensable gas, *International Journal of Heat and Mass Transfer* 82 (2015) 588-603.
- [56] H. Cao, Computational fluid dynamics simulations of convective pure vapor condensation inside vertical cylindrical condensers, *Journal of Heat Transfer* 139(6) (2017) 061503.
- [57] H.B. Komandiwirya, P. Hrnjak, T. Newell, An experimental investigation of pressure drop and heat transfer in an in-tube condensation system of ammonia with and without miscible oil in smooth and enhanced tubes, *Air Conditioning and Refrigeration Center. College of Engineering. University of Illinois at Urbana-Champaign.*, 2005.
- [58] A. Cavallini, G. Censi, D. Del Col, L. Doretti, G.A. Longo, L. Rossetto, C. Zilio, Condensation inside and outside smooth and enhanced tubes -a review of recent research, *International Journal of Refrigeration* 26(4) (2003) 373-392.
- [59] L. Doretti, C. Zilio, S. Mancin, A. Cavallini, Condensation flow patterns inside plain and microfin tubes: A review, *International Journal of Refrigeration* 36(2) (2013) 567-587.
- [60] B.M. Fronk, S. Garimella, In-tube condensation of zeotropic fluid mixtures, *International Journal of Refrigeration* 36(2) (2012) 534-561.
- [61] O. García-Valladares, Review of in-tube condensation heat transfer correlations for smooth and microfin tubes, *Heat Transfer Engineering* 24(4) (2003) 6-24.
- [62] J.R. Thome, Condensation inside tubes, *Wolverine Engineering Data Book III2006*, pp. 1-29.
- [63] R. Enright, N. Miljkovic, J.L. Alvarado, K. Kim, J.W. Rose, Dropwise condensation on micro- and nanostructured surfaces, *Nanoscale and Microscale Thermophysical Engineering* 18(3) (2014) 223-250.
- [64] B.M. Fronk, S. Garimella, In-tube condensation of zeotropic fluid mixtures: A review, *International Journal of Refrigeration* 36(2) (2013) 534-561.
- [65] A.P. Kryukov, V.Y. Levashov, N.V. Pavlyukevich, Condensation from a vapor-gas mixture, *Journal of Engineering Physics and Thermophysics* 83(4) (2010) 679-687.
- [66] H. Louahli-Gualous, B. Mecheri, Unsteady steam condensation flow patterns inside a miniature tube, *Applied Thermal Engineering* 27(8-9) (2007) 1225-1235.

- [67] J.M. Martín-Valdepeñas, M.A. Jiménez, F. Martín-Fuertes, J.A.F. Benítez, Comparison of film condensation models in presence of non-condensable gases implemented in a CFD Code, *Heat and Mass Transfer/Waerme- und Stoffuebertragung* 41(11) (2005) 961-976.
- [68] A. Odaymet, H. Louahlia-Gualous, Experimental study of slug flow for condensation in a single square microchannel, *Experimental Thermal and Fluid Science* 38 (2012) 1-13.
- [69] J.W. Rose, Enhanced condensation heat transfer, *JSME International Journal, Series B: Fluids and Thermal Engineering* 49(3) (2006) 626-635.
- [70] B. Shen, E.A. Groll, A critical review of the influence of lubricants on the heat transfer and pressure drop of refrigerants - Part II: Lubricant influence on condensation and pressure drop, *HVAC&R Research* 11(4) (2005) 511-526.
- [71] S. Lips, J.P. Meyer, Stratified flow model for convective condensation in an inclined tube, *International Journal of Heat and Fluid Flow* 36 (2012) 83-91.
- [72] S. Lips, J.P. Meyer, Experimental study of convective condensation in an inclined smooth tube. Part I: Inclination effect on flow pattern and heat transfer coefficient, *International Journal of Heat and Mass Transfer* 55(1) (2012) 395-404.
- [73] D. Jung, Y. Cho, K. Park, Flow condensation heat transfer coefficients of R22, R134a, R407C, and R410A inside plain and microfin tubes, *International Journal of Refrigeration* 27(1) (2004) 25-32.
- [74] M.H. Kim, J.S. Shin, Condensation heat transfer of R22 and R410A in horizontal smooth and microfin tubes, *International Journal of Refrigeration* 28(6) (2005) 949-957.
- [75] G. Arslan, N. Eskin, Heat transfer characteristics for condensation of R134a in a vertical smooth tube, *Experimental Heat Transfer* 28(5) (2014) 430-445.
- [76] E. van Rooyen, M. Christians, L. Liebenberg, J.P. Meyer, Probabilistic flow pattern-based heat transfer correlation for condensing intermittent flow of refrigerants in smooth horizontal tubes, *International Journal of Heat and Mass Transfer* 53(7-8) (2010) 1446-1460.
- [77] A.S. Dalkilic, S. Wongwises, Two-phase heat transfer coefficients of R134a condensation in vertical downward flow at high mass flux, in: P.A. Belmiloudi (Ed.) *Heat Transfer - Theoretical Analysis, Experimental Investigations and Industrial Systems*, 2011, pp. 15-32.
- [78] A.S. Dalkilic, S. Wongwises, Experimental study on the modeling of condensation heat transfer coefficients in high mass flux region of refrigerant HFC-134a inside the vertical smooth tube in annular flow regime, *Heat Transfer Engineering* 32(1) (2011) 33-44.
- [79] A.S. Dalkilic, S. Laohalertdecha, S. Wongwises, Experimental investigation of heat transfer coefficient of R134a during condensation in vertical downward flow at high mass flux in a smooth tube, *International Communications in Heat and Mass Transfer* 36(10) (2009) 1036-1043.

- [80] L. Liebenberg, J.R. Thome, J.P. Meyer, Flow visualization and flow pattern identification with power spectral density distributions of pressure traces during refrigerant condensation in smooth and micro-fin tubes, *Journal of Heat Transfer* 127(3) (2005) 209-220.
- [81] R. Suliman, L. Liebenberg, J.P. Meyer, Improved flow pattern map for accurate prediction of the heat transfer coefficients during condensation of R-134a in smooth horizontal tubes and within the low-mass flux range, *International Journal of Heat and Mass Transfer* 52(25-26) (2009) 5701-5711.
- [82] A. Cavallini, G. Censi, D.D. Col, L. Doretti, L. Rossetto, G.A. Longo, Heat transfer coefficients of HFC refrigerants during condensation at high temperature inside an enhanced tube, 9th International Refrigeration and Air Conditioning Conference, Purdue, USA, 2002, p. Paper 563.
- [83] A. Cavallini, G. Censi, D. Del Col, L. Doretti, G.A. Longo, L. Rossetto, Experimental investigation on condensation heat transfer and pressure drop of new HFC refrigerants (R134a, R125, R32, R410, R236ea) in a horizontal smooth tube, *International Journal of Refrigeration* 24 (2001) 73-87.
- [84] L. Liebenberg, J.P. Meyer, A review of flow pattern-based predictive correlations during refrigerant condensation in horizontally smooth and enhanced tubes, *Heat Transfer Engineering* 29(1) (2008) 3-19.
- [85] L. Liebenberg, J.P. Meyer, Refrigerant condensation flow regimes in enhanced tubes and their effect on heat transfer coefficients and pressure drops, *Heat Transfer Engineering* 29(6) (2008) 506-520.
- [86] C. Aprea, A. Greco, G.P. Vanoli, Condensation heat transfer coefficients for R22 and R407C in gravity driven flow regime within a smooth horizontal tube, *International Journal of Refrigeration* 26 (2003) 393-401.
- [87] M. Awad, A. Dalkılıç, S. Wongwises, A critical review on condensation heat transfer in microchannels and minichannels, *Journal of Nanotechnology in Engineering and Medicine* 5(1) (2014) 010904.
- [88] M.M. Shah, A general correlation for heat transfer during film condensation inside pipes, *International Journal of Heat and Mass Transfer* 22(4) (1979) 547-556.
- [89] M.M. Shah, An improved and extended general correlation for heat transfer during condensation in plain tubes, *HVAC&R Research* 15(5) (2009) 889-913.
- [90] M.M. Shah, A new flow pattern based correlation for heat transfer during condensation in horizontal tubes, *International Heat Transfer Conference (IHTC)*, Kyoto Japan, 2014.
- [91] M.M. Shah, Prediction of heat transfer during condensation in inclined plain tubes, *Applied Thermal Engineering* 94 (2016) 82-89.



- [92] A.O. Adelaja, J. Dirker, J.P. Meyer, Convective condensation heat transfer of R134a in tubes at different inclination angles, *International Journal of Green Energy* 13(8) (2016) 812-821.
- [93] I.Y. Chen, G. Kocamustafaogullari, Condensation heat transfer studies for stratified, cocurrent two-phase flow in horizontal tubes, *International Journal of Heat and Mass Transfer* 30(6) (1987) 1133-1148.
- [94] J.R. Thome, J. El Hajal, A. Cavallini, Condensation in horizontal tubes, Part 2: New heat transfer model based on flow regimes, *International Journal of Heat and Mass Transfer* 46(18) (2003) 3365-3387.
- [95] A. Cavallini, D.D. Col, L. Doretti, M. Matkovic, L. Rossetto, C. Zilio, G. Censi, Condensation in horizontal smooth tubes: A new heat transfer model for heat exchanger design, *Heat Transfer Engineering* 27(8) (2006) 31-38.
- [96] M.M. Shah, Comprehensive correlations for heat transfer during condensation in conventional and mini/micro channels in all orientations, *International Journal of Refrigeration* 67 (2016) 22-41.
- [97] J. El Hajal, J.R. Thome, A. Cavallini, Condensation in horizontal tubes, Part 1: Two-phase flow pattern map, *International Journal of Heat and Mass Transfer* 46(18) (2003) 3349-3363.
- [98] D. Khoeini, M.A. Akhavan-Behabadi, A. Saboonchi, Experimental study of condensation heat transfer of R-134a flow in corrugated tubes with different inclinations, *International Communications in Heat and Mass Transfer* 39(1) (2012) 138-143.
- [99] S.G. Mohseni, M.A. Akhavan-Behabadi, M. Saeedinia, Flow pattern visualization and heat transfer characteristics of R-134a during condensation inside a smooth tube with different tube inclinations, *International Journal of Heat and Mass Transfer* 60 (2013) 598-602.
- [100] S.G. Mohseni, M.A. Akhavan-Behabadi, Flow pattern visualization and heat transfer characteristics of R-134a during evaporation inside a smooth tube with different tube inclinations, *International Communications in Heat and Mass Transfer* 59 (2014) 39-45.
- [101] S.G. Mohseni, M.A. Akhavan-Behabadi, Visual study of flow patterns during condensation inside a microfin tube with different tube inclinations, *International Communications in Heat and Mass Transfer* 38(8) (2011) 1156-1161.
- [102] F. Xing, J. Xu, J. Xie, H. Liu, Z. Wang, X. Ma, Froude number dominates condensation heat transfer of R245fa in tubes: Effect of inclination angles, *International Journal of Multiphase Flow* 71 (2015) 98-115.
- [103] Y. Lyulin, I. Marchuk, S. Chikov, O. Kabov, Experimental study of laminar convective condensation of pure vapor inside an inclined circular tube, *Microgravity Science and Technology* 23(4) (2011) 439-445.

- [104] W.A. Davies, Heat transfer and visualization in large flattened-tube condensers with variable inclination, Mechanical Science and Engineering, University of Illinois at Urbana-Champaign, USA, 2016, p. 112.
- [105] W.A. Davies III, Y. Kang, P. Hrnjak, A.M. Jacobi, Heat transfer and visualization in large flattened-tube condensers with variable inclination, 16th International Refrigeration and Air Conditioning Conference Purdue, USA, 2016, p. Paper 1700.
- [106] M.A. Akhavan-Behabadi, S.G. Mohseni, S.M. Razavinasab, Evaporation heat transfer of R-134a inside a microfin tube with different tube inclinations, Experimental Thermal and Fluid Science 35(6) (2011) 996-1001.
- [107] E. Grolman, J.M.H. Fortuin, Gas-liquid flow in slightly inclined pipes, Chemical Engineering Science 52 (1997) 4461-4471.
- [108] A.J. Ghajar, C.C. Tang, Heat transfer measurements, flow pattern maps, and flow visualization for non-boiling two-phase flow in horizontal and slightly inclined pipe, Heat Transfer Engineering 28(6) (2007) 525-540.
- [109] J.C. Chato, Laminar condensation inside horizontal and inclined tubes, ASHRAE Journal 4 (1962) 52-60.
- [110] R. Würfel, T. Kreutzer, W. Fratzscher, Turbulence transfer processes in adiabatic and condensing film flow in an inclined tube, Chemical engineering & technology 26(4) (2003) 439-448.
- [111] J. Tepe, A. Mueller, Condensation and subcooling inside an inclined tube, Chemical Engineering Progress 43(5) (1947) 267-278.
- [112] Y. Yang, L. Jia, Experimental investigation on heat transfer coefficient during upward flow condensation of R410A in vertical smooth tubes, Journal of Thermal Science 24(2) (2015) 155-163.
- [113] T. Nitheanandan, H.M. Soliman, Analysis of the stratified/nonstratified transition boundary in horizontal and slightly inclined condensing flows, Canadian Journal of Chemical Engineering 72 (1994) 26-34.
- [114] Y.-J. Kim, J.-M. Cho, M.-S. Kim, Studies on the evaporative heat transfer characteristics and pressure drop of CO<sub>2</sub> flowing upward in inclined (45°) smooth and micro-fin tubes, Transactions of the Korean Society of Mechanical Engineers B 32(8) (2008) 612-620.
- [115] D. Barnea, A unified model for predicting flow-pattern transitions for the whole range of pipe inclinations, International Journal of Multiphase Flow 13 (1987) 1-12.
- [116] J.C. Chato, Laminar condensation inside horizontal and inclined tubes, Department of Mechanical Engineering, Massachusetts Institute of Technology, USA, 1960.
- [117] K.E. Hassan, M. Jakob, Laminar film condensation of pure saturated vapours on inclined circular cylinders, ASME Journal of Heat Transfer 80(4) (1958) 887-894.

- [118] B.X. Wang, X.Z. Du, Condensation on the outside surface of a small/mini diameter tube for vapor flowing through a horizontal annulus surround by an adiabatic concentric tube, *International Journal of Heat and Mass Transfer* 43(8) (2000) 1391-1398.
- [119] I. Park, H. Lee, I. Mudawar, Determination of flow regimes and heat transfer coefficient for condensation in horizontal tubes, *International Journal of Heat and Mass Transfer* 80 (2015) 698-716.
- [120] I. Park, I. Mudawar, Climbing film, flooding and falling film behavior in upflow condensation in tubes, *International Journal of Heat and Mass Transfer* 65 (2013) 44-61.
- [121] H. Lee, C.R. Kharangate, N. Mascarenhas, I. Park, I. Mudawar, Experimental and computational investigation of vertical downflow condensation, *International Journal of Heat and Mass Transfer* 85 (2015) 865-879.
- [122] I. Park, S.-M. Kim, I. Mudawar, Experimental measurement and modeling of downflow condensation in a circular tube, *International Journal of Heat and Mass Transfer* 57(2) (2013) 567-581.
- [123] K.-E. Hassan, *Laminar film condensation of pure saturated vapors on inclined circular cylinders*, Mechanical Engineering, Illinois Institute of Technology, USA, 1955.
- [124] R. Suliman, M. Kyembe, J.P. Meyer, Experimental investigation and validation of heat transfer coefficients during condensation of R-134a at low mass fluxes, 7th International Conference on Heat Transfer, Fluid Mechanics and Thermodynamics (HEFAT), Antalya, Turkey, 2010, pp. 1-7.
- [125] M.B. Ould Didi, N. Kattan, J.R. Thome, Prediction of two-phase pressure gradients of refrigerants in horizontal tubes, *International Journal of Refrigeration* 25(7) (2002) 935-947.
- [126] A. Cavallini, D. Del Col, L. Doretti, G. Longo, L. Rossetto, Heat transfer and pressure drop during condensation of refrigerants inside horizontal enhanced tubes, *International Journal of Refrigeration* 23(1) (2000) 4-25.
- [127] D. Del Col, D. Torresin, A. Cavallini, Heat transfer and pressure drop during condensation of the low GWP refrigerant R1234yf, *International Journal of Refrigeration* 33(7) (2010) 1307-1318.
- [128] L.M. Schlager, M.B. Pate, A.E. Bergles, Heat transfer and pressure drop during evaporation and condensation of R22 in horizontal micro-fin tubes, *International Journal of Refrigeration* 12(1) (1989) 6-14.
- [129] G.A. Longo, Heat transfer and pressure drop during hydrocarbon refrigerant condensation inside a brazed plate heat exchanger, *International Journal of Refrigeration* 33(5) (2014) 944-953.
- [130] A. Briggs, C. Kelemenis, J.W. Rose, Heat transfer and pressure drop measurements for in-tube condensation of CFC-113 using microfin tubes and wire inserts, *Experimental Heat Transfer* 13(3) (2000) 163-181.

- [131] C. Guo, T. Wang, X. Hu, D. Tang, Experimental and theoretical investigation on two-phase flow characteristics and pressure drop during flow condensation in heat transport pipeline, *Applied Thermal Engineering* 66(1) (2014) 365-374.
- [132] L. Wang, C. Dang, E. Hihara, Experimental study on condensation heat transfer and pressure drop of low GWP refrigerant HFO1234yf in a horizontal tube, *International Journal of Refrigeration* 35(5) (2012) 1418-1429.
- [133] M.E.G. Ferguson, P.L. Spedding, Measurement and prediction of pressure drop in two-phase flow, *Journal of Chemical Technology & Biotechnology* 63(3) (1995) 262-278.
- [134] A.S. Dalkılıç, A. Çebi, O. Acikgoz, S. Wongwises, Prediction of frictional pressure drop of R134a during condensation inside smooth and corrugated tubes, *International Communications in Heat and Mass Transfer* 88 (2017) 183-193.
- [135] F. Aakenes, S.T. Munkejord, M. Drescher, Frictional pressure drop for two-phase flow of carbon dioxide in a tube: Comparison between models and experimental data, *Energy Procedia* 51(Supplement C) (2014) 373-381.
- [136] M.A. Hossain, H.M.M. Afroz, A. Miyara, Two-phase frictional multiplier correlation for the prediction of condensation pressure drop inside smooth horizontal tube, *Procedia Engineering* 105(Supplement C) (2015) 64-72.
- [137] J.E. Laurinat, T.J. Hanratty, J.C. Dallman, Pressure drop and film height measurements for annular gas-liquid flow, *International Journal of Multiphase Flow* 10(3) (1984) 341-356.
- [138] C. Lu, R. Kong, S. Qiao, J. Larimer, S. Kim, S. Bajorek, K. Tien, C. Hoxie, Frictional pressure drop analysis for horizontal and vertical air-water two-phase flows in different pipe sizes, *Nuclear Engineering and Design* 332 (2018) 147-161.
- [139] T. Layssac, S. Lips, R. Revellin, Experimental study of flow boiling in an inclined mini-channel: Effect of inclination on flow pattern transitions and pressure drops, *Experimental Thermal and Fluid Science* (2018).
- [140] R. Akasaka, K. Tanaka, Y. Higashi, Thermodynamic property modeling for 2,3,3,3-tetrafluoropropene (HFO-1234yf), *International Journal of Refrigeration* 33(1) (2010) 52-60.
- [141] A.E. Dukler, M.I. Wicks, R.G. Cleveland, Frictional pressure drop in two-phase flow: A comparison of existing correlations for pressure loss and holdup, *AIChE Journal* 10(1) (1964) 38-43.
- [142] H.M. Mekisso, Comparison of frictional pressure drop correlations for isothermal two-phase horizontal flow, Oklahoma State University 2013.
- [143] J. Mandhane, G. Gregory, K. Aziz, Critical evaluation of friction pressure-drop prediction methods for gas-liquid flow in horizontal pipes, *Journal of Petroleum Technology* 29(10) (1977) 1,348-1,358.

- [144] M. Wambsganss, J. Jendrzeczyk, D. France, Two-phase flow and pressure drop in flow passages of compact heat exchangers, SAE Technical Paper, 1992.
- [145] R.W. Lockhart, R.C. Martinelli, Proposed correlation of data for isothermal, two-phase, two-component flow in pipes, Chemical Engineering Progress Symposium Series 45 (1949) 39-48.
- [146] R. Grønnerud, Investigation of liquid hold-up, flow-resistance and heat transfer in circulation type evaporators, part iv: two-phase flow resistance in boiling refrigerants, Bull. De l'Inst. Du Froid, Annexe 1 (1972).
- [147] L. Sun, K. Mishima, Evaluation analysis of prediction methods for two-phase flow pressure drop in mini-channels, International Journal of Multiphase Flow 35(1) (2009) 47-54.
- [148] S.-M. Kim, I. Mudawar, Universal approach to predicting two-phase frictional pressure drop for adiabatic and condensing mini/micro-channel flows, International Journal of Heat and Mass Transfer 55(11) (2012) 3246-3261.
- [149] Y. Xu, X. Fang, A new correlation of two-phase frictional pressure drop for condensing flow in pipes, Nuclear Engineering and Design 263 (2013) 87-96.
- [150] J. Lee, I. Mudawar, Two-phase flow in high-heat-flux micro-channel heat sink for refrigeration cooling applications: Part I—pressure drop characteristics, International Journal of Heat and Mass Transfer 48(5) (2005) 928-940.
- [151] W. Zhang, T. Hibiki, K. Mishima, Correlations of two-phase frictional pressure drop and void fraction in mini-channel, International Journal of Heat and Mass Transfer 53(1) (2010) 453-465.
- [152] T. Tran, M.-C. Chyu, M. Wambsganss, D. France, Two-phase pressure drop of refrigerants during flow boiling in small channels: an experimental investigation and correlation development, International Journal of Multiphase Flow 26(11) (2000) 1739-1754.
- [153] S.H. Yoon, E.S. Cho, Y.W. Hwang, M.S. Kim, K. Min, Y. Kim, Characteristics of evaporative heat transfer and pressure drop of carbon dioxide and correlation development, International Journal of Refrigeration 27(2) (2004) 111-119.
- [154] A. Cavallini, G. Censi, D. Col, L. Doretti, Condensation of halogenated refrigerants inside smooth tubes, HVAC&R Research 8(4) (2002) 429-451.
- [155] Y.W. Hwang, M.S. Kim, The pressure drop in microtubes and the correlation development, International Journal of Heat and Mass Transfer 49(11) (2006) 1804-1812.
- [156] K. Mishima, T. Hibiki, Some characteristics of air-water two-phase flow in small diameter vertical tubes, International Journal of Multiphase Flow 22(4) (1996) 703-712.
- [157] A. Pamitran, K.-I. Choi, J.-T. Oh, P. Hrnjak, Characteristics of two-phase flow pattern transitions and pressure drop of five refrigerants in horizontal circular small tubes, International Journal of Refrigeration 33(3) (2010) 578-588.

- [158] W. Yu, D. France, M. Wambsganss, J. Hull, Two-phase pressure drop, boiling heat transfer, and critical heat flux to water in a small-diameter horizontal tube, *International Journal of Multiphase Flow* 28(6) (2002) 927-941.
- [159] M. Awad, Y. Muzychka, Effective property models for homogeneous two-phase flows, *Experimental Thermal and Fluid Science* 33(1) (2008) 106-113.
- [160] C. Lombardi, E. Pedrocchi, A pressure drop correlation in two-phase flow, *Energy. Nucl.(Milan)* 19(2) (1972) 91-99.
- [161] W. McAdams, Vaporization inside horizontal tubes-II Benzene-oil mixtures, *Trans. ASME* 39 (1949) 39-48.
- [162] D. Beattie, P. Whalley, A simple two-phase frictional pressure drop calculation method, *International Journal of Multiphase Flow* 8(1) (1982) 83-87.
- [163] S. Lin, C.C.K. Kwok, R.Y. Li, Z.H. Chen, Z.Y. Chen, Local frictional pressure drop during vaporization of R-12 through capillary tubes, *International Journal of Multiphase Flow* 17(1) (1991) 95-102.
- [164] H. Mukherjee, J.P. Brill, Pressure drop correlations for inclined two-phase flow, *Journal of Energy Resources Technology* 107(4) (1985) 549-554.
- [165] L. Cheng, G. Ribatski, J.M. Quibén, J.R. Thome, A flow pattern based phenomenological two-phase frictional pressure drop model for CO<sub>2</sub> evaporation in macro-and micro-channels, *Eurotherm 2008.Tue.Nl* (2008).
- [166] J. Xiao, P. Hrnjak, A pressure drop model for condensation accounting for non-equilibrium effects, *International Journal of Heat and Mass Transfer* 126 (2018) 421-430.
- [167] D.R.E. Ewim, R. Kombo, J.P. Meyer, Flow pattern and experimental investigation of heat transfer coefficients during the condensation of R134a at low mass fluxes in a smooth horizontal tube, *12th International Conference on Heat Transfer, Fluid Mechanics and Thermodynamics (HEFAT), Costa del Sol, Malaga, Spain, 2016*, pp. 264-269.
- [168] D.R.E. Ewim, J.P. Meyer, Pressure drop during condensation at low mass fluxes in smooth horizontal and inclined tubes, *International Journal of Heat and Mass Transfer* 133 (2019) 686-701.
- [169] S. Rouhani, E. Axelsson, Calculation of void volume fraction in the subcooled and quality boiling regions, *International Journal of Heat and Mass Transfer* 13(2) (1970) 383-390.
- [170] S.Z. Rouhani, Subcooled void fraction, Internal Report. AE-RTV841, AB Atomenergi Sweden, Sweden, 1969.
- [171] K.P. Traviss, W.M. Rohsenow, A.B. Baron, Forced convection condensation in tubes: a heat transfer correlation for condenser design, *ASHRAE Transactions* 9(1) (1973) 57-65.

- [172] G. Breber, J.W. Palen, J. Taborek, Prediction of horizontal tubeside condensation of pure components using flow regime criteria, *Journal of Heat Transfer* 102(3) (1980) 471-476.
- [173] H.M. Soliman, J.R. Schuster, P.J. Berenson, A general heat transfer correlation for annular flow condensation, *ASME Journal of Heat Transfer* 90(1) (1968) 67-76.
- [174] T.N. Tandon, H.K. Varma, C.P. Gupta, A new flow regime map for condensation inside horizontal tubes, *ASME Journal of Heat Transfer* 104 (1982) 763-768.
- [175] T.N. Tandon, H.K. Varma, G.C. P., Prediction of flow patterns during condensation of binary mixtures in a horizontal tube, *ASME Journal of Heat Transfer* 107(2) (1985) 424-430.
- [176] M.K. Dobson, J.C. Chato, Condensation in smooth horizontal tubes, *ASME Journal of Heat Transfer* 120 (1998) 193-213.
- [177] J.W. Coleman, S. Garimella, Two-phase flow regimes in round, square and rectangular tubes during condensation of refrigerant R134a, *International Journal of Refrigeration* 26(1) (2003) 117-128.
- [178] R.G. Sardesai, R.G. Owen, D.J. Pulling, Flow regimes for condensation of a vapour inside a horizontal tube, *Chemical Engineering Science* 36(7) 1173-1180.
- [179] R.W. Lockhart, R.C. Martinelli, Proposed correlation of data for isothermal, two-phase, two-component flow in pipes, *Chemical Engineering Progress Symposium Series* 45 39-48.
- [180] J.P. Holman, *Heat Transfer*, 9th ed., McGraw-Hill, New York, 2002.
- [181] F.M. White, *Fluid Mechanics*, 6th ed., McGraw-Hill, Singapore, 2009.
- [182] J. Palen, G. Breber, J. Taborek, Prediction of flow regimes in horizontal tube-side condensation, *Heat Transfer Engineering* 1(2) (1979) 47-57.
- [183] L. Cheng, G. Ribatski, J.R. Thome, Two-phase flow patterns and flow-pattern maps: Fundamentals and applications, *Applied Mechanics Reviews* 61(5) (2008) 050802-050802.
- [184] S.Z. Rouhani, M.S. Sohal, Two-phase flow patterns: A review of research results, *Progress in Nuclear Energy* 11(3) (1983) 219-259.
- [185] M. Christians, Flow pattern-based heat transfer and pressure drop correlations for condensing refrigerants in smooth tubes, M. Eng, Mechanical and Aeronautical Engineering, Thesis, University of Pretoria, 2007.
- [186] L.P.M. Colombo, A. Lucchini, A. Muzzio, Flow patterns, heat transfer and pressure drop for evaporation and condensation of R134a in microfin tubes, *International Journal of Refrigeration* 35(8) (2012) 2150-2165.
- [187] A.S. Dalkilic, S. Wongwises, An investigation of a model of the flow pattern transition mechanism in relation to the identification of annular flow of R134a in a vertical tube using various void fraction models and flow regime maps, *Experimental Thermal and Fluid Science* 34(6) (2010) 692-705.

- [188] A.J. Ghajar, C.C. Tang, Void fraction and flow patterns of two-phase flow in upward and downward vertical and horizontal pipes, *Advances in Multiphase Flow and Heat Transfer* 4(Chapter 7) (2012) 175-201.
- [189] S. Grauso, R. Mastrullo, A.W. Mauro, J.R. Thome, G.P. Vanoli, Flow pattern map, heat transfer and pressure drops during evaporation of R-1234ze(E) and R134a in a horizontal, circular smooth tube: Experiments and assessment of predictive methods, *International Journal of Refrigeration* 36(2) (2013) 478-491.
- [190] S.G. Kandlikar, Two-phase flow patterns, pressure drop, and heat transfer during boiling in minichannel flow passages of compact evaporators, *Heat Transfer Engineering* 23(1) (2002) 5-23.
- [191] F.T. Kanizawa, G. Ribatski, Two-phase flow patterns and pressure drop inside horizontal tubes containing twisted-tape inserts, *International Journal of Multiphase Flow* 47 (2012) 50-65.
- [192] D.W. Shao, E. Granryd, Flow pattern, heat transfer and pressure drop in flow condensation; Part I: Pure and azeotropic refrigerants, *HVAC&R Research* 6(2) (2000) 175-195.
- [193] D.W. Shao, E. Granryd, Flow pattern, heat transfer and pressure drop in flow condensation; Part II: zeotropic refrigerants, *HVAC&R Research* 6(2) (2000) 197-209.
- [194] W. Xu, L. Jia, Visualization on flow patterns during condensation of R410A in a vertical rectangular channel, *Journal of Thermal Science* 23(3) (2014) 269-274.
- [195] O. Baker, Simultaneous flow of oil and gas, *Oil and Gas Journal* 53(12) (1954) 185-195.
- [196] Y. Taitel, A.E. Dukler, A model for predicting flow regime transitions in horizontal and near-horizontal gas-liquid flow, *American Institute of Chemical Engineering (AIChE) Journal* 22(1) (1976) 47-55.
- [197] J.M. Mandhane, G.A. Gregory, K. Aziz, A flow pattern map for gas-liquid flow in horizontal pipes, *International Journal of Multiphase Flow* 1 (1974) 537-553.
- [198] G.F. Hewitt, D. Roberts, *Studies of two-phase flow patterns by simultaneous x-ray and flash photography*, Atomic Energy Research Establishment, Harwell, England (United Kingdom), 1969.
- [199] J.R. Fair, What you need to design thermosiphon reboilers, *Petroleum Refinery Journal* 39 (1960) 105-123.
- [200] N. Kattan, J.R. Thome, D. Favrat, Flow boiling in horizontal tubes: Part 1- Development of a diabatic two phase flow pattern, *ASME Journal of Heat Transfer* 120 (1998) 140-147.
- [201] J.R. Thome, J.E. Hajal, Two-phase flow pattern map for evaporation in horizontal tubes: latest version, *Heat Transfer Engineering* 24(6) (2003) 3-10.
- [202] N. Kattan, J.R. Thome, D. Favrat, Flow boiling in horizontal tubes: Part 3- Development of a new heat transfer model based on flow pattern, *ASME Journal of Heat Transfer* 120 (1998) 156-165.



- [203] D. Steiner, Heat transfer to boiling saturated liquids, Verein Deutscher Ingenieure (Ed.), VDI-Warmeatlas (VDI Heat Atlas), VDI-Gesellschaft Verfahrenstechnik und Chemieingenieurwesen (GCV), Düsseldorf, 1993.
- [204] O. Zürcher, D. Favrat, J.R. Thome, Development of a diabatic two-phase flow pattern map for horizontal flow boiling, *International Journal of Heat and Mass Transfer* 45(2) (2002) 291-301.
- [205] A. Cavallini, G. Censi, D. Del Col, L. Doretti, L. Rosetto, A tube-in-tube water/zeotropic mixture condenser: Design procedure against experimental data, *Experimental Thermal Fluid Sciences* 25 (2002) 495-501.
- [206] P.G. Kosky, F.W. Staub, Local condensing heat transfer coefficients in the annular flow regime, *American Institute of Chemical Engineering (AIChE) Journal* 17 (1971) 1037-1043.
- [207] A. Cavallini, R. Zecchin, A dimensionless correlation for heat transfer in forced convection condensation, *Proceedings of the Sixth International Heat Transfer Conference*, 1974, pp. 309-313.
- [208] W.W. Akers, H.A. Deans, O.K. Crosser, Condensation heat transfer within horizontal tubes, *Chemical Engineering Progress Symposium Series* 55 (1959) 171-176.
- [209] W.W. Akers, H.F. Rosson, Condensation inside a horizontal tube, *Chemical Engineering Progress Symposium Series* 50 (1960) 145-149.
- [210] H. Haraguchi, S. Koyama, T. Fujii, Condensation of refrigerants HCFC 22, HFC134a and HCFC 123 in a horizontal smooth tube (2nd report, proposals of empirical expressions for the local heat transfer coefficient), *Transactions of the JSME, Part B* 574(69) (1994) 2117-2124.
- [211] L. Tang, Empirical study of new refrigerant flow condensation inside horizontal smooth and micro-fin tubes, *Mechanical Engineering*, University of Maryland at College Park, 1997.
- [212] K. Moser, R.L. Webb, B. Na, A new equivalent Reynolds number model for condensation in smooth tubes, *ASME Journal of Heat Transfer* 120(2) (1998) 410-417.
- [213] J.C. Chato, Laminar condensation inside horizontal and inclined tubes, *ASHRAE Journal* 4 (1962) 52-60.
- [214] M.M. Chen, An analytical study of laminar film condensation: Part 1 – Flat Plates, *ASME Journal of Heat Transfer* 8 (1961) 48-54.
- [215] H. Jaster, P.G. Kosky, Condensation heat transfer in a mixed flow regime, *International Journal of Heat and Mass Transfer* 19(1) (1976) 95-99.
- [216] H.F. Rooson, J.A. Meyers, Point of values of condensing film coefficients inside a horizontal tube, *Chemical Engineering Progress Symposium Series* 61 (1965) 190-199.
- [217] F. Dittus, L. Boelter, Heat transfer in automobile radiators of the tubular type, *International Communications in Heat and Mass Transfer* 12(1) (1985) 3-22.

- [218] S.M. Zivi, Estimation of steady state void fraction by means of minimum entropy generation, *Journal of Heat and Mass Transfer* 86 (1964) 247-252.
- [219] W. Nusselt, Die oberflächenkondensation des wasserdampfes, *Zietschrift des Vereins deutscher Ingenieure* 60(27) (1916) 541-546.
- [220] E.F. Carpenter, A.P. Colburn, The effect of vapour velocity on condensation inside tubes, *Proceedings of the general discussions on heat transfer, published by the Institute of Mechanical Engineers and ASME, 1951, pp. 20-26.*
- [221] D. Traviss, W. Rohsenow, Flow regimes in horizontal two-phase flow with condensation, *ASHRAE Trans* 79(2) (1973) 31-39.
- [222] T. Von Karman, The analogy between fluid friction and heat transfer, *ASME Transactions* 61 (1939) 705-711.
- [223] A. Singh, M.M. Ohadi, S.V. Dessiatoun, Empirical modelling of stratified wavy flow condensation heat transfer in smooth horizontal tubes, *ASHRAE Transactions: Symposia* 9 (1996) 596-603.
- [224] M. Azzolin, S. Bortolin, L.P. Le Nguyen, P. Lavieille, A. Glushchuk, P. Queeckers, M. Miscevic, C.S. Iorio, D. Del Col, Experimental investigation of in-tube condensation in microgravity, *International Communications in Heat and Mass Transfer* 96 (2018) 69-79.
- [225] B.-X. Wang, X.-Z. Du, Study on laminar film-wise condensation for vapor flow in an inclined small/mini-diameter tube, *International Journal of Heat and Mass Transfer* 43(10) (2000) 1859-1868.
- [226] T. Nitheanandan, H.M. Soliman, Influence of tube inclination on the flow regime boundaries of condensing steam, *The Canadian Journal of Chemical Engineering* 71(1) (1993) 35-41.
- [227] L. Liebenberg, J.P. Meyer, The characterization of flow regimes with power spectral density distributions of pressure fluctuations during condensation in smooth and micro-fin tubes, *Experimental Thermal and Fluid Science* 31(2) (2006) 127-140.
- [228] W.E.I. Xiaoyong, F. Xiande, S.H.I. Rongrong, A comparative study of heat transfer coefficients for film condensation, *Energy Science and Technology* 3(1) (2012) 1-9.
- [229] D.J. Kukulka, R. Smith, W. Li, Comparison of tubeside condensation and evaporation characteristics of smooth and enhanced heat transfer IEHT tubes, *Applied Thermal Engineering* (2015) 1-8.
- [230] A. Miyara, K. Nonaka, M. Taniguchi, Condensation heat transfer and flow pattern inside a herringbone-type micro-fin tube, *International Journal of Refrigeration* 23(2) (2000) 141-152.
- [231] S. Wongwises, M. Polsongkram, Condensation heat transfer and pressure drop of HFC-134a in a helically coiled concentric tube-in-tube heat exchanger, *International Journal of Heat and Mass Transfer* 49(23-24) (2006) 4386-4398.

- [232] N.-H. Kim, Condensation heat transfer and pressure drop of R-410A in a 7.0 mm O.D. microfin tube at low mass fluxes, *Heat and Mass Transfer* (2016) 1-15.
- [233] S.N. Sapali, P.A. Patil, Heat transfer during condensation of HFC-134a and R-404A inside of a horizontal smooth and micro-fin tube, *Experimental Thermal and Fluid Science* 34(8) (2010) 1133-1141.
- [234] D.W. Shao, E. Granryd, Heat transfer and pressure drop of HFC134a-oil mixtures in a horizontal condensing tube, *International Journal of Refrigeration* 18(8) (1995) 524-533.
- [235] C.-C. Wang, C.-S. Chiang, Two-phase heat transfer characteristics for R-22 /R-407C in a 6.5 mm smooth tube, *International Journal of Heat and Fluid Flow* 18(November 1996) (1997) 550-558.
- [236] Z. Wu, B. Sundén, L. Wang, W. Li, Convective condensation inside horizontal smooth and microfin tubes, *Journal of Heat Transfer* 136(5) (2014).
- [237] X. Zhuang, G. Chen, X. Zou, Q. Song, M. Gong, Experimental investigation on flow condensation of methane in a horizontal smooth tube, *International Journal of Refrigeration* 78 (2017) 193-214.
- [238] X. Zhuang, M. Gong, G. Chen, X. Zou, J. Shen, Two-phase flow pattern map for R170 in a horizontal smooth tube, *International Journal of Heat and Mass Transfer* 102 (2016) 1141-1149.
- [239] X. Zhuang, M. Gong, X. Zou, G. Chen, J. Wu, Experimental investigation on flow condensation heat transfer and pressure drop of R170 in a horizontal tube, *International Journal of Refrigeration* 66 (2016) 105-120.
- [240] J.P. Meyer, J. Dirker, S.M.A. Noori Rahim Abadi, A review of condensation in inclined tubes, *Encyclopedia of Two-Phase Heat Transfer and Flow III*, World Scientific 2018, pp. 243-280.
- [241] Z. Olujić, Predicting two-phase flow friction loss in horizontal pipes, *Chemical Engineering (New York)* 92(13) (1985) 45-50.
- [242] A. Cavallini, L. Doretti, M. Matkovic, L. Rossetto, Update on condensation heat transfer and pressure drop inside minichannels (keynote), *ASME 3rd International Conference on Microchannels and Minichannels*, American Society of Mechanical Engineers, 2005, pp. 19-31.
- [243] A. Cavallini, L. Doretti, M. Matkovic, L. Rossetto, Update on condensation heat transfer and pressure drop inside minichannels, *Heat Transfer Engineering* 27(4) (2006) 74-87.
- [244] S. Wongwises, M. Pipathattakul, Flow pattern, pressure drop and void fraction of two-phase gas–liquid flow in an inclined narrow annular channel, *Experimental Thermal and Fluid Science* 30(4) (2006) 345-354.
- [245] M.K. Maddi, D.P. Rao, Experimental studies on flow boiling in inclined tubes: In the regions encountered in solar collectors, *The Canadian Journal of Chemical Engineering* 73(1) (1995) 73-84.

- [246] C.J. Baroczy, Correlation of liquid fraction in two-phase flow with application to liquid metals, *Chemical Engineering Progress Symposium Series* 61(57) (1965) 179-191.
- [247] A. Autee, S.S. Rao, R. Puli, R. Shrivastava, An experimental study on two-phase pressure drop in small diameter horizontal, downward inclined and vertical tubes, *Thermal Science* 19(5) (2015) 1791-1804.
- [248] S.M. Bhagwat, A.J. Ghajar, A flow pattern independent drift flux model based void fraction correlation for a wide range of gas-liquid two phase flow, *International Journal of Multiphase Flow* 59 (2014) 186-205.
- [249] E.W. Lemmon, M.L. Huber, M.O. McLinden, NIST standard reference database 23: reference fluid thermodynamic and transport properties (REFPROP), version 9.1, National Institute of Standards and Technology, Standard reference data program, Gaithersburg, (2013).
- [250] ASHRAE, ASHRAE Standard 41.4: Method for measurement of proportion of lubricant in liquid refrigerant, American Society for Heating, Refrigeration, and Air-conditioning Engineers, USA, 2006.
- [251] J.R. Lamarsh, Introduction to nuclear reactor theory, Addison-Wesley Reading, Massachusetts 1966.
- [252] B. Zohuri, P. McDaniel, Thermodynamics in nuclear power plant systems, Springer 2015.
- [253] F.M. White, Fluid mechanics, 5th edition ed., McGraw-Hill 2003.
- [254] M.J. Moran, H.N. Shapiro, D.D. Boettner, M.B. Bailey, Fundamentals of engineering thermodynamics, John Wiley & Sons 2010.
- [255] S. Glasstone, A. Sesonske, Nuclear reactor engineering: reactor systems engineering, Springer Science & Business Media 2012.
- [256] V.P. Carey, Liquid-vapor phase-change phenomena, Hemisphere, New York, United States, 1992.
- [257] P.F. Dunn, Measurement and data analysis for engineering and science, CRC Press, Boca Raton, 2010.
- [258] L. Liebenberg, A.E. Bergles, J.P. Meyer, A review of refrigerant condensation in horizontal micro-fin tubes, The 2001 International Mechanical Engineering Congress and Exposition, Orlando, Florida, 5-10 November 2001, AES-Vol. 40, 2000, pp. 155-168.
- [259] A.O. Adelaja, J. Dirker, J.P. Meyer, A condensation heat transfer correlation for inclined smooth tubes, 12th International Conference on Heat Transfer, Fluid Mechanics and Thermodynamics, Costa del Sol, Malaga, Spain, 2016.
- [260] J.G. Collier, J.R. Thome, Convective boiling and condensation, Condensation, Oxford University Press, USA, 1994, pp. 430-487.

- [261] S.J. Kline, The purposes of uncertainty analysis, *Journal of Fluids Engineering* 107(2) (1985) 153-160.
- [262] F.A. McClintock, Describing uncertainties in single-sample experiments, *Mechanical Engineering* 75(1) (1953) 3-8.
- [263] R.J. Moffat, Describing the uncertainties in experimental results, *Experimental Thermal and Fluid Science* 1(1) (1988) 3-17.
- [264] S. Bell, A beginner's guide to uncertainty of measurement, *Measurement good practice guide*, National Physical Laboratory, United Kingdom, 1999, pp. 1-30.
- [265] S.J. Kline, Describing uncertainty in single sample experiments, *Mechanical Engineering* 75 (1953) 3-8.
- [266] S. Coetzee, The development of an experimental set-up to investigate heat transfer enhancement in tube-in-tube heat exchangers, M. Ing. Thesis, Mechanical Engineering, University of Johannesburg, 2000.
- [267] E. Van Rooyen, Time-fractional analysis of flow patterns during refrigerant condensation, M.Eng. Thesis, Mechanical and Aeronautical Engineering, University of Pretoria, 2007.
- [268] S. Abu-Eishah, Correlations for the thermal conductivity of metals as a function of temperature, *International Journal of Thermophysics* 22(6) (2001) 1855-1868.

## Appendix A: Experimental Uncertainty Analysis

---

### A.1. Introduction

Any honest experimenter must be able to present to the reader what the uncertainties in the results of his experiments are. Uncertainties emanate from human error, machine error, calculation error and calibration error. It is therefore imperative that this chapter in the appendix is devoted to this important subject. The experimental set-up returns information based on the input to it and the confidence level in the output from the set-up is partly dependent on its sensitivity and accuracy in interpreting the inputs. Therefore, proper care should be taken when calculations are made because of the cascading effects of using wrong output values which renders an otherwise correct equation bad due to errors introduced from direct measurements (outputs) [257, 261-264].

Uncertainty is a phenomenon that is unavoidable and arises in partially observable and/or stochastic environments as well as due to ignorance and/or indolence. It is the estimated amount or percentage by which an observed or calculated value may differ from the true value. Some laboratories, such as test laboratories, may not have the resources to undertake detailed uncertainty analyses even though increasingly, quality management standards such as the ISO 9000 series are requiring that all measurement results be accompanied by statements of uncertainty.

The first step in the uncertainty evaluation is the definition of the result to be reported for the test item for which uncertainty is required. The computation of the standard deviation depends on the number of repetitions on the test item and the range of environmental and operational conditions over which the repetitions were made, in addition to other sources of error, such as calibration uncertainties for reference standards, which influence the final result. If the value for the test item cannot be measured directly but must be calculated from measurements on secondary quantities, the equation for combining the various quantities must be defined.

Single sample uncertainty analysis will be used in this work as it clearly first into the picture wherein the data used have been averaged and evaluated using similar data sampling rates.

### A.2. General uncertainty analysis procedures

The magnitude cum weight of an error can be described as uncertainty Kline and McClintock [265] (1953). It is usually given as a percentage and is represented as  $\delta$  (measurand). Let us consider an experimental variable  $X_1$ , its associated uncertainty must be represented as  $\delta X_1$ . Usually, we can represent uncertainties with a statistical confidence level where it must fall in.

Uncertainties are a function of two components; the Precision ( $P_1$ ) which can be a ransom error in the measurement and a fixed error ( $F_1$ ) known as the Bias. Representing the uncertainty in a Euclidean norm of the two, we have that:

$$\delta X_1 = \{(F_1)^2 + (P_1)^2\}^{\frac{1}{2}} \quad (\text{A.1})$$

Coetzee [266] and Van-Rooyen [267] dealt with uncertainties directly as opposed to other cases where there was a dichotomy that necessitated the use of the Bias and Precision components. In this study, we followed the method of Coetzee and Van-Rooyen except on rare occasions when we needed to use both Bias and Precision components.

Let us assume that an experimental quantity  $Z$  is a function of  $n$  variables,  $X_0$  through  $X_n$  each with an uncertainty  $\delta X_i$ . Hence,

$$Z = f(X_0, X_1, \dots, X_n) \quad (\text{A.2})$$

The effect of the uncertainty of a single variable on quantity  $Z$  is the partial derivative of  $Z$  with respect to that single variable (i.e.  $X_i$ ), multiplied by the variable's uncertainty ( $\delta X_i$ ). Mathematically,

$$\delta Z_{X_i} = \frac{\partial}{\partial X_i} (Z) \delta X_i \quad (\text{A.3})$$

By summing all the uncertainties of  $Z$  in terms of its variables, the limiting uncertainty is found. The Euclidean form of the individual uncertainties can be written as:

$$\delta Z = \left\{ \sum_{i=1}^n \left( \frac{\partial}{\partial X_i} (Z) \delta X_i \right)^2 \right\}^{\frac{1}{2}} \quad (\text{A.4})$$

This equation is valid only when:

- ❖ The errors and uncertainties of each variable are mutually exclusive
- ❖ All the  $X_i$  are quoted at the same odds.
- ❖ The distribution of the errors or uncertainties is Gaussian, for all  $X_i$

It is the practice to normalize Eq. A.4 with respect to the full value of  $Z$ . However, there are some exceptions such as when the temperature measured is 0 °C.

### A.3. Temperature measurement uncertainties

Temperature measurements for this investigation were done using T-type thermocouples (copper-constantan). The cold junction used was built into the National Instruments' SCXI-1303 card. All the

thermocouples used were calibrated using a linear scale against a high precision platinum resistance temperature (Pt100) detector in a thermal bath to an accuracy of  $\pm 0.1$  °C. The temperature range set was between 10 and 60 °C.

There were 28 thermocouples in all and the precision of each measurement is known to be the standard deviation from the steady-state value it measures. Then, the uncertainty in each thermocouple's reading is:

$$\delta T_i = \sqrt{F^2 + P^2} \quad (\text{A.5})$$

It can be deduced that the precision  $P$  is equal to the standard deviation of the reading,  $\sigma$ . In this work, the average temperatures were normally used and it can be written as:

$$T_m = \frac{T_1 + T_2 + T_3 + \dots + T_n}{n} \quad (\text{A.6})$$

Representing this in terms of partial derivatives, we have that:

$$\frac{\partial T_{m,T_i}}{\partial T_i} = \frac{1}{n} \delta T_i \quad (\text{A.7})$$

Taking the Euclidean form with the assumption that all the thermocouples have an identical uncertainty, we have that:

$$\delta T_m = \left\{ \sum_{i=1}^n \left( \frac{1}{n} \delta T_i \right)^2 \right\}^{\frac{1}{2}} = \left( \frac{n}{n^2} \delta T_i^2 \right)^{\frac{1}{2}} = \left( \frac{1}{n} \right)^{\frac{1}{2}} \delta T_i \quad (\text{A.8})$$

#### A.4. Wall temperature uncertainty

For the inner tube through which the refrigerant flowed, 28 grooves were made at seven positions marked (A-G) equidistant to one another along the tube. Each position had four grooves marked (1-4) at equal distances around the circumference of the tube. Our interest here is on the average wall temperature hence following from Eq. A. 8, the uncertainty becomes:

$$\delta T_{w,o} = \frac{1}{\sqrt{28}} \delta T_{w,i} \quad (\text{A.9})$$



### A.5. Temperature difference uncertainty

The temperature difference is clearly a function of the inlet and outlet temperatures and noting that the uncertainty in each thermocouple measurement is approximately the same, temperature difference uncertainty can be written as:

$$\delta\Delta T = (\delta T_1^2 + \delta T_2^2)^{\frac{1}{2}} \quad (\text{A.10})$$

Here, the average uncertainty in the wall temperatures is used as the single uncertainty.

### A.6. Refrigerant mass flow rate uncertainty

The Coriolis mass flow meters have an accuracy of 0.1% of the nominal reading. Hence the uncertainty in the Coriolis CMF-010 can be written as:

$$\delta\dot{m} = \frac{1}{1000} \dot{m}_{ind} \quad (\text{A.11})$$

### A.7. Mass flux uncertainty

Mass flux ( $G$ ), is the ratio of the mass flow of the refrigerant to the cross-sectional area of the inner tube:

$$G = \frac{\dot{m}}{A_{cs}} \quad (\text{A.12})$$

The uncertainty in the mass flux will then be a function of both the mass flow rate and the area. Writing Eq. A.12 as an uncertainty in the Euclidean form, we get that:

$$\delta G = \left( \left( \frac{\partial G \delta \dot{m}}{\partial \dot{m}} \right)^2 + \left( \frac{\partial G \delta A_{cs}}{\partial A_{cs}} \right)^2 \right)^{\frac{1}{2}} \quad (\text{A.13})$$

Where in the partial derivatives are:

$$\frac{\partial G}{\partial \dot{m}} = \frac{1}{A_{cs}} \quad (\text{A.14})$$

$$\frac{\partial G}{\partial A_{cs}} = -\frac{\dot{m}}{A_{cs}^2} \quad (\text{A.15})$$

### A.8. Water mass flow rates uncertainty

The accuracy of the CMF-010 and 0-25 used to measure the water flow rates have is within 0.1% of the nominal reading. Thus the water flow uncertainty is:

$$\delta\dot{m} = \frac{1}{1000} \dot{m}_{ind} \quad (\text{A.16})$$

The Bürkert flow meters model nos. DIN-015 and DIN-025 have an uncertainty of 0.2% of the indicated reading hence its uncertainty is:

$$\delta\dot{m} = \frac{2}{1000} \dot{m}_{ind} \quad (\text{A.17})$$

### A.9. Pressure measurement uncertainty

The pressure transducers, Sensotec FP-2000s with a full scale of  $\pm 3447$  kPa (500 psi) have an uncertainty of 0.1% of the full scale. This results in:

$$\delta P_{tr} = \pm \frac{1}{1000} P_{ind} \quad (\text{A.18})$$

### A.10. REFPROP uncertainty analysis

REFPROP [249] uses the input of two-point functions (pressure and temperature) to calculate the correct thermodynamic properties of the R134a. However, the uncertainties in terms of percentages are found in the .fld files in the REFPROP directory. The exceptions to these are the uncertainties of the specific enthalpy and entropy which are calculated using the governing equation of state and from REFPROP [249] we deduce that the typical uncertainties are:

$$\delta h = 0.5\%$$

$$\delta \sigma = 0.05\%$$

$$\delta C_p = 1\%$$

$$\delta \mu_l = 1.1\%$$

$$\delta \rho_v = 0.1\%$$

$$\delta \rho_l = 0.1\%$$

$$\delta\mu_v = 1.1\%$$

$$\delta k_{l,v} = 3.7\%$$

Similarly, the waterside uncertainties are found in the water fluid file from REFPROP and others relating to enthalpy, thermal conductivity and surface tension are inferred from Van-Rooyen [267] as:

$$\delta h = 0.5\%$$

$$\delta\sigma = 0.05\%$$

$$\delta C_p = 1\%$$

$$\delta\mu_l = 1.1\%$$

$$\delta\rho_v = 0.1\%$$

$$\delta\rho_l = 0.1\%$$

$$\delta\mu_v = 1.1\%$$

$$\delta k_{l,v} = 3.7\%$$

#### **A.11. Uncertainty in the measurement of condenser length**

For this uncertainty, we will use the principle of precision and bias. The precision was assumed to be the smallest increment of the tape measure while a bias limit of 0.5 mm was used. Thus the uncertainty in the length if the condenser is:

$$\delta L = \sqrt{0.5^2 + 0.5^2} = 0.7 \text{ mm}$$

#### **A.12. Uncertainty in the measurement of tube diameter**

The inside tube diameter was measured by Wolverine Tube Inc. [62] and cross-checked in the laboratory and the uncertainty is  $25 \times 10^{-6}$  m, that is  $\delta d_i = 25 \times 10^{-6}$  m.

#### **A.13. Uncertainty in the thermal conductivity of the copper tubes**

This uncertainty is deduced from the work of Abu-Eishah [268] who performed a detailed uncertainty analysis on the thermal conductivity of copper and this is given as:

$$\frac{\delta k_{Cu}}{k_{Cu}} * 100 = \frac{0.04}{400} * 100 = 0.01\%$$

This is only valid for the region of the temperatures which the copper was subjected to in this study (i.e. 0 – 50 °C)

#### A.14. Uncertainty in the measurement of surface area

The tube surface area ( $A$ ) is defined as:

$$A = \pi d_i L \quad (\text{A.19})$$

Then the uncertainty in  $A$  is:

$$\delta A = \left[ \left( \frac{\partial A \delta L}{\partial L} \right)^2 + \left( \frac{\partial A \delta d_i}{\partial d_i} \right)^2 \right]^{\frac{1}{2}} \quad (\text{A.20})$$

The partial derivatives are:

$$\frac{\partial A}{\partial L} = \pi d_i \quad (\text{A.21})$$

$$\frac{\partial A}{\partial d_i} = \pi L \quad (\text{A.22})$$

#### A.15. Uncertainty in the wall thermal resistance

The wall thermal resistance derived from Fourier's law of heat conduction is:

$$R_w = \frac{\ln\left(\frac{d_o}{d_i}\right)}{2\pi k_{cu} L} \quad (\text{A.23})$$

The partial derivatives are:

$$\frac{\partial R_w}{\partial d_o} = \frac{1}{2\pi k_{cu} L d_o} \quad (\text{A.24})$$

$$\frac{\partial R_w}{\partial d_i} = -\frac{1}{2\pi k_{cu} L d_i} \quad (\text{A.25})$$

$$\frac{\partial R}{\partial k_{cu}} = -\frac{\ln\left(\frac{d_o}{d_i}\right)}{2\pi L k_{cu}^2} \quad (\text{A.26})$$

$$\frac{\partial R}{\partial L} = -\frac{\ln\left(\frac{d_o}{d_i}\right)}{2\pi L^2 k_{cu}} \quad (\text{A.27})$$

The overall wall thermal resistance uncertainty is then given as:

$$\delta R_w = \left( \left( \frac{\partial R_w}{\partial d_o} \delta d_o \right)^2 + \left( \frac{\partial R_w}{\partial d_i} \delta d_i \right)^2 + \left( \frac{\partial R_w}{\partial k_{cu}} \delta k_{cu} \right)^2 + \left( \frac{\partial R_w}{\partial L} \delta L \right)^2 \right)^{\frac{1}{2}} \quad (\text{A.28})$$

#### A.16. Refrigerant side heat balance uncertainty

The total heat lost by the refrigerant is the product of the refrigerant mass flow rate and the change in specific enthalpy (inlet of the pre-condenser to the exit of the post condenser). Mathematically, it is:

$$\dot{Q}_r = \dot{m}_r \Delta h = \dot{m}_r (h_{in} - h_{out}) \quad (\text{A.29})$$

$$\delta \dot{Q}_r = \left( \left( \frac{\partial(\dot{Q}_r)}{\partial \dot{m}} \delta \dot{m} \right)^2 + \left( \frac{\partial(\dot{Q}_r)}{\partial \Delta h} \delta \Delta h \right)^2 \right)^{\frac{1}{2}} \quad (\text{A.30})$$

where:

$$\delta \Delta h = \left( \left( \frac{\partial \Delta h}{\partial h_{in}} \delta h_{in} \right)^2 + \left( \frac{\partial \Delta h}{\partial h_{out}} \delta h_{out} \right)^2 \right)^{\frac{1}{2}} \quad (\text{A.31})$$

#### A.17. Waterside heat balance uncertainty

The heat gained by the water in the three condensers is the summation of the heat gained in each and is written as:

$$\dot{Q}_w = \sum \dot{Q}_{i,w} \quad (\text{A.32})$$

Hence the uncertainty is:

$$\delta \dot{Q}_w = \left( \sum_{i=1}^3 \left( \frac{\partial}{\partial \dot{Q}_i} \dot{Q}_w (\delta \dot{Q}_i) \right)^2 \right)^{\frac{1}{2}} \quad (\text{A.33})$$

However,

$$\dot{Q}_i = \dot{m}_{w,i} C_{p,i} \Delta T_i \quad (\text{A.34})$$

It can be deduced that the uncertainty is a function of the mass flow of water, specific heat and water temperature difference and is:

$$\delta \dot{Q}_i = \left[ \left( \frac{\partial \dot{Q}_i}{\partial \dot{m}} \delta \dot{m} \right)^2 + \left( \frac{\partial \dot{Q}_i}{\partial C_{p,i}} \delta C_{p,i} \right)^2 + \left( \frac{\partial \dot{Q}_i}{\partial \Delta T_i} \delta \Delta T_i \right)^2 \right]^{\frac{1}{2}} \quad (\text{A.35})$$

## A.18. Inlet and outlet vapour quality uncertainty analysis

### A.18.1. Inlet vapour quality uncertainty

The vapour quality at the inlet of the test section is calculated using measured data including temperature, pressure and water-side heat transferred and REFPROP properties and is given as:

Where  $h_v$  and  $h_l$  are evaluated from REFPROP at saturation point functions at the inlet and outlet of the test section. The inlet specific enthalpy is:

$$h_{test,in} = h_{pre,in} - \frac{|\dot{Q}_{pre}|}{\dot{m}_r} \quad (\text{A.36})$$

Thus, the uncertainty in the test inlet enthalpy is:

$$\delta h_{in,test} = \left[ \left( \frac{\partial}{\partial \dot{Q}_{pre,H_2O}} (h_{in,test}) \delta \dot{Q}_{pre,H_2O} \right)^2 + \left( \frac{\partial}{\partial h_{in,pre}} (h_{in,test}) \delta h_{in,pre} \right)^2 + \left( \frac{\partial}{\partial \dot{m}_r} (h_{in,test}) \delta \dot{m}_r \right)^2 \right]^{\frac{1}{2}} \quad (\text{A.37})$$

Where the partial derivatives are:

$$\frac{\partial h_{in,test}}{\partial h_{in,pre}} = 1 \quad (\text{A.38})$$

$$\frac{\partial h_{in,test}}{\partial \dot{Q}_{pre,w}} = -\frac{1}{\dot{m}_r} \quad (\text{A.39})$$

$$\frac{\partial h_{in,test}}{\partial \dot{m}_r} = -\frac{\dot{Q}_w}{\dot{m}_r^2} \quad (\text{A.40})$$

It also follows that the uncertainty in  $x_{in}$  is:

$$\delta x_{in} = \left[ \left( \frac{\partial}{\partial h_{l,test\ in}}(x_{in}) \delta h_{l,test\ in} \right)^2 + \left( \frac{\partial}{\partial h_{in,test}}(x_{in}) \delta h_{in,test} \right)^2 + \left( \frac{\partial}{\partial h_{v,test\ in}}(x_{in}) \delta h_{v,test\ in} \right)^2 \right]^{\frac{1}{2}} \quad (\text{A.41})$$

And the partial derivatives are:

$$\frac{\partial x_{in}}{\partial h_{in,test}} = \frac{1}{h_{v,test\ in} - h_{l,test\ in}} \quad (\text{A.42})$$

$$\frac{\partial x_{in}}{\partial h_{v,test\ in}} = \frac{h_l - h_{in,test}}{(h_v - h_l)^2} \quad (\text{A.43})$$

$$\frac{\partial x_{in}}{\partial h_{l,test\ in}} = -\frac{1}{h_{v,test\ in} - h_{l,test\ in}} - \frac{h_{in,test} - h_{l,test\ in}}{(h_{v,test\ in} - h_{l,test\ in})^2} \quad (\text{A.44})$$

### A.18.2. Outlet vapour quality uncertainty

Analogous to the inlet vapour quality, the outlet vapour quality takes the same form as the inlet vapour quality and is calculated from:

$$x_{out} = \frac{h_{out,test} - h_l}{h_v - h_l} \quad (\text{A.45})$$

And following the same route as the inlet, we finally arrive at:

$$\delta x_{out} = \left[ \left( \frac{\partial}{\partial h_{l,test\ out}}(x_{out}) \delta h_{l,test\ out} \right)^2 + \left( \frac{\partial}{\partial h_{out,test}}(x_{out}) \delta h_{out,test} \right)^2 + \left( \frac{\partial}{\partial h_{v,test\ out}}(x_{out}) \delta h_{v,test\ out} \right)^2 \right]^{\frac{1}{2}} \quad (\text{A.46})$$

And the partial derivatives are:

$$\frac{\partial x_{out}}{\partial h_{out,test}} = \frac{1}{h_{v,test\ out} - h_{l,test\ out}} \quad (\text{A.47})$$

$$\frac{\partial x_{out}}{\partial h_{v,test\ out}} = \frac{h_{l,out} - h_{out,test}}{(h_{v,out} - h_{l,out})^2} \quad (\text{A.48})$$

$$\frac{\partial x_{out}}{\partial h_{l,test\ out}} = -\frac{1}{h_{v,test\ out} - h_{l,test\ out}} - \frac{h_{out,test} - h_{l,test\ out}}{(h_{v,test\ out} - h_{l,test\ out})^2} \quad (\text{A.49})$$

### A.18.3. Average test vapour quality uncertainty

The average test vapour quality is:

$$x_{avg} = \frac{x_{in} + x_{out}}{2} \quad (\text{A.50})$$

And the uncertainty becomes:

$$\delta\delta x_{avg} = \left( \left( \frac{\partial(x_{avg}\delta x_{in})}{\partial x_{in}} \right)^2 + \left( \frac{\partial(x_{avg}\delta x_{out})}{\partial x_{out}} \right)^2 \right)^{\frac{1}{2}} \quad (\text{A.51})$$

### A.19. Inner wall temperature uncertainty

The mean inner wall temperature is:

$$\overline{T_{w,i}} = \overline{T_{w,o}} + |Q_{test}R_w| \quad (\text{A.52})$$

Then the partial derivatives are:

$$\frac{\partial \overline{T_{w,i}}}{\partial \overline{T_{w,o}}} = 1 \quad (\text{A.53})$$

$$\frac{\partial \overline{T_{w,i}}}{\partial Q_{test}} = R_w \quad (\text{A.54})$$

$$\frac{\partial \overline{T_{w,i}}}{\partial R_w} = Q_{test} \quad (\text{A.55})$$

Therefore, the inner wall temperature uncertainty is:

$$\delta T_{w,i} = \left[ (\delta T_{w,o})^2 + (R_w \delta \dot{Q}_w)^2 + (\dot{Q}_w \delta R_w)^2 \right]^{\frac{1}{2}} \quad (\text{A.56})$$

### A.20. Heat transfer coefficient uncertainty analysis

The overall coefficient of heat transfer through the test condenser was calculated from Newton's law of cooling as shown:



$$\alpha_{conv} = \left| \frac{\dot{Q}_{w,test}}{A(\bar{T}_{w,i} - T_{sat})} \right| \quad (A.57)$$

where  $A$  is the inner surface area of the inner tube of the test section,  $T_{sat}$  is the mean saturation temperature at the inlet and outlet of the test section,  $\bar{T}_{w,i}$  is the mean inner wall temperature and it is related to the mean outer-wall temperature  $\bar{T}_{w,o}$  of the tube through the thermal resistance of the wall of the copper tube  $R_w$  [K/W]. The uncertainty in the temperature difference was derived in A.5.

The partial derivatives are:

$$\frac{\partial \alpha_{conv}}{\partial \dot{Q}_{w,test}} = \frac{1}{A(T_{sat} - \bar{T}_{w,i})} \quad (A.58)$$

$$\frac{\partial \alpha_{conv}}{\partial A} = -\frac{\dot{Q}_{w,test}}{A^2(T_{sat} - \bar{T}_{w,i})} \quad (A.59)$$

$$\frac{\partial \alpha_{conv}}{\partial \Delta T} = -\frac{\dot{Q}_{w,test}}{A} \quad (A.60)$$

The uncertainty is:

$$\delta \alpha_{conv} = \left[ \left( \frac{1}{A \Delta T} \delta \dot{Q}_{w,test} \right)^2 + \left( -\frac{\dot{Q}_{w,test}}{A^2 \Delta T} \delta A \right)^2 + \left( -\frac{\dot{Q}_{w,test}}{A \Delta T} \delta \Delta T \right)^2 \right]^{\frac{1}{2}} \quad (A.61)$$

## A.21. Pressure drop uncertainty analysis

The measured test pressure drop over the test condenser is a function of both friction and pressure drop and momentum pressure drop as shown in Eqs. A.62 - A.64. Accordingly, the uncertainty in the pressure drop is a function of the accuracy of the pressure transducers and the measurement of the inclination angle. It is also a function of vapour quality and the thermodynamic properties of the R134a.

$$\Delta p_{meas} = \Delta p_{mom} + \Delta p_{fri} \quad (A.62)$$

$$\Delta p_{meas} = p_{in} - p_{out} \quad (A.63)$$

$$\Delta p_{fri} = p_{in} - p_{out} - \Delta p_{mom} \quad (A.64)$$

### A.21.1. Measured pressure drop uncertainty

The uncertainty in the measured pressure drop is a function of the accuracy and uncertainty of the pressure transducers only. Three sets of pressure taps were mounted between the sight glass and the

test section on either side. Two of the taps were connected to different sensor pressure transducers to measure the absolute pressures at the inlet and outlet of the test condenser while the third set was connected to a differential pressure transducer. The resultant pressures at the inlet and outlet are means of the three individual transducers each having the same uncertainty. Thus mathematically,

$$p_{in/out} = \frac{1}{3} \sum_1^3 p_{meas,j} \quad (\text{A.65})$$

$$\delta p_{in/out,meas} = \left( \sum_{j=1}^3 \left( \frac{\partial}{\partial p_j} p_{in/out,meas} \delta p_j \right)^2 \right)^{\frac{1}{2}} \quad (\text{A.66})$$

It is assumed that all the pressure transducers have the same uncertainty given as:

$$\delta p_{in/out,meas} = \left( \frac{1}{3} \right)^{\frac{1}{2}} \delta p_j \quad (\text{A.67})$$